2011

Modulators of Ion Channels Crucial to Rodent Olfaction

Thomas G. Mast

THE FLORIDA STATE UNIVERSITY

COLLEGE OF ARTS AND SCIENCES

MODULATORS OF ION CHANNELS CRUCIAL TO RODENT OLFACTION

By

THOMAS G. MAST

A Dissertation submitted to the
Department of Biological Science
in partial fulfillment of the
requirements for the degree of
Doctor of Philosophy

Degree Awarded:
Fall Semester, 2011

Thomas G. Mast defended this dissertation on July, 15 2011.

The members of the supervisory committee were:

Debra Ann Fadool
Professor Directing Dissertation

Choogon Lee
University Representative

Wu-Min Deng
Committee Member

Frank Johnson
Committee Member

Michael Meredith
Committee Member

The Graduate School has verified and approved the above-named committee members, and certifies that the dissertation has been approved in accordance with university requirements.

To Amy and Eden.

ACKNOWLEDGEMENTS

I would not have been able to complete the work described here without the help of many people. To begin, I thank Dr. Debra Ann Fadool for taking me into her laboratory. The following results are only possible because of the guidance and support of Debi.

My family has provided me with tremendous emotional and financial support during the long days and years in Tallahassee. I thank them as much as I possibly can. In particular, I want to thank my wife, Amy, for still loving me during the ugly times; to Rebecca and Kevin for helping out with Edie when she was sick (and with some daycare cash!); to my parents, Katie and Jerry, for encouraging and supporting the worst student in the family—I thank you very much.

To my friends and peers whom gave me their time, shoulders and minds, especially: Kristal Tucker, Joe Breza, John Thompson, Jenn Stratford, Chris Kovach, Todd Stincic, Heidi Rivera, Joanne and Dave Garcia, Ariel Simonton, Chad Samuelsen, Greg Loney and Ann Marie Torregrossa, your friendship made my life and studies more fun and rewarding.

I thank my committee members, Drs. Frank Johnson, Michael Meredith, Wu-Min Deng and Choogon Lee, for their comments and help. And thanks to Dr. James Smith for guidance on insect chemical senses.

Many thanks to the staff members in both the Department of Biological Science and in the Program in Neuroscience who were very helpful. Charles Badland without whom most of the figures in this dissertation would not be publishable and to Jay Thigpen and Chris Gillis as well, for without their help my computer situation would have been dire. And to the office help who sheltered me from too much paperwork: Judy Bowers, Linda Sims and Janice Parker.

Lastly, I wish to thank the Program in Neuroscience for the two-year Neuroscience Fellowship and for continued support via the Chemical Senses Training Program. The Department of Biological Science provided a teaching appointment and the Robert B. Short Scholarship in Zoology for off-campus education. The Graduate School and the FSU Council on Research and Creativity provided funding for supplies with the Dissertation Research and LEAD Grants.

TABLE OF CONTENTS

LIST OF FIGURES

LIST OF ABBREVIATIONS

AP-5	D-(-)-2-Amino-5-phosphonopentanoic acid
ACSF	Artificial cerebrospinal fluid
ANOVA	Analysis of variance
AOB	Accessory olfactory bulb
AOS	Accessory olfactory system
BDNF	Brain derived neurotrophic factor, mature
BK	Big conductance potassium channel
Ca^+	Calcium
CaNS	Calcium-activated, non-selective ion channel
CMV	Cytomegalovirus
Da	Daltons
DAG	Diacylglycerol
DAPI	Diamidino-phenyindole
EPL	External plexiform layer
oEPL	Outer external plexiform layer
FITC	Fluorescein isothiocyanate
$G\alpha_{i2}$	GTP binding protein, alpha inhibiting polypeptide 2
$G\alpha_o$	GTP binding protein, alpha activating polypeptide O
GOB	Goblet cell
GABA	γ-Aminobutyric acid
GPCR	G-protein coupled receptor
GTP	Guanosine-5'-triphosphate
G-protein	Guanidine trisphosphate-binding protein
GL	Glomerular layer
Gr	Granule cell
HEK293	Human embryonic kidney 293 cells
IgG	Immunoglobulin G
IP_3	Inositol trisphosphate
IP_3R	Inositol trisphosphate receptor
IP_3R_3	Inositol trisphosphate receptor, type 3
ir	immunoreactive
K^+	Potassium
Kv1.3	Voltage-gate potassium channel, *Shaker* family member 3
LB	Lysis buffer
M	Mitral cell
MΩ	Mega ohms
MCL	Mitral cell layer
MHC	Major histocompatability complex
M10	MHC class 1b, 10
MOE	Main olfactory epithelium
MOS	Main olfactory system
M_r	Molecular weight, relative
mRNA	Messenger ribonucleic acid
N	Number of samples

Na^+	Sodium
Na_3VO_4	Sodium pervanadate
NBQX	2,3-Dioxo-6-nitro-1,2,3,4-tetrahydrobenzo[*f*]quinoxaline-7-sulfonamide
NGF	Nerve growth factor, mature
NT-3	Neurotrophin 3, mature
NT-4	Neurotrophin 4, mature
OB	Olfactory bulb
OE	Olfactory epithelium
ONL	Olfactory nerve layer
OR	Olfactory receptor
OSN	Olfactory sensory neuron
P	Postnatal day
P75NTR	p75 neurotrophin receptor
PBS	Phosphate buffered saline
PG	Periglomerular cell
PIP_2	phosphatidylinositol 4,5-bisphosphate
PLC	Phospholipase C
PPI	Protease and phosphatase inhibitor solution
proBDNF	Brain derived neurotrophic factor, immature
proNGF	Nerve growth factor, immature
proNT-3	Neurotrophin-3, immature
proNT-4	Neurotrophin-4, immature
REEP1	Receptor expression enhancing protein 1
RTP1	Receptor transporting protein 1
SCSB	Sodium citrate stripping buffer
SDS-PAGE	Sodium dodecyl polyacrylamide gel electrophoresis
snk	Student-Newman-Keuls post-hoc test
TEB	Tissue extract buffer
TH	Tyrosine hydroxylase
TIFF	Tagged-image file format
TRPC2	Transient receptor potential 2 channel
TrkA	Tyrosine receptor kinase A
TrkB	Tyrosine receptor kinase B
TrkC	Tyrosine receptor kinase C
TSB	Tris stripping buffer
VNO	Vomeronasal organ
VR	Vomeronasal receptor
V1R	Type 1 vomeronasal receptors
V2R	Type 2 vomeronasal receptors
VSNs	Vomeronasal sensory neurons
WB	Wash buffer
YFP	Yellow fluorescent protein

ABSTRACT

Olfaction allows vertebrates to sense their chemical environment, and plays an important role in feeding behavior, reproduction, memory and learning. The first portion of the dissertation examined the signal transduction cascade in the rodent vomeronasal organ (VNO). The proteins in this cascade have been individually well-characterized over the last 20 years; however, little attention has been paid to the role of protein-protein interactions among these molecules. I found two novel binding partners for the transient receptor potential 2 channel (TRPC2), which establishes the first electrical signal in the pheromone transduction pathway, in the native VNO. Homer 1b/c was found to co-immunoprecipitate with TRPC2 and the inositol trisphosphate receptor (IP_3R) from rat VNO lysates. The second new protein partner was chaperone with previously no known function in the VNOs. Receptor transporting protein 1 (RTP1) expression was investigated with immunohistochemical techniques and was localized to to the VNO sensory epithelium. RTP1 also co-immunoprecipitated with TRPC2 from rat VNO lysates and, additionally, RTP1 increased TRPC2 surface expression as measured by cell-surface biotinylation. When co-expressed with RTP1 in human embryonic kidney cells, TRPC2 formed a functional channel as measured with whole-cell electrophysiology.

The second portion of this dissertation is a commentary on the function and importance of the VNO in human mate selection. The published literature on human vomeronasal function is briefly examined. With this in mind, I concluded that VNO has no role in human behavior.

The last portion of this doctoral dissertation examined the role of brain-derived neurotrophic factor (BDNF) in the mouse olfactory bulb (OB). Mitral cells, the principle output cells of the OB, express tyrosine receptor kinase B (TrkB) the high-affinity BDNF receptor. OB interneurons express the low-affinity BDNF receptor, p75NTR. Following naris-occlusion more mitral cells became immunoreactive and interneurons became less BDNF immunoreactive. In the OB, only the unprocessed proBDNF was detected with immunoblot. In a slice preparation, proBDNF did not alter mitral cell excitability while mature BDNF did. Interestingly, intranasal delivery of proBDNF, but not BDNF, induced activated-caspase 3 immunoreactivity in OB interneurons and reduced tyrosine hydroxylase immunoreactivity. Thus, BDNF modulates mitral cell excitability and proBDNF modulates interneuron markers of cell death.

CHAPTER ONE

INTRODUCTION

The Olfactory System: An Overview

In the mouse and rat, the olfactory pathway can be partitioned into three anatomically separated areas: an olfactory epithelium, the olfactory bulb (OB), and the olfactory cortex. The olfactory epithelia contain the cell bodies and sensory transduction machinery that physically detects environmental chemicals. At least four olfactory epithelia exist: the gruenbuerg ganglion (Koos and Fraser 2005), the septal organ (Ma *et al.* 2003), the vomeronasal organ (VNO) (Halpern and Martinez-Marcos 2003; Meredith and O'Connell 1979; Wysocki *et al.* 1980), and the main olfactory epithelium (MOE) (Schild and Restrepo 1998). The OB receives the synaptic input from the olfactory epithelia and is functionally the primary, unimodal olfactory cortex (Haberly 2001; Swanson 2000). The olfactory system has two major divisions: the main olfactory system (MOS) and the accessory olfactory system (AOS). The MOS is the pathway that arises as MOE axons synapse within an area of the OB called the main olfactory bulb (MOB). The AOS is the neural pathway extending from VNO axons synapse within an area of the OB called the accessory olfactory bulb (AOB) (Halpern and Martinez-Marcos 2003; Kratskin 1995; Ma 2007) (Figure 1.1). Projections from the OB then synapse within deeper brain regions commonly referred to as the olfactory cortex (Swanson 2000).

Olfaction allows vertebrates to sense their chemical environment, and it plays an important role in feeding behavior, reproduction, memory and learning. The primary function of the MOS is to detect general environmental chemicals, such as food odors (Ma 2007). The MOS is then connected to brain areas associated with memory. For example, rodents are good at forming and then remembering odor-place associations between those general odors and where the animal detected them (Gibb *et al.* 2006; Lipton *et al.* 1999). The MOS does not only detect general odors. The MOS is also able to detect 'social' odors generated by conspecifics (Lin *et al.* 2007; Schaefer *et al.* 2002; Spehr *et al.* 2006; Woodley and Baum 2004). Thus, the MOS is crucial for finding food and negotiating the environmental terrain.

The mammalian AOS functions as a detector for those 'social' chemical signals (chemosignals) concerning social organization and conspecific reproductive status

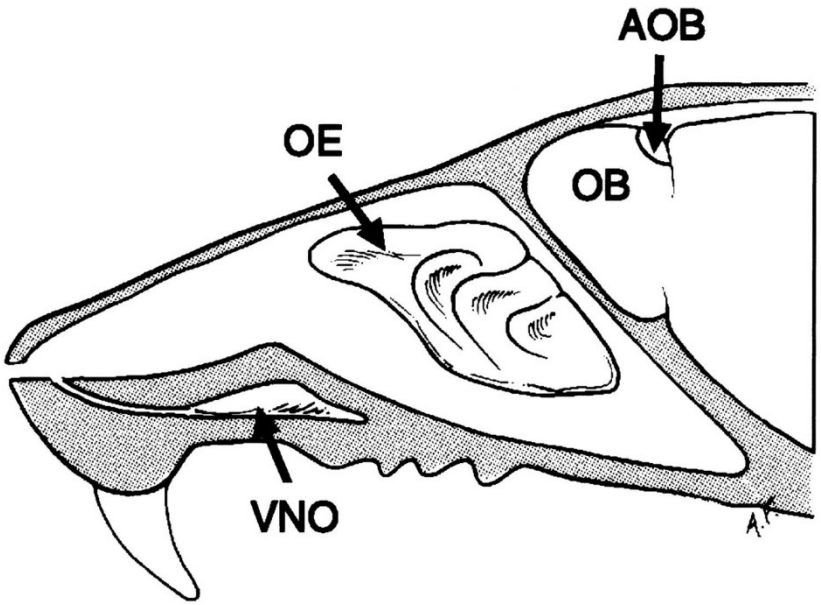

Figure 1.1 Schematic of the rodent nasal cavity with an emphasis on the main and accessory olfactory pathways. The vomeronasal organ (VNO) is shown in the roof of the mouth, embedded in the hard palate. The main olfactory epithelium (OE) covers the olfactory turbinates. The olfactory bulb (OB) in shown in the braincase. The accessory olfactory bulb (AOB) is a dorsal, rostral subdivision of the OB. Modified from Liman and Corey, 1996.

(Halpern and Martinez-Marcos 2003; Meredith *et al.* 1980). The AOS has been repeatedly linked to social behaviors and, as such, is a powerful model for sensory neuroscience, neuronal circuitry, and the neurobiology of behavior (Ben-Shaul *et al.* 2010; Halpern and Martinez-Marcos 2003; Kimchi *et al.* 2007; Leypold *et al.* 2002; Meredith 1986; Stowers *et al.* 2002). The AOS appears to also make odor-place associations (Jang T 2001; Martínez-Ricós *et al.* 2007).

My dissertation investigates channel function in the first two stages of the olfactory system—neurons within the VNO of the AOS and neurons within the MOB of the MOS. Chapter 2 investigates the AOS by examining VNO function at the level of protein-protein interactions inherent to the signal transduction cascade of the individual vomeronasal sensory neurons (VSNs). Chapter 3 briefly reviews VNO function in humans. Chapter 4 investigates the MOS by examining the effect sensory input loss has on the MOB protein expression and localization. Lastly, Chapter 5 investigates MOB sensory input loss on histological and electrophysiological changes.

Accessory Olfactory System Details

Vomeronasal sensory transduction and AOS pathway

The VNO lies along either side of the midline as a blind-ended tube and contains sensory neurons called vomeronasal sensory neurons (VSNs) (Halpern and Martinez-Marcos 2003; Inamura and Kashiwayanagi 2000; Wysocki *et al.* 1980). VSNs are bipolar neurons with a microvillar dendrite that projects into the VNO lumen (Berghard *et al.* 1996; Liman *et al.* 1999; Vaccarezza *et al.* 1981; Wysocki *et al.* 1980) and an axon that project centrally. VSNs express a G-protein coupled receptor (GPCR) in the dendrite microvilli. Here, these GPCRs are from one of the vomeronasal receptor (VR) families, either a V1R or a V2R receptor protein, and are responsible for binding to chemical stimuli (Berghard *et al.* 1996; Dulac and Axel 1995; Herrada and Dulac 1997; Matsunami and Buck 1997; Ryba and Tirindelli 1997). Upon binding of a chemosignal, V1Rs and V2Rs activate the G-proteins, $G\alpha_{i2}$ and $G\alpha_o$, respectively (Halpern and Martinez-Marcos 2003) (Figure 1.2). The G-protein activates phospholipase C (PLC), an enzymatic pathway that is stimulated upon ligand binding to a VR (Berghard *et al.* 1996; Dulac and Axel 1995; Halpern and Martinez-Marcos 2003; Matsunami and Buck 1997). PLC reacts with phosphoinositol bisphosphate (PIP_2) and hydrolyzes it into diacylglycerol (DAG) and inositol trisphosphate (IP_3). IP_3 binds to, and facilitates, the opening of IP_3-receptors

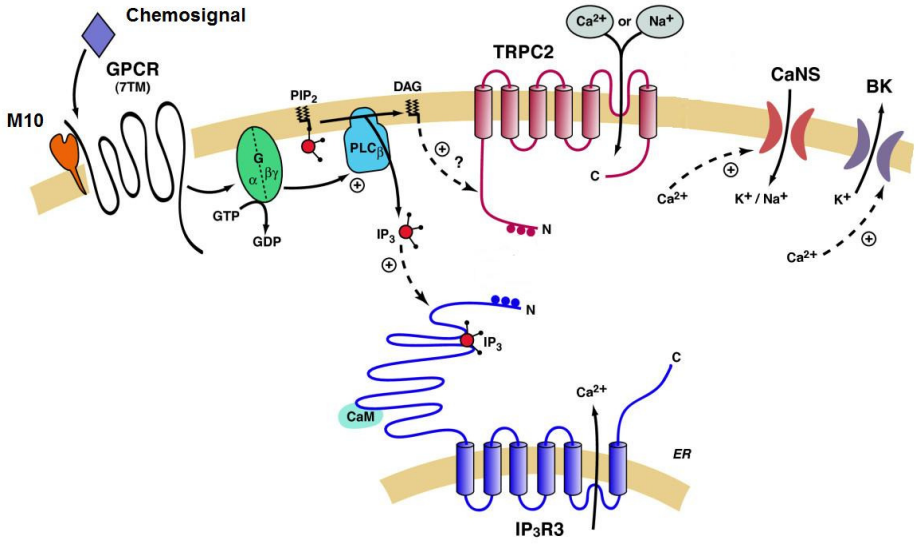

Figure 1.2 Schematic of vomeronasal signal transduction. The vomeronasal organ (VNO) signal transduction pathway begins when a chemosignal binds to either a type 1 vomeronasal (V1R) or type 2 vomeronasal (V2R) G-protein coupled receptor (GPCR); V2Rs may be associated with a member of the M10 major histocompatibility protein family. V1R/ V2R activate a guanidine trisphosphate-binding protein (G-protein). The activated G-protein stimulates the cleavage of phosphatidylinositol 4,5-bisphosphate (PIP_2) into 1,4,5-inositol trisphosphate (IP_3) and diacylglycerol (DAG) via phospholipase C (PLC). DAG has been reported to gate the non-specific cation current through the type 2 canonical transient receptor potential channel (TRPC2). Two isoforms of IP_3R (IP_3R_2 and IP_3R_3) are expressed in the VNO, and IP_3R_3 forms a complex with TRPC2. IP_3 activation of IP_3R_3 may increase the calcium current. A calcium-activated non-selective ion channel (CaNS) can amplify the chemosignal-induced current following the rise in intracellular calcium. This rise in intracellular calcium also activates the calcium-activated big conductance potassium ion channels (BK). Modified from Fadool, 2005.

allowing calcium to enter the cell (Brann *et al.* 2002; Fadool 2005; Inamura *et al.* 1997b; Keverne 1999; Taylor and Laude 2002). VSN dendrites also express the type 2 canonical transient receptor potential (TRPC2) non-selective cation channel (Lucas *et al.* 2003). In the VSNs, TRPC2 appears to gated by DAG (Lucas *et al.* 2003). TRPC2 is thought to be the primary signal amplification process necessary for VSN function (Leypold *et al.* 2002; Lucas *et al.* 2003; Stowers *et al.* 2002). Further signal amplification, however, could come from other channels (Liman 2003). Signal adaptation is likely to come from calcium-calmodulin inhibition of both IP_3R_3 (Taylor and Laude 2002) and TRPC2 (Spehr *et al.* 2009), calcium-activated big conductance potassium channels (BK) (Ukhanov *et al.* 2007; Zhang *et al.* 2008), and metabolism of DAG into the lipid arachidonic acid (Spehr *et al.* 2002; Zhang *et al.* 2008). Each VSN extend an axon into the AOB and form an excitatory glutamatergic synapse (Jia *et al.* 1999).

The AOB is a layered, cortical-like structure (Halpern and Martinez-Marcos 2003; Jia *et al.* 1999; Kaba and Keverne 1992; Larriva-Sahd 2008) (Figure 1.3). Moving from superficial to deep, the layers are: the vomeronasal nerve layer, the glomerular layer, the external cellular layer, the lateral olfactory tract, and the internal cellular layer (Larriva-Sahd 2008). The glomerular and cellular layers are populated with distinct sets of neurons. The glomerular layer contains vomeronasal nerve terminals, mitral/tufted dendrites and interneurons (Halpern and Martinez-Marcos 2003; Jia *et al.* 1999; Larriva-Sahd 2008). The external cellular layer contains the cell bodies of output neurons and the internal cell layer contains granule interneurons (Larriva-Sahd 2008).

The AOB neurons form a complex circuit. For example, granule neurons of the granule layer make dendo-dendritic synapses with mitral neurons of the external cellular layer. Through these dendo-dendritic synapses, granule cells inhibit output neurons including mitral cells (Jia *et al.* 1999). The glomeruli are spherical regions of neuropil surrounded by interneurons and output neuron cell bodies (Larriva-Sahd 2008) (Figure 1.3). This differs from the main olfactory bulb where glomeruli are exclusively delimited by interneurons (Kosaka *et al.* 1998). Most AOB output neurons have branched axons that project to several targets (Kang *et al.* 2011).

AOB axons synapse directly into cortical regions, and thus, together with the other olfactory projections, constitute the only sensory pathway that is not relayed through the

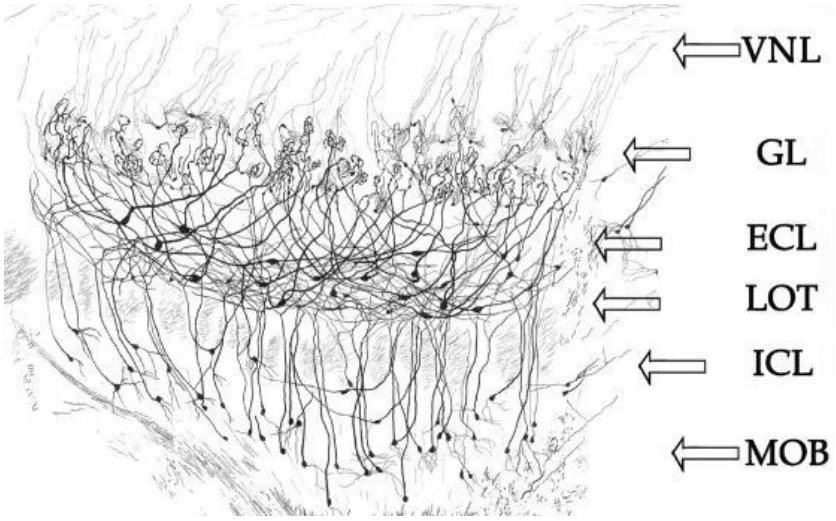

Figure 1.3 Schematic of the accessory olfactory bulb. Axons from the vomeronasal nerve layer (VNL) project into glomeruli in the glomerular layer (GL). Also projecting into the glomeruli are dendrites from output neurons, the cell bodies of which lie in the external cellular layer (ECL). Beneath the ECL is another layer of cells called the internal cellular layer (ICL). The lateral olfactory tract extending from the main olfactory bulb (MOB) separated the ECL from the ICL. Modified from Larriva-Sahd, 2008.

thalamus prior to reaching cortical regions (Swanson 2000). AOB output cells project to both the anterior amygdala and the medial amygdala (Halpern and Martinez-Marcos 2003; Kang *et al.* 2011; Meredith and Westberry 2004); as well as the bed nucleus of the stria terminalis and bed nucleus of the accessory olfactory tract (Halpern and Martinez-Marcos 2003; Mohedano-Moriano *et al.* 2007). The olfactory cortex then projects to the hippocampus, thalamus, hypothalamus, and brainstem (Haberly 2001; Halpern and Martinez-Marcos 2003; Kratskin 1995).

VSN physiology

The VNO has long been considered a chemosensory organ based on histological similarities with the MOS (Halpern and Martinez-Marcos 2003). This view was supported by the discovery that the VNO contains a physical pump (Meredith *et al.* 1980; Meredith and O'Connell 1979), and thus, a mechanism for introducing chemical stimuli into VNO lumen. Living *ex vivo* preparations of both the MOE (Scott and Scott-Johnson 2002) and VNO (Tucker 1963) can be induced to generate a summed electrical potential. The potentials generated from the VNO epithelia, the so-called electrovomeronasogram (EVG) can be elicited following presentation of chemical stimuli (Tucker 1963). EVG response to specific chemicals is abolished following gene-targeted deletion of VRs (Del Punta *et al.* 2002a). The molecular receptor found in the MOE, the olfactory receptors, (Buck L 1991; Godfrey *et al.* 2004) and the signaling transduction components are not present in the VNO (Berghard *et al.* 1996; Dulac and Axel 1995; Herrada and Dulac 1997). Thus, the VNO and VRs use a different physiological pathway.

Research into the ionic currents and protein interactions that underlie VSN physiology continues to be informed by several experimental findings. VSN physiological experiments were geared toward finding channels and currents, and signal transduction molecules. Disassociated VSNs respond to urine, a rich source of chemosignals (Meredith and Westberry 2004; Samuelsen and Meredith 2009) by firing many spikes (action potentials). Underlying these spikes are at least one voltage-gated sodium current and multiple voltage-gated potassium currents (Labra *et al.* 2005; Trotier *et al.* 1998). VSN responses to urine are also dependent upon calcium influx as low extracellular calcium blocks chemosensory currents (Inamura and Kashiwayanagi 2000). Additionally, isolated calcium currents are blocked by low external calcium (Inamura *et al.* 1997b) and by T-type and L-type calcium channel blockers (Liman and

Corey 1996). These calcium currents may function to activate an unidentified calcium-activated non-selective cation channel (Liman 2003). Calcium may be a coordinating molecule in the VNO, as chemical stimulation of the VNO generates the second-messenger, and calcium-store ligand (Taylor and Laude 2002), IP_3 (Luo *et al.* 1994; Wekesa and Anholt 1997). Dialysis of IP_3 into VSNs generates both sodium currents and calcium currents, but not action potentials (Inamura *et al.* 1997b). VSN responses to urine are blocked by IP_3R and PLC antagonists (Inamura *et al.* 1997a; Spehr *et al.* 2002). Thus, VSNs require conductance's generated by IP_3, but these are not sufficient to generate the entire receptor potential. Primary amplification of the receptor potential comes from TRPC2 expressed in the VSN dendrite (Liman *et al.* 1999). This hypothesis is supported by experiments that demonstrated an IP_3R_3-TRPC2 protein-protein interaction *in vivo* (Brann *et al.* 2002). WithoutTRPC2 mice have altered social behavior (Leypold *et al.* 2002; Stowers *et al.* 2002), not unlike animals lacking a VNO (Meredith 1986). TRPC2 deficient animals also lack EVG responses to chemical stimuli (Leypold *et al.* 2002). Lastly, the TRPC2 channel is not gated by IP_3 or Ca^{2+} store depletion (Lucas *et al.* 2003), but is gated by the other product of PLC activation, DAG (Lucas *et al.* 2003; Spehr *et al.* 2009) and biophysically is a non-selective cation channel.

The physiology of VSNs is fascinating, and specific. For example, VSNs, unlike OSNs, do not exhibit strong and rapid signal adaption (Ukhanov *et al.* 2007). Instead, VSN have persistent spiking behavior following stimulation (Inamura *et al.* 1999; Leinders-Zufall *et al.* 2000; Trotier *et al.* 1998; Ukhanov *et al.* 2007). VSNs also appear to be able to differentiate between genders and among individuals (He *et al.* 2008). The best evidence for narrow and specific tuning at the receptor level is the fact that individual neurons are highly sensitive (i.e. 10^{-11}M) to their ligand (Leinders-Zufall *et al.* 2000). These neurons do not respond to other ligands and, in slice preparations, individual chemosignals produce distinct, non-overlapping sets of activated VSNs (Leinders-Zufall *et al.* 2000). Given this specificity it appears that VNO chemosignal responses are discreet and simply a function of one or a few VSN response profiles. For example, mice form preferences toward urine based on MHC haplotype (Doty 2003) and individual VSNs respond to MHC class I peptides encoded by these haplotypes (Leinders-Zufall *et al.* 2004). MHC peptides are not the full stimulus (or story), as the activation patterns generated by the peptide do not overlap with the urine activation patterns (ie the fluid that naturally contains the stimulus) (He *et al.* 2008). Sulfated steroids are also present in urine, may

be behaviorally relevant in terms of mating, and are active ligands for VSNs (Nodari *et al.* 2008). Each individual VSN, and presumably each encoded VR, responds to a functional group (i.e. structural specificity) present on the steroid; however, the activation pattern across the VNO is complex, as each VSN can respond to one of several sulfated steroids containing the functional group (i.e. broad tuning) (Nodari *et al.* 2008). Thus, although VSN response profiles are rather specific, the VNO likely respond to chemosignals broadly. Molecular evidence for a broad response comes from the V1rb2-deficient mouse. V1rb2 expressing VSNs respond to 2-heptanone and not similar compounds; however, the V1rb2-deficient VNO still produces an EVG in response to 2-heptanone stimulation. This indicates that at least one more 2-heptanone receptor exists in the VNO (Boschat C 2002; Del Punta *et al.* 2002a). Therefore, the specificity of the VNO may not be due to a requirement of chemosignal detection. It may be due to a mechanism of selection termed 'sensory drive' in which environment forces the cue and sensory apparatus for the cue to adapt (Boughman 2002). In this case of steroids in a terrestrial environment, the chemosignal is likely to neither disperse widely nor be in great quantities; therefore, it is reasonable that highly-sensitive receptors would evolve to help detect these discreet quantities.

Questions on VSN function

This VSN signaling cascade is not fully described and at least three interesting problems in vomeronasal function remain. The first question revolves around the role of MHC proteins in VSN function. MHC 1b proteins are expressed only in V2R- and $G\alpha_o$- expressing cells (Ishii *et al.* 2003; Loconto *et al.* 2003), which are exclusively located in the basal VNO sensory epithelium (Herrada and Dulac 1997) (Figure 1.4). *In vivo* the MHC 1b proteins localize to the VSN dendrite (Loconto *et al.* 2003). Importantly, β-2-microglobin, a protein that helps traffic and stabilize MHC 1b proteins (Crowley *et al.* 1997), immunoprecipitates with both MHC and V2R proteins (Loconto *et al.* 2003). *In vitro*, co-expression of V2Rs with M10 and β2-microglobulin leads to increased receptor surface expression (Loconto *et al.* 2003). This work suggests that the MHC molecules ensure proper V2R localization. It has also been suggested, however, that the MHC proteins may act to sort VSN axons. $G\alpha_{i2}$-positive V1R-positive axons synapse in the rostral half of the AOB whereas $G\alpha_o$-postive V2R-positive axons synapse in the caudal AOB (Del Punta *et al.* 2002b; Jia and Halpern 1996; Rodriguez *et al.* 1999) (Figure 1.4).

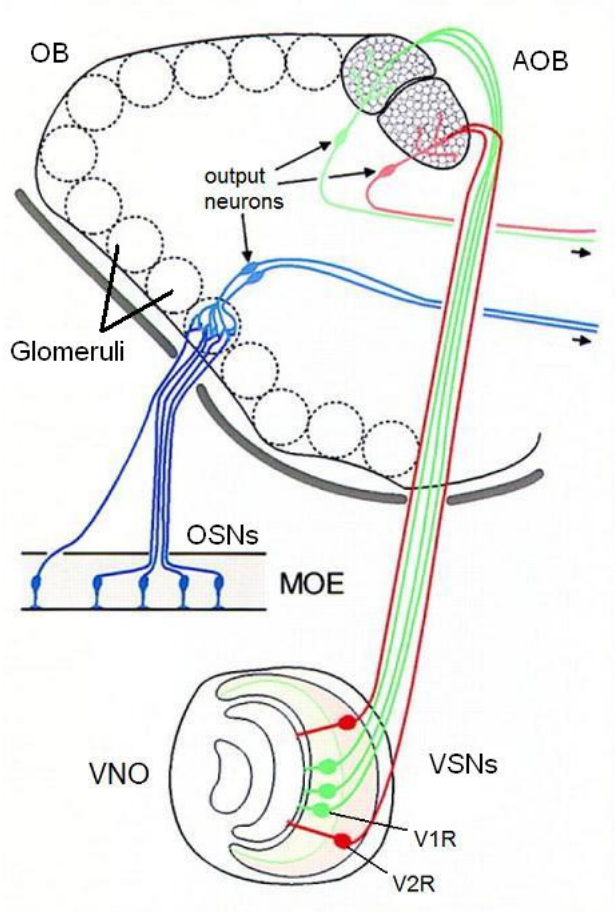

Figure 1.4 Schematic of the vomeronasal and main olfactory sensory projections to the OB. Vomeronasal sensory neurons (VSNs) are shown projecting from the vomeronasal organ (VNO) to the accessory olfactory bulb (AOB). Note that V1R expressing neurons are in the apical VNO and project to the rostral AOB and the V2R expressing neurons are in the basal VNO and project to the caudal AOB. The main olfactory epithelium (MOE) contains olfactory sensory neurons that project to glomeruli within the OB. The output neurons are projecting to the olfactory cortex. Modified from Herrada and Dulac, 1997.

MHC proteins may help V2R axons recognize 'like' axons so that synaptic convergence can occur in the glomeruli (Del Punta *et al.* 2002b; Ishii *et al.* 2003). In support of this hypothesis, it has been shown that not all V2R-positive cells are MHC 1b-positve (Ishii and Mombaerts 2008), giving V2R cells flexibility during axon fasciculation. The second question of VSN signaling cascade concerns the number of V2R genes expressed per neuron. It is commonly thought that each VSN expresses one, and only one, VR (Rodriguez 2007), just as olfactory sensory neurons express only one odorant receptor (Chess *et al.* 1994; McClintock 2010; Mombaerts *et al.* 1996; Serizawa *et al.* 2003). This has only been documented for the V1R family (Rodriguez *et al.* 1999; Roppolo *et al.* 2007). Interestingly, a recent report suggests that in each V2R-positive neuron, two different V2R genes are sequentially expressed (Ishii and Mombaerts 2011). Ishii and Mombaerts (2011) present data only at the gene expression level (i.e. mRNA) and further studies need to be conducted to both confirm these results and look to for evidence at the receptor level (i.e. protein). The last question surrounding VSN signal transduction involves TRPC2 expression and is addressed in Chapter 2. TRPC2 is crucial for generating the VSN response to chemical ligands (Lucas *et al.* 2003) and gene-targeted deletion of TRPC2 results in mice with altered sexual and social behaviors (Kimchi *et al.* 2007; Leypold *et al.* 2002; Stowers *et al.* 2002). TRPC2 biophysical properties and protein binding partners, however, have been difficult to determine due to poor expression in heterologous expression systems (Hofmann *et al.* 2000; Jungnickel *et al.* 2001).

Vomeronasal experimental focus

In light of the problems listed above, Chapter 2 of this dissertation describes a method to express TRPC2 with an olfactory specific chaperone, receptor transporting protein 1 (RTP1) (Saito *et al.* 2004; Zhuang and Matsunami 2007). Chapter 2 also describes a role for a scaffolding protein called Homer 1b/c. Scaffolding proteins work to link-up other proteins. Homers have been shown to tether glutamate receptors, IP_3 receptors, and other calcium sensitive proteins together (Brakeman *et al.* 1997; Kammermeier and Worley 2007; Kim *et al.* 2006b; Tu *et al.* 1999; Worley *et al.* 2007a; Xiao *et al.* 1998; Yuan *et al.* 2003). Chapter 2 describes a role for Homer 1b/c in keeping TRPC2 and IP_3 receptors together in the VSN signaling cascade.

Main Olfactory System Details

Like the AOB, the MOB is a layered, cortical-like structure (Kratskin 1995; Shepherd and Greer 1998) (Figure 1.5). Moving from superficial to deep, these layers are the: olfactory nerve layer (ONL), glomerular layer (GL), external plexiform layer (EPL), mitral cell layer (MCL), internal plexiform layer (IPL), and the granule layer (GL). The glomeruli are spherical regions of neuropil where OSN axon terminals make glutamatergic synapses (Berkowicz *et al.* 1994; De Saint Jan and Westbrook 2007; Trombley and Westbrook 1990) with mitral/tufted dendrites and interneurons (Kratskin 1995; Shepherd and Greer 1998). The glomeruli are delimited by interneurons (Kosaka *et al.* 1998). Most glomerular interneurons are considered inhibitory as they contain the neurotransmitter γ-aminobutyric acid (GABA); a few of these neurons are also catecholamine neurons that express tyrosine hydroxylase (Baker *et al.* 1993; Baker *et al.* 1988; Brunjes *et al.* 1985; Deng *et al.* 2007; Kiyokage *et al.* 2010; Kosaka *et al.* 1998; Parrish-Aungst *et al.* 2011). The mitral and tufted cells are the output neurons of the olfactory bulb (Price and Powell 1970). Mitral cells have a unique anatomy including a lack of spines (Price and Powell 1970) and long, lateral dendrites (Cajal 1995). Granule cells are another kind of interneuron located in a large layer, deep to the mitral cells (Kratskin 1995).

This dissertation examines mitral cell electrical excitability and uses this excitability to measure the activation of endogenous signaling pathways (Chapter 5). Odorant activity in the nasal cavity induces glutamate release into glomeruli by OSNs (Berkowicz *et al.* 1994; De Saint Jan and Westbrook 2007; De Saint Jan and Westbrook 2005; Trombley and Westbrook 1990). The activated glomeruli generate a pattern of activity (Johnson *et al.* 2010; Lin *et al.* 2005; Schaefer *et al.* 2002; Woodley and Baum 2004). The mitral cells that synapse within the glomeruli (Kratskin 1995), then project this information to the olfactory cortex in a pattern of activity (Haberly 2001). Individual mitral cells have differing responses to odors (Griff *et al.* 2008a) and to respiration (Griff *et al.* 2008b). Mitral cell responses are thought to be sculpted by local lateral excitation/ inhibition via dendro-dendritic synapse between granule and mitral cells (Chen and Shepherd 1997; Kratskin 1995; Whitman and Greer 2007). Lateral excitation is likely due to glutamate release at dendro-dendritic synapses along mitral cell lateral dendrites (Chen and Shepherd 1997; De Saint Jan and Westbrook 2007; Maher *et al.* 2009) (Figure 1.5). Odor-evoked mitral cell lateral inhibition that can be recorded *in vivo* (Margrie *et al.* 2001) is likely due to GABA release at dendro-dendritic synapses between mitral cell lateral dendrites

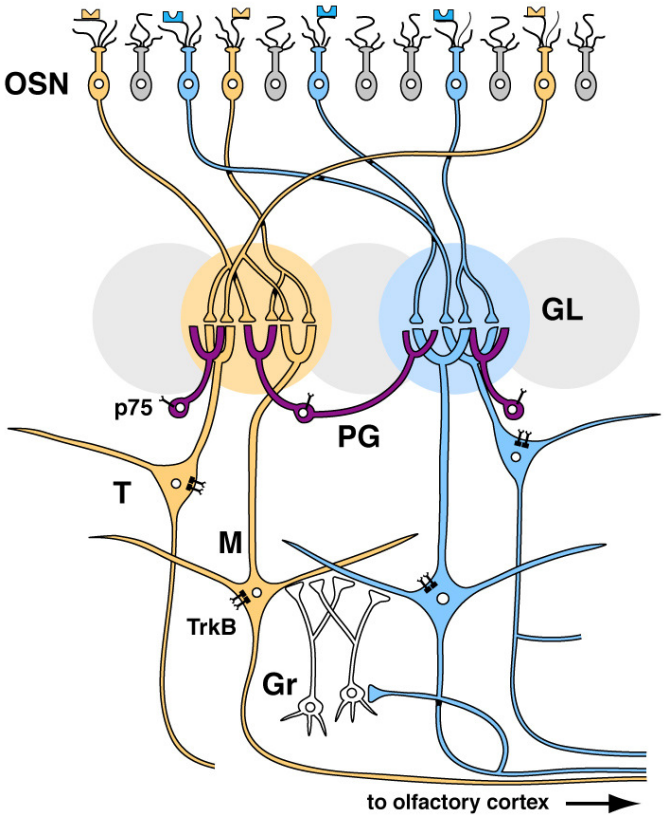

Figure 1.5 Schematic of the main olfactory bulb. Olfactory sensory neurons (OSNs) expressing the same olfactory receptor (tan and blue) project into the same glomerulus (GL) a region of neuropil in the glomerular layer. The glomeruli are surrounded by interneurons, including periglomerular cells (PG). PG cells express the p75 neurotrophin receptor (p75). OSNs synapse with glomerular layer interneurons and the output neurons, mitral (M) and tufted (T) cells. Mitral and tufted cells express the tyrosine receptor kinase B (TrkB) neurotrophin receptor. Mitral cell lateral dendrites form synapses with adjacent mitral cells and granule interneurons (Gr) of the granule layer.

and granule cell dendrites (Kratskin 1995; Lagier *et al.* 2007; Lledo *et al.* 2004; Margrie *et al.* 2001) (Figure 1.5). Mitral cell response to odor input is also shaped by presynaptic inhibition. The glomerular cells that surround the glomeruli are able to reduce the activity of neighboring glomeruli via GABA inhibition of OSNs (McGann *et al.* 2005; Olsen and Wilson 2008; Root *et al.* 2008) where OSNs and the interneurons form synapses (Kosaka *et al.* 1998; Kratskin 1995). Mitral cells also have differing spontaneous activities based upon latency and rate (Nica *et al.* 2010) and in relation to the respiratory cycle (Griff *et al.* 2008b). Thus, mitral cells may have intrinsic differences in excitability based on ion channel expression (Maher and Westbrook 2005; Padmanabhan and Urban 2010). Electrically-stimulated mitral cells generate sub-threshold oscillations that involve the slow inactivating potassium current I_D (Balu *et al.* 2004; Chen and Shepherd 1997). The slow inactivating potassium current I_D is associated with Kv1.3 (Balu *et al.* 2004; Bean 2007; Fadool and Levitan 1998). It is unclear whether Kv1.3 is functioning in homomeric channels (Kv1.3 only) or in heteromertic Kv1.3 channels (with other *Shaker* subunits) (Balu *et al.* 2004). It is clear that Kv1.3 is necessary for proper mitral cell electrical activity as Kv1.3 gene-targeted deletion severely alters mitral cell evoked activity (Fadool *et al.* 2004).

Neurotrophin family

Neurotrophins are proteins that support neuron growth and survival (Barker 2009; Kalb 2005; Reichardt 2006). Studies on mouse tumors transplanted *in vivo* and on snake venom *in vitro* (Levi-Montalcini 1987) led to the discovery of the first neurotrophin, nerve growth factor (NGF), originally purified from the mouse salivary gland (Cohen 1960). Twenty-five years later a similar protein called brain-derived neurotrophic factor (BDNF) was purified from pig brain (Barde *et al.* 1982). The similarity between NGF and BDNF allowed for molecular cloning techniques to be used to discover neurotrophin-3 (NT3) (Ernfors *et al.* 1990) and neurotrophin-4 (Hallböök *et al.* 1991; Ip *et al.* 1992) within a decade. P75 neurotrophin receptor (p75NTR) was identified as the first neurotrophin receptor (Rodriguez-Tébar *et al.* 1990). The receptor binds all neurotrophins with similar, low affinity (Reichardt 2006; Rodriguez-Tébar *et al.* 1990) (Kalb 2005) (Figure 1.6). The second class of neurotrophin receptors, the tyrosine receptor kinases (Trk), demonstrate a degree of ligand specificity and higher binding affinities (Kalb 2005; Reichardt 2006). Here, NGF binds to TrkA; BDNF binds to TrkB, NT4 binds to TrkC, and NT3 binds to each (Reichardt 2006) (Figure 1.6). Different receptor-

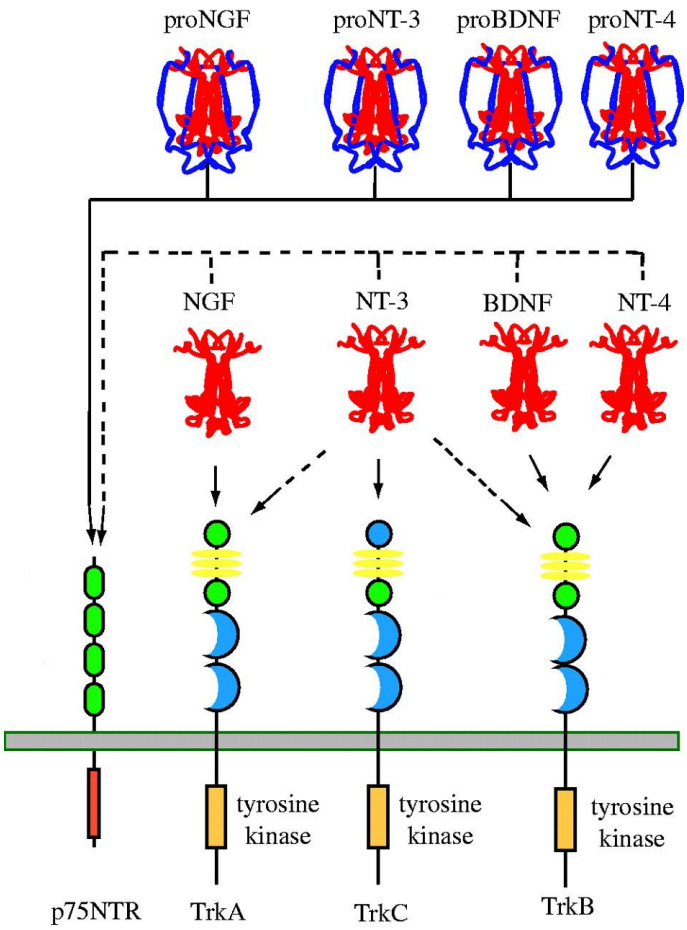

Figure 1.6 Schematic of the neurotrophin family receptor interactions. All proneurotrophins bind to p75NTR. Cleaved, mature neurotrophins bind to p75NTR with low affinity. Nerve growth factor (NGF) binds to TrkA; BDNF and NT4 bind to TrkB; NT3 activates TrkC with high affinity. NT3 has also low affinity for TrkA and TrkB, as well. Low-affinity interactions are shown with dashed lines and high-affinity interactions are shown with solid lines. Note the cytoplasmic kinase domain on the Trk receptors and not p75NTR. Modified from Reichardt, 2006.

neurotrophin binding patterns are achieved via enzymatic processing. Neurotrophins are secreted as a a longer 'pro' isoform (i.e. proBDNF, proNGF) that requires processing by an extracellular protease (Lee *et al.* 2001) that cleaves the pro domain from the rest of the protein (Figure 1.6). For example, the *bdnf* gene product is secreted into the extracellular matrix as proBDNF which typically requires enzymatic processing by proteases to become an active TrkB ligand (Pang *et al.* 2004). The cleaved 'mature' neurotrophins (i.e. BDNF, NGF) are the preferred ligands for the Trk receptors (TrkA, TrkB and TrkC) (Fayard *et al.* 2005; Kalb 2005; Reichardt 2006). TrkB is the high-affinity receptor for BDNF (Fayard *et al.* 2005; Kalb 2005; Reichardt 2006). The proneurotrophins have a higher affinity for the p75NTR than for their respective Trk receptor (Kalb 2005; Lee *et al.* 2001; Reichardt 2006). The increased affinity for p75NTR receptors by proneurotrophins is likely due to binding to the p75NTR co-receptor sortilin (Beattie *et al.* 2002; Kalb 2005; Reichardt 2006; Teng *et al.* 2005).

BDNF and cell death

Neurotrophins have been demonstrated to induce cell death (Bamji *et al.* 1998; Beattie *et al.* 2002; Kalb 2005; Lee *et al.* 2001; Teng *et al.* 2005). The cell death promoting role of neurotrophins is due to activation of p75NTR (Bamji *et al.* 1998; Beattie *et al.* 2002; Kalb 2005; Lee *et al.* 2001; Teng *et al.* 2005). However, it was demonstrated in an *in vitro* assay that proBDNF can bind to and activate the TrkB receptor (Fayard *et al.* 2005). Regardless of the ligand-receptor interaction, both proBDNF and proNGF have been shown to induce p75NTR dependent cell-death. ProNGF has been shown to induce p75NTR-dependent apoptosis in smooth muscle cells, sympathetic neurons, and in a pheochromocytoma cell line (Lee *et al.* 2001) *in vitro*. ProNGF stimulates cell death in oligodendrocytes in an *in vivo* model of nerve damage (Beattie *et al.* 2002). Examining the glia in the dying nerve at multiple time points reveals that the oligodendrocytes first up regulate p75NTR and caspase 3 before succumbing to apoptosis (Beattie *et al.* 2002). At a high concentration, BDNF (200 ng/ml; ~4 nM) can induce apoptosis in cultured sympathetic ganglion neurons (Bamji *et al.* 1998). The number of BDNF-induced apoptotic neurons is reduced when BDNF signaling is perturbed with co-application of a function-blocking antiserum or when the stimulated neurons are cultured from p75NTR-null mice (Bamji *et al.* 1998). In a different study, a lower concentration of BDNF (100 ng/ml) did not induce apoptosis in cultured sympathetic ganglion neurons (Teng *et al.* 2005). In this study, a 10-fold lower concentration of proBDNF (10 ng/ml; 0.2 nM) induced apoptosis in a sortilin-

p75NTR receptor complex dependent manner (Teng *et al.* 2005). This same concentration of proBDNF also initiated apoptosis in cultured cerebellar granule neurons, inhibited neurite growth in cultured basal forebrain neurons, and decreased spine density in cultured hippocampal neurons (Koshimizu *et al.* 2009). Crucial to this dissertation is that the mouse OB glomerular interneurons are both p75NTR positive (Cao *et al.* 2007; Imamura and Greer 2009) (Figure 1.5) and prone to sensory deprivation-induced cell death (Kim *et al.* 2006a; Najbauer and Leon 1995). Despite the data cited above, proBDNF has not been demonstrated to induce cell death *in vivo*. The work presented here will test the hypothesis that proBDNF directly alters long-term OB plasticity by facilitating cell death in OB interneurons via the p75NTR.

The loss of sensory afferents (i.e. inputs) has been demonstrated to induce cell death in the brain regions or nuclei receiving these afferents (Biju *et al.* 2008; Bush *et al.* 2008; Leon 1998; Nucci *et al.* 2003; Scholz *et al.* 2005). The type of neuron that will die following sensory deprivation is different across modalities and is tissue specific. Visual (Nucci *et al.* 2003) and auditory (Bush *et al.* 2008) nuclei affected by sensory loss respond by losing relay or projection neurons. Interneurons die following loss of sensory input to the spinal cord dorsal horn (Scholz *et al.* 2005) and to the OB (Biju *et al.* 2008; Kim *et al.* 2006a; Leon 1998). OB interneuron death can be induced by both deafferentation (direct insult to the peripheral neuron) (Kim *et al.* 2006a; Margolis *et al.* 1974) and by sensory deprivation (indirect insult by loss of odorant stimulation) (Biju *et al.* 2008; Brunjes *et al.* 1985; Kelsch *et al.* 2009; Kim *et al.* 2006a; Yamaguchi and Mori 2005). One study has examined these two methods of inducing sensory-dependent cell loss in the mouse OB and demonstrated that each method produced similar results (Kim *et al.* 2006a) in terms of the number of and the phenotype of the neurons that died. Although olfactory sensory deprivation was originally developed as model to study cell death during 'critical periods' in development (Brunjes *et al.* 1985), this model of neuronal insult works well in the adult mouse OB (Baker *et al.* 1993; Hamilton *et al.* 2008; Kelsch *et al.* 2009; Kim *et al.* 2006a; Parrish-Aungst *et al.* 2011; Yamaguchi and Mori 2005). Lastly, not all interneurons die at the same rate in mouse OBs affected by sensory deprivation. OB catecholamine glomerular interneurons have been shown to be particularly sensitive to sensory-deprivation induced cell death as measured by OB dopamine concentrations (Baker *et al.* 1988) and by the number of tyrosine hydroxylase positive interneurons (Kelsch *et al.* 2009; Kim *et al.* 2006a; Yamaguchi and Mori 2005) in the deprived OB relative to control OBs. The exact

mechanism of this cell loss is not yet known. After sensory deprivation granule cells, the other major class of OB interneurons, express the apoptotic enzyme activated-caspase 3 (Yamaguchi and Mori 2005) whereas catecholamine neurons express activated-caspase 3 prior to methamphetamine-induced apoptosis (Deng *et al.* 2007). Chapter 4 examines the localization of BDNF following naris-occlusion in the mouse and Chapter 5 examines activated-caspase 3 and TH following naris-occlusion.

OB plasticity

Neurons in the OB can be broadly classified into two categories: those that project to external sites (output neurons) and those that project to internal sites (interneurons) (Figure 1.5). Mitral cells are the principle output neurons of the mammalian OB (Price and Powell 1970) and receive information about volatile chemicals via synaptic input from OSNs that are located in the nasal epithelium (Schild and Restrepo 1998; Strausfeld and Hildebrand 1999). Mitral cells then transmit this information to the olfactory cortex and other downstream processing centers. Mitral cells express TrkB the high-affinity receptor for BDNF (Imamura and Greer 2009) (Figure 1.5). We have shown that mitral cells respond to BDNF stimulation via TrkB activation (Tucker and Fadool 2002). Activated TrkB is a surface membrane-bound kinase that phosphorylates tyrosine residues within many proteins (Reichardt 2006) including the predominant voltage-gated potassium channel species expressed by mitral cells, the *Shaker*-family member, Kv1.3 (Colley *et al.* 2004). Upon phosphorylation at tyrosine residuesY111-113, Y137, and Y479, Kv1.3 conductance is reduced and the total potassium current is suppressed (Colley *et al.* 2004; Tucker and Fadool 2002). This alters both the electrical properties of, and the information transmitted by, the mitral cell. We have also determined OB BDNF localization following naris-occlusion—a model of neuronal insult where mitral cells become immunoreactive for BDNF and the mitral cells are resistant to cell death (Chapter 4). In contrast, interneurons, the other class of OB neurons, have a dramatic loss of BDNF immunoreactivity and are susceptible to cell death (Chapter 4). Many of these cell-death prone interneurons express the other, low-affinity, BDNF receptor, p75NTR (Imamura and Greer 2009). We have also discovered that the mouse OB has undetectable levels of mature BDNF and that BDNF immunoreactivity in the mouse OB appears to be proBDNF (Chapter 4). Lastly, proBDNF has been shown to induce cell death in neurons by binding to and activating p75NTR

(Teng *et al.* 2005). Thus, proBDNF may act as a pro-life signal to TrkB-positive mitral cells and as a pro-death signal to p75NTR-positive interneurons in the mouse OB.

Experiments conducted in Chapter 5 directly measure the actions of BDNF isoforms on OB neurons. The resultant data will be used to clarify the role of the proBDNF isoform as a putative pro-death signal and the role of the mature BDNF isoform as a pro-survival signal. Only the pro-survival isoform, mature BDNF, is a modulator of short-term plasticity in the brain, even though both isoforms have been found in the extracellular space and are thus available as neurotrophin receptor ligands. The two aims of this chapter provide valuable, novel data that can explain the complicated processes of how BDNF affects cell-to-cell communication and cell survival.

Mitral cell electrical properties and the *Shaker* channel family member Kv1.3

Voltage-gated potassium channels (Kv) comprise a family of channels that are crucial for action potential generation and membrane potential (Bean 2007; Chandy and Gutman 1993). The Kv family member important to this proposal is a member of the *Shaker* family. The founding gene of the *Shaker* family was discovered following behavioral screens of mutated *drosophila* strain, Sh (Catsch 1948). These flies had a mutation on the X chromosome that induced erratic leg and wing twitches during ether anesthesia. Further descriptions of the mutant Sh flies (Kaplan and Trout 1969) indicated a family of genes. The Sh gene was described as a Kv channel crucial for neuromuscular junction function (Jan and Jan 1997; Jan *et al.* 1977). In all neurons, Kv channels regulate action potential firing (Balu *et al.* 2004; Bean 2007; Chen and Shepherd 1997; Misonou and Trimmer 2004).

The Kv channel studied during the completion of this dissertation was Kv1.3. Kv1.3 is expressed in the OB projection neurons, the mitral cells, where it is responsible for 60-80% of the potassium current (Fadool and Levitan 1998; Kues and Wunder 1992; Veh *et al.* 1995). Electrically-excited mitral cells demonstrate sub-threshold oscillations that involve the slow inactivating potassium current (Balu *et al.* 2004; Chen and Shepherd 1997). The slow inactivating potassium current I_D is associated with Kv1.3 (Balu *et al.* 2004; Bean 2007; Fadool and Levitan 1998). Blocking the I_D in electrically stimulated mitral cells reduces the latency to first action potential and lengthens the 'burst' duration (i.e. discreet periods of high frequency activity interspersed among periods of low frequency activity) of action potentials (Balu *et al.* 2004). Kv1.3 is important in the timing, rate, and patterning of mitral cell action potentials and

is thus important in the output of the OB to higher brain centers. Altering this output to higher brain centers can alter the way the brain senses and perceives an olfactory stimulus.

BDNF, Kv1.3 and olfaction

Kv1.3 current is important for sensing and perceiving an olfactory stimulus. Mice can associate an arbitrary scent with a food reward and will dig through bedding material 'spiked' with this scent in search of the food award. Kv1.3-null mice trained in such a paradigm can detect an odor at dilutions 1-to-3-orders of magnitude lower when compared to similarly trained wild-type mice (Fadool *et al.* 2004). Kv1.3-null mice are also better at finding a hidden, novel food item and are able to discriminate between two alcohols that differ only by a single carbon atom (Fadool *et al.* 2004). These results indicate that inhibiting the Kv1.3 current improves mouse olfactory ability.

Kv1.3 current is inhibited by activated receptor tyrosine kinases, such as TrkB kinase and insulin receptor kinase, which can alter animal behavior. When Kv1.3 tyrosine residues are phosphorylated by the insulin receptor this reduces the peak evoked current by 25-45% (Colley *et al.* 2004; Fadool and Levitan 1998; Fadool *et al.* 2000). When the BDNF-activated TrkB receptor phosphorylates Kv1.3 tyrosine residues, the evoked potassium current is reduced by ~35% (Colley *et al.* 2004; Tucker and Fadool 2002). Genetic deletion of Kv1.3 eliminates BDNF- and insulin-evoked suppression of voltage-dependent potassium currents in mitral cells (Fadool *et al.* 2004). Topical application of BDNF (Tucker and Fadool 2002) to intact OB tissue or intranasally delivered insulin (Marks *et al.* 2009) to the mouse OB *in vivo* causes Kv1.3 channels tyrosine phosphorylation. Chronic application of insulin to the OB *in vivo* by intranasal delivery (IND) results in phosphorylated Kv1.3 and altered olfactory discrimination by awake, behaving mice (Marks *et al.* 2009). It is not known if IND application of proBDNF can induce interneuron cell death in a manner similar to that of sensory deprivation.

OB experimental focus

The goals of Chapters 4 and 5 in this dissertation were to test the hypothesis that BDNF alters mouse OB plasticity by acting in both a short- and a long-term manner on two different neuronal populations as defined by neurotrophin receptor expression. The short-term effects of BDNF on mouse olfactory plasticity are mediated by the TrkB receptor that is expressed by the mitral cells and can be measured by changes in electrical excitability. Conversely, the long-term

effects of BDNF on mouse OB plasticity are mediated by the p75NTR expressed by interneurons located in the external plexiform layer and can be measured by changes in cell survival following loss of synaptic input or exposure to proBDNF. Chapter 5 presents the first *in vivo* data on the action of BDNF and proBDNF on easily identifiable, central nervous system neuronal populations that express either p75NTR or TrkB, but not both. Since mitral cells lack spines (Price and Powell 1970) these results will be interesting to compare to the work done on spiny neurons in the hippocampus (Chapleau *et al.* 2009; Pang *et al.* 2004; Woo *et al.* 2005). In the hippocampus, BDNF facilitates synaptic strengthening (Chapleau *et al.* 2009; Pang *et al.* 2004) and proBDNF facilitates synaptic weakening (Woo *et al.* 2005).

CHAPTER TWO

THE TRPC2 CHANNEL FORMS PROTEIN-PROTEIN INTERACTIONS WITH HOMER AND RTP IN THE RAT VOMERONASAL ORGAN[1]

Introduction

The mammalian accessory olfactory system (AOS) functions as a detector for chemical signals (chemosignals) concerning social organization and conspecific reproductive status (Halpern and Martinez-Marcos 2003; Meredith *et al.* 1980). The vomeronasal organ (VNO) is the primary sensory organ for the AOS. In rodents, the VNO is an encapsulated neuroepithelium containing a lumen and is able to aspirate fluids via a vascular pump (Meredith and O'Connell 1979; Vaccarezza *et al.* 1981). Vomeronasal sensory neurons (VSN) express vomeronasal receptors (VRs) belonging to one of the two families of G-protein coupled receptors (GPCRs) specific to the VNO, the V1Rs and V2Rs (Dulac and Axel 1995; Matsunami and Buck 1997; Ryba and Tirindelli 1997). Upon binding of a chemosignal, V1Rs and V2Rs activate the G-proteins, $G\alpha_{i2}$ and $G\alpha_{o}$, respectively (Halpern and Martinez-Marcos 2003). G-protein activation can ultimately result in a non-specific cation current through the canonical transient receptor potential channel type 2 (TRPC2) (Liman *et al.* 1999; Lucas *et al.* 2003; Vannier *et al.* 1999).

VNO function is dependent upon TRPC2 (Kimchi *et al.* 2007; Leypold *et al.* 2002; Stowers *et al.* 2002). Adaptor proteins scaffold TRPC to proteins such as inositol 1,4,5-trisphosphate receptor type 3 (IP_3R_3) (Brann and Fadool 2006; Kim *et al.* 2006b; Yuan *et al.* 2003). In the invertebrate retina TRP is in a scaffold-mediated complex whereby deletion of the scaffold leads to complex degradation and altered light responses (Huber 2001). The TRP channel and IP_3 receptor are co-localized in VSN microvilli (Brann *et al.* 2002) whereby peptide disruption of the protein-protein interaction between them inhibits chemosignal-induced currents (Brann and Fadool 2006).

[1] Portions of this chapter were duplicated from the original article Mast TG, Brann JH, Fadool DA. (2010) The TRPC2 channel forms protein-proteininteractions with Homer and RTP in the rat vomeronasal organ. BMC Neurosci. 11:61. The authors retain copyright.

Homers are adaptor proteins that bind to proline-rich sequences on proteins associated with calcium signalling (Worley *et al.* 2007a). Long Homer isoforms (1b/c, 2a/b, 3) contain, whereby the immediate-early gene encoded short isoform (1a) lacks, a coiled-coil motif that mediates multimerization (Brakeman *et al.* 1997; Worley *et al.* 2007a). Homers alter the function and distribution of metabotropic glutamate receptors (mGluRs) (Brakeman *et al.* 1997; Kammermeier and Worley 2007; Xiao *et al.* 1998).

TRPC2 clones have poor surface expression *in vitro* and may require a chaperone for proper formation (Hofmann *et al.* 2000; Jungnickel *et al.* 2001). Receptor transporting protein 1 (RTP1) and receptor expression enhancing protein 1 (REEP1) are putative transmembrane protein chaperones expressed in the main olfactory system, which target olfactory GPCRs to the membrane and form protein-protein interactions with olfactory GPCRs *in vitro* (Saito *et al.* 2004). RTP1 and REEP1 mRNAs are expressed in the mouse VNO, but as of yet, neither protein has been reported in VSNs, and have not been proposed to have any functional interactions with vomeronasal GPCRs (Saito *et al.* 2004).

Given the role of TRPC2 in chemosignal detection, the interactions of TRPC2 with adaptor proteins in other sensory systems, and chaperone mRNA expression in the VNO, we sought to test the hypothesis that TRPC2 forms protein-protein associations with partners that could alter channel function or localization. Specifically, we sought to identify interactions between TRPC2 and Homer family members and interactions between TRPC2 and RTP1 or REEP1. First, we demonstrate VNO protein expression of RTP1, Homer, and TRPC2. Next we describe novel, *in vivo,* interactions between TRPC2 and Homer 1b/c as well as TRPC2 and RTP1. Lastly, we demonstrate a physiological role for the interaction between RTP1 and TRPC2; *in vitro* co-expression of RTP1 with TRPC2 leads to increased cell-surface expression of functional TRPC2.

Materials and Methods

Animal care and maintenance

Postnatal Day 30 (P30) Sprague-Dawley rats were used for biochemistry experiments and were housed on a 12h:12h light:dark cycle in the Florida State University (FSU) vivarium. All procedures were performed in accordance with the FSU Animal Care and Use Committee and NIH-approved guidelines.

Solutions

Solutions used for protein sample or tissue preparation, including phosphate buffered saline (PBS), lysis buffer (LB), wash buffer (WB), and protease and phosphatase inhibitor solution (PPI), were made as described in (Colley *et al.* 2007). Tissue extract buffer (TEB) was prepared as in (Xiao *et al.* 1998). Cell-surface biotinylation solutions, including biotinylation lysis buffer and biotinylation quench buffer, were made as described by (Fu *et al.* 2006). Immunoblot stripping buffers, including tris stripping buffer (TSB) and sodium citrate stripping buffer (SCSB), were also made as described in Colley *et. al.* (2007). Electrophysiology solutions were prepared as in (Jungnickel *et al.* 2001) and were as follows (in mM): intracellular pipette 150 KCl, 10 HEPES pH 7.2, 2 $MgCl_2$, 10 glucose; extracellular bath 140 $NaCl_2$, 10 HEPES pH 7.4, 4 KCl, 4 $CaCl_2$, 1 $MgCl_2$, and 10 glucose. All chemicals were obtained from either Sigma Chemical Company (St. Louis, MO, USA) or Fisher Scientific (Suwanne, GA, USA).

Plasmids and antibodies

All encoded cDNAs were downstream from a cytomegalovirus (CMV) promoter. TRPC2 clone 14, with an N-terminal myc-epitope (EQKLISEEDL), was prepared in the $pcDNA_3$ vector and was a kind gift from Dr. L Birnbaumer (National Institute of Environmental Health Sciences) (Vannier *et al.* 1999). RTP1 and REEP1were in the pCI vector and were kind gifts of Dr. H. Matsunami (Duke University) (Saito *et al.* 2004). pCDM8 was a kind gift from Dr. Brian Seed (Harvard University) (Jurman *et al.* 1994). DNA encoding human CD8 was amplified from pCDM8 and subcloned into the $pcDNA_3$ vector (Carlsbad, CA, Invitrogen) between the BamH1 and EcoR1 restriction sites. cDNA encoding Kv1.3 was subcloned into the $pcDNA_3$ vector (Carlsbad, CA, Invitrogen) at the unique HindIII restriction site within the multiple cloning region (Fadool *et al.* 1997). Kv1.3 was also epitope-tagged via insertion of the myc sequence on the extracellular face of the channel between the S1and S2 transmembrane domains (Colley *et al.* 2007).

T1NH, T2NH, and T3NH are anti-peptide polyclonal antibodies specific for the type-1, -2 and -3 IP_3R isoforms, respectively, and were raised against the following amino terminal sequences (amino acid position in parentheses): T1NH = CLATGHYLAAEVDPDQEVDPDQ-DASR (308–326), T2NH = CPDYRDAQNEGKTVRDGKTVRDGELP (320–338) and T3NH = CENPSYKGDVSDPGDVSDPKAAGPGA (319–337). These antibodies were a generous gift of

Dr Gregory Mignery (Loyola University Chicago, Stritch College of Medicine, Maywood, IL, USA) (Ramos-Franco *et al.* 1998). An antiserum detecting TRPC2 as raised in guinea pig and directed against the N-terminal cytosolic domain CSSDASGAGPGGPLRNVE was a generous gift of Dr. Richard Axel (Columbia University, New York, NY, USA) (Leypold *et al.* 2002). Anti-peptide polyclonal antibodies detecting the different forms of Homer were made by immunizing rabbits with the synthetic C-terminal peptides of Homer 1b/c (IFELTELRDNLAKLLECS), 2a/b (GKIDDLHDFRRGLSKLGTDN), or 3 (RLFELSELRE-GLARLAEAA) conjugated to thyroglobulin with glutaraldehyde (Xiao *et al.* 1998). A fourth, rabbit polyclonal antiserum recognizing all Homer 1 (1a, 1b, and 1c) isoforms was generated against the full-length GST-Homer 1a fusion protein (Brakeman *et al.* 1997). These antibodies were a generous gift of Dr. Paul Worley (Johns Hopkins University, Baltimore, MD, USA). A polyclonal antibody recognizing all Homer proteins (Pan-Homer; 1a, 1b, 1c, 2a, 2b, 3) was made by immunizing rats with recombinant Homer 1a (AB5875, Chemicon/Millipore, St. Louis, MO, USA). The mouse monoclonal antiserum for the c-myc epitope was from Roche (Indianapolis, IN, USA). Rabbit polyclonal antiserum specific to RTP1 was a kind gift of Dr. Hiro Matsunami (Duke University, Durham, NC, USA) (Zhuang and Matsunami 2007). When necessary to validate equal protein loading, a rabbit polyclonal antibody detecting cellular actin was used. The immunogen for this antibody was SGPSIVHRKCF attached to a Multiple Antigen Peptide (MAP) backbone (Sigma Chemical).

Tissue homogenization and Western blotting

Tissue extracts were prepared as in (Xiao *et al.* 1998). Briefly, P30 rats were killed by CO_2 inhalation, decapitated, and VNOs were rapidly dissected and placed in ice cold TEB with PPI. Samples on ice were sonicated (Sonic Dismembrator, Model 60, Fisher Scientific) twice for eight seconds on setting number five. Non-soluble matter was removed by ultracentrifugation (Beckman Coulter, Fullerton, CA, USA) at 37,000 x *g* for 30 min at 4°C. The supernatants were aliquoted and stored at –80°C until use. The pellets were solubilized in 2% sodium dodecyl sulfate (SDS), aliquoted, and stored at –80°C in case the initial screening of the lysates did not yield results.

Immunoprecipitations were performed as in (Brann *et al.* 2002). In brief, P30 rat VNOs were homogenized with a size 20 Kontes glass tissue-homogenizer (Kontes Glass, Vineland, NJ,

USA) on ice in LB with PPI. Lysis was continued on a Roto-Torque (Model 7637, Cole-Parmer Instruments, Vernon Hills, IL, USA) for 30 min at 4°C. Lysates were clarified by centrifugation at 15,000 x g (Eppendorf, Model 5415C, Westbury, NY, USA) for 10 min at 4°C and then precleared for 1 hour (hr) with 3 mg/ml protein A sepharose (GE Healthcare, Uppsalla). This was followed by another centrifugation step to remove the protein A sepharose. Proteins of interest (Homer 1b/c, Homer 2, Homer 3, TRPC2, IP_3R_3, RTP1) were immunoprecipitated from the clarified lysates by overnight incubation on a Roto-Torque at 4°C with 5 μg/ml of appropriate antiserum. Samples were then incubated for 3 hr with protein A sepharose and centrifuged as above. Immunoprecipitates were washed four times with WB. Lysates and washed immunoprecipitates were diluted in SDS gel loading buffer containing (Sambrook *et al.* 1989) 1 mM Na_3VO_4 and stored at –20°C until use.

Purified VNO tissue extracts or immunoprecipitated proteins were separated on 6 to 15% acrylamide gels by SDS-PAGE and electro-transferred to nitrocellulose membranes. Equal protein loading (30 μg) was controlled by Bradford protein assay (BioRad, Hercules, CA, USA) and confirmed by 0.1% Fast Green staining and α-β-actin labeling. The nitrocellulose membrane was blocked with 5% non-fat milk for 60 min, incubated overnight at 4°C in primary antisera against TRPC2 (1:2000), IP_3R_3 (1:2000), RTP1 (1:1000), Homer 1b/c (1:1000), Homer 2a/b (1:2000), Homer 3 (1:2000), Homer 1 isoforms (Worley, 1:1000), all Homer isoforms (Chemicon, 1:1000), or RTP1 (1:1000). Membranes were then incubated with horseradish peroxidase-conjugated species-specific secondary antibody (donkey anti-rabbit, Amersham Biosciences or rabbit anti-guinea pig, Sigma) for 90 min at room temperature (rt). Labeled protein was detected with enhanced chemiluminescence (ECL; Amersham Biosciences, Piscataway, NJ, USA) using Classic Blue autoradiography film BX (MidSci, St. Louis, MO, USA). To ensure equal loading, nitrocellulose membranes were stripped by incubating blots in eight ten-minute washes of TSB, followed by eight ten-minute washes of SCSB, then re-probed using α-β-actin (1:1000). Autoradiographs were scanned using a Hewlett-Packard Photosmart Scanner (Model 106-816; Hewlett-Packard, San Diego, CA, USA) and quantified by line scanning densitometry using Quantiscan Software (Biosoft, Cambridge, UK).

RNA extraction and reverse-transcriptase PCR

P30 rats were killed by CO_2 inhalation, decapitated, and VNOs were rapidly dissected and placed on dry ice. RNA was extracted using the SV Total RNA Isolation System as per the manufacturer's protocol (Promega, Madison, WI, USA). RNA purity and concentration was determined by UV spectroscopy (NanoDrop-1000, Wilmington, DE, USA). cDNA was reverse-transcribed using the ImPromII kit as per manufacturer's protocol (Promega). Gene-specific primers have been previously reported (Behrens *et al.* 2006) and were as follows: RTP1_forward, AAGCGTGACCACAGATGAGTG; RTP1_reverse, GAGCAGAAGTTCCAGCCTGAG; REEP1_forward, CAATGAATTCCCACCATGGTGTCATGGATCATCTCCAGGC; REEP1_reverse, GACTAGCGGCCGCCTAGGCGGTGCCTGAGCTGCTAG. PCR products were resolved using 1.0% agarose gel electrophoresis and visualized via UV excitation of the incorporated ethidium bromide.

Human embryonic kidney cell (HEK293) maintenance and transfection

HEK 293 cells were maintained in minimum essential medium (MEM), 2% penicillin/streptomycin, and 10% FBS (Gibco BRL). Before transfection, cells were grown to confluence (~7 days), dissociated with trypsin, and re-plated to low density onto Corning substrate-coated plasticware on poly-d-lysine-treated glass coverslips as previously described (Fadool *et al.* 1997). HEK293 cells were transfected for 4-5 hrs at 37ºC with plasmid cDNA and LipofectamineTM transfection reagent (Invitrogen, Carlsbad, CA, USA) in OptiMEM serum-reduced media (Gibco BRL). Either 1.5 µg of plasmid DNA and 7.5 µl Lipofectamine were applied to 30-50% confluent glass coverslips in 35 mm dishes or 3.0 µg of plasmid DNA and 15 µl Lipofectamine were applied to 80-95% confluent 60 mm dishes, for immunocytochemical and biochemical experiments, respectively. $pcDNA_3$ vector was used to normalize total DNA concentration in co-transfection conditions, as previously (Cook and Fadool 2002).

Immunocytochemistry

Thirty-six hrs post-transfection, HEK293 cells were washed in PBS and fixed in ice-cold St. Marie's fixative (1.0% acetic acid in 95% ethanol). Cells were washed three times in PBS and incubated for 30 min at rt in PBST-block (0.1% Triton x-100 in PBS and 1% Bovine Serum Albumin). Cells were immunolabeled with primary antisera diluted in PBST-block for 90 min at

rt or overnight at 4ºC with α-c-myc. To determine that the RTP1 carboxyl-terminus is located on the extracelluar face of the HEK cell surface membrane, transfected cells were first incubated with either 200 μg/μl proteinase K or PBS and immunolabled with αRTP1 without any detergents (Manganas and Trimmer 2000). Cells were then washed three times in PBS. The secondary antisera were applied at rt for 1.5 hr in PBS using fluorescein isothiocyanate-conjugated goat anti-mouse antiserum (1:200). Following three washes in PBS, cells were counter-stained with a five-minute incubation in diamidino-phenyindole (DAPI) in PBS (1:5000). The cells were mounted on glass slides with Vectashield (Vector Laboratories, Burlingame, CA, USA) to prevent photobleaching.

Tissue sections (~16 μm) were prepared from P30 rats that had been fixed-perfused (4% paraformaldehyde) and sucrose cryoprotected as previously described (Brann *et al.* 2002). Sections were air-dried on the bench for 60 minutes, re-hydrated with PBS, and then incubated at 80ºC in 10 mM sodium citrate for 30 minutes for antigen retrieval (Jiao *et al.* 1999). The sections were cooled and non-specific binding was blocked by a 60-minute incubation in blocking solution (5% normal goat serum/ 2.5% BSA/ 0.3% triton in PBS). During the block, the primary antibodies were treated with L-glutathione to cap reactive SH-functional groups. On ice, an L-glutathione/ Tris-EDTA solution was diluted in the blocking solution containing the primary antiserum to a final concentration of 30 mM L-glutathione Tris-EDTA / 1.25% normal goat serum/ 0.625% BSA/ 0.075% triton (Rogers *et al.* 2006). After the block, sections were rinsed with Tris-EDTA - 0.3% triton and incubated with antiserum overnight in a darkened, humidified chamber. Antiserum for RTP1 was used at a final dilution of 1:200 and antisera for TRPC2 was used at 1:400. Sections to be stained using the ABC method were treated according to the manufacturer's protocol (Vector, Burlingham, CA, USA) and the precipitate was visualized with the chromagen AEC (Sigma). Immunofluorescence was detected with either donkey anti-rabbit Texas Red (Amersham Biosciences) or rabbit anti-guinea pig FITC (Sigma).

Microscopy

Conventional light microscopy was performed on an Axiovert S-100 (Zeiss, Thornwood, NY, USA) equipped with epifluoresence, an AxioCam camera (#412-312, Zeiss), and Axiovision data capture software (version 3.1, Zeiss). Images were captured with a pixel resolution of 1300 x 1030. Laser confocal microscopy was performed on an Axioplan 2

microscope attached to an LSM510 two-confocal system (Zeiss). FITC was excited at 488 and DAPI at 700 nm with argon/2 and titanium/ sapphire lasers, respectively. Images were captured at 1024 × 1024 pixels resolution in LSM file format, and then were converted to a 16-bit TIFF file format using LsMB software (Zeiss). The TIFF file was opened in NIH ImageJ (http://rsb.info.nih.gov/ij/) and a uniform rectangle of 200 pixels × 20 pixels was applied across the center of the cell (Z-axis) to obtain the plot density profile of the pixels underneath as previously described (Marks and Fadool 2007).

Transfection efficiency analysis

Three to nine fields of view for each transfection condition (TRPC2 + $pcDNA_3$, TRPC2 + RTP1, TRPC2 + REEP1, and Kv1.3 + $pcDNA_3$) were captured under a fluorescent and either a brightfield or a DAPI emission. Each field of view was approximately 90,000 μm^2. Transfection efficiency was calculated for each field of view as the ratio of the number of fluorescent cells divided by the total number of cells. Cell counts were performed using NIH ImageJ software.

Cell-surface biotinylation

Cell-surface biotinylation was performed as described (Fu *et al.* 2006). Briefly, either 24- or 48-hr post-transfection, HEK293 cells were washed with ice-cold PBS and then incubated with 1.0 mg/ml biotin (Pierce, Rockford, Ill, USA) in PBS for 30 min at 4ºC. Following a PBS rinse, cells were incubated for 30 min at 4ºC in quench buffer, rinsed again, and then lysed for 30 min at 4ºC in lysis buffer. Lysed cells were scraped, triturated, and centrifuged at 12,000 rpm for 10 min at 4ºC. The supernatants were collected and aliquots were set aside for confluency controls. Protein concentration was calculated using a Bradford assay (BioRad). Equal amounts of protein were brought up to 1 ml with PBS (pH 8.0) and incubated overnight at 4ºC with 40 µl streptavidin-conjugated agarose-beads (Pierce). The beads were pelleted with a centrifugation of 12,000 rpm for 10 min at 4ºC, washed, and then stored at -20ºC until further use.

Whole-cell electrophysiology

Hoffman modulation contrast optics was used to visualize cells at 40× magnification (Axiovert 135, Carl Zeiss). Thirty-six hrs post-transfection, HEK293 cells were rinsed with bath solution and incubated with anti-hCD8 beads (Dyna-Beads, Invitrogen) to mark transfected cells

(either hCD8+/TRPC2+/RTP1- or hCD8+/TRPC2+/RTP1+) (Jurman *et al.* 1994). Co-expression with CD8 allows visualization of cells taking up the cDNA encoding the channel or receptor of interest by marking transfected cells with a red polypropylene-antibody-linked bead. We (Cook and Fadool 2002) and others (Jurman *et al.* 1994) have demonstrated that single cells take up multiple constructs equivalently and that the density of the beads is proportional to the expression of channel of interest. Cells were rinsed two times before beginning a recording session to remove any unbound beads. Cells were rinsed two more times before beginning a recording session. Electrophysiological records were analyzed using software from Microcal Origin (Northampton, MA) and Quattro Pro (Borland International, Scotts Valley, CA).

Patch electrodes were fabricated from Jencons glass (Jencons Limited, Bridgeville, PA) with pipette resistances between 9 and 14 MΩ. Macroscopic currents were recorded in the whole-cell configuration using an Axopatch-200B amplifier (MDS Analytical Technologies/Axon Instruments, Sunnyvale, CA), filtered at 5 kHz, digitized at 5 kHz, and stored for later analysis. All voltage signals were generated and data were acquired with the use of an Axon Digidata 1200 board with pClamp v9.2 software (Axon Instruments). Cells were held routinely at a holding potential (V_h) of -60 mV, stepped to 80 mV (V_c), held for 40 milliseconds (ms), and then changed to a ramp protocol by falling to -80 mV over 100 ms (-1.6 mV/ ms). The total pulse duration was 140 ms and the inter pulse interval was 60 seconds. Several sweeps were taken over the 3-6 minutes after establishing the whole-cell configuration to establish a stable baseline. ATP stimulation was achieved with bath application of 0.5 ml of 500 μM for a final bath concentration of ~166 mM ATP. Peak inward current amplitude was measured at -80 mV from a subsequent sweep.

Data analysis

Numerical data were statistically analyzed using Prizm software (version 4, GraphPad, San Diego, CA, USA). One-way Analysis of Variance (ANOVA) with either a Student-Newman-Keuls (*snk*) or a Dunnett's post-hoc test was performed with statistical significance determined at the 95% confidence interval.

Results

Homer, RTP1, and REEP1 are Expressed in the Vomeronasal Organ

TRPC2 forms a protein-protein interaction with IP_3R_3 in rat VSNs (Brann *et al.* 2002) and a peptide blocker of this interaction functionally reduces odor-activated currents (Brann and Fadool 2006). We therefore questioned whether adaptor proteins might moderate the scaffold complex. Rat VNO tissue was screened with an antiserum that recognized all homer isoforms (Pan-Homer). Pan-Homer antiserum was observed to label proteins at the predicted molecular weight via SDS-PAGE followed by Western analysis on NP40-solubilized tissue extracts from the hippocampus (H), cerebellum (Ce), cerebral hemisphere (CH), olfactory bulb (OB), and vomeronasal organ (VNO) (Figure 2.1A). Only long forms (M_r = 45 kDa) were detected using the pan-Homer antiserum, presumably because the short form of Homer (H1a) is a transient product of an activity-dependent immediate early gene (Brakeman *et al.* 1997), making detection difficult. The commercial pan-Homer antiserum, and not the investigator-generated antisera (Figure 2.1 B-E) (see Methods), produced a non-selective band at 45 kDa, and therefore was not utilized in subsequent biochemical analyses.

Isoform-specific antisera were then utilized to further probe which Homer isoforms were predominantly found in the VNO. Homer 1b/c and Homer 3 were expressed in all neural tissues tested including the OB and the VNO (Figure 2.1B and 2.1E). Repetition of SDS-PAGE and Western analysis using the same tissue extracts as in Figure 2.1B resulted in no immunoreactive labelling with preimmune serum used to generate the homer 1b/c antiserum (Figure 2.1C). Homer 2 was weakly detected in the VNO, but was found in the OB, as well as other brain regions tested (Figure 2.1D). In our previous studies we have noted sexual dimorphism in the VNO (Fadool *et al.* 2001; Murphy *et al.* 2001), therefore, male and female VNO lysates were separately probed with Homer antisera. An appreciable sex difference was not consistently detected (Figure 2.1A- 2.1E). Equal protein loading was confirmed for all Western blots by stripping the blot and then re-probing for actin immunoreactivity (see Figure 2.3A).

RTP1 and REEP1 mRNAs have only been demonstrated in the mouse (Saito *et al.* 2004), therefore rat VNO cDNA was screened using gene-specific primers and reverse-transcriptase PCR (RT-PCR) for chaperone expression. RTP1 and REEP1 expression in the rat VNO is

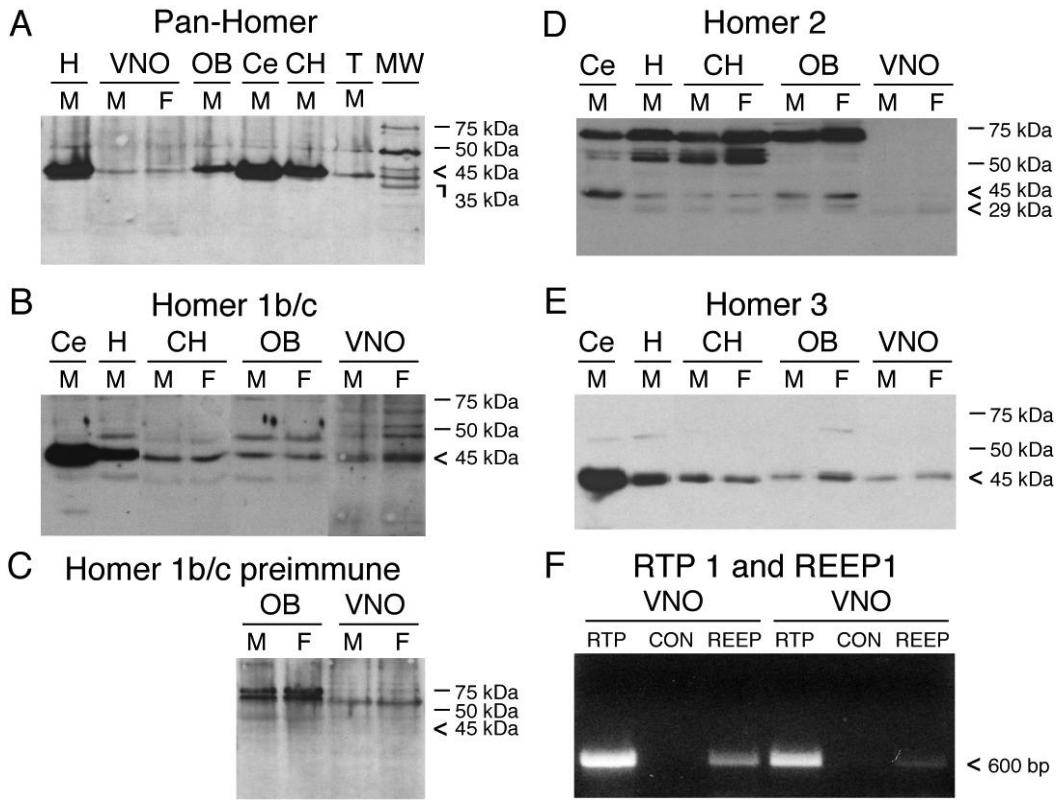

Figure 2.1 Adaptor protein expression in the rat vomeronasal organ. (VNO). (A-E) Representative Western blots of NP40-solubilized proteins incubated with Homer family antisera as labeled. Proteins were separated by SDS-PAGE and then electro-transferred to nitrocellulose as described in the text. Expected M r= 45/47, 29 kDa. Abbreviations: H = hippocampus, OB = olfactory bulb, Ce = cerebellum, CH = cerebral hemispheres, T = testis, M = male, F = female. Representative of 3-4 individual preparations for each antiserum. (F) Two representative trials of RT-PCR products specific for RTP1 (RTP) and REEP1 (REEP), respectively. The expected PCR products were 597 bp (RTP1) and 623 bp (REEP1). CON = no reverse transcriptase negative control.

reported in Figure 2.1F. Each RT-PCR reaction produced a single band and the identity of the band was confirmed by sequencing.

Since RTP1 cellular localization has not been previously explored in the olfactory system, the determination of the cells or cellular processes that express RTP1 was made using immunoctyochemistry (ICC). Coronal sections of the rat nasal cavity containing both the vomeronasal and the main olfactory epithelium (MOE) were incubated with an antiserum for RTP1 (Figure 2.2). Using an avidin-peroxidase chromagen method, RTP1 immunoreactivity was evident in the rat MOE cilia (osn; Figure 2.2B), VNO microvilli (vsn; Figure 2.2B), goblet cells (gob; Figure 2.2B), and the soft palate (sp; Figure 2.2B). Higher resolution micrographs of the MOE cilia and VNO microvilli can be seen in Figure 2.2C and 2.2E, respectively. RTP1 immunoreactivity was absent from all other structures including the respiratory epithelium (res; Figure 2.2D) and from the VNO microvilli that were processed without primary antiserum (Figure 2.2F). To determine whether the labeling of RTP1 might overlap with previous TRPC2 microvillar localization reported by our laboratory and others (Brann *et al.* 2002; Liman *et al.* 1999) we used dual-colored ICC with fluorescently-tagged secondary antisera to test for co-localization of TRPC2 and RTP1. As shown in Figures 2.2G-I, the signals for the two proteins extensively overlap at the microvilli (m) as evidenced in the merged image overlay (Figure 2.2I). Omission of primary antisera eliminated the fluorescent signal in each condition tested (Figures 2.2J-L). To control for RTP1 antiserum specificity human embryonic kidney 293 (HEK293) cells were transfected with an RTP1 expression vector and then processed in non- permeablizing conditions for RTP1 immunoreactivity. Pre-incubating the cells with proteinase K abolished the RTP1 immunoreactivity (Figure 2.3B, C). Additionally RTP1 immunodetection was present across development in the mouse main olfactory epithelium (Figure 2.3A) and absent when the primary antiserum was removed from immunoprecipitation experiments (Figure 2.3D).

Homer and RTP1 form protein-protein interaction with TRPC2

Previous *in vitro* data have demonstrated that TRPC2 and Homer 1 form a protein-protein interaction (Yuan *et al.* 2003). Our discovered co-localization of TRPC2 and RTP1 suggests that these proteins may also bind *in vivo*. To test the rigor of potential protein-protein interactions, reciprocal co-immunoprecipitations were performed in native rat VNO lysates (Figure 2.4). TRPC2 was clearly immunoprecipitated with both Homer 1b/c (Figures 2.4C and 2.4D) and RTP1 (Figures 2.4E and 2.4F). Interestingly, Homer 1b/c could co-immunoprecipitate

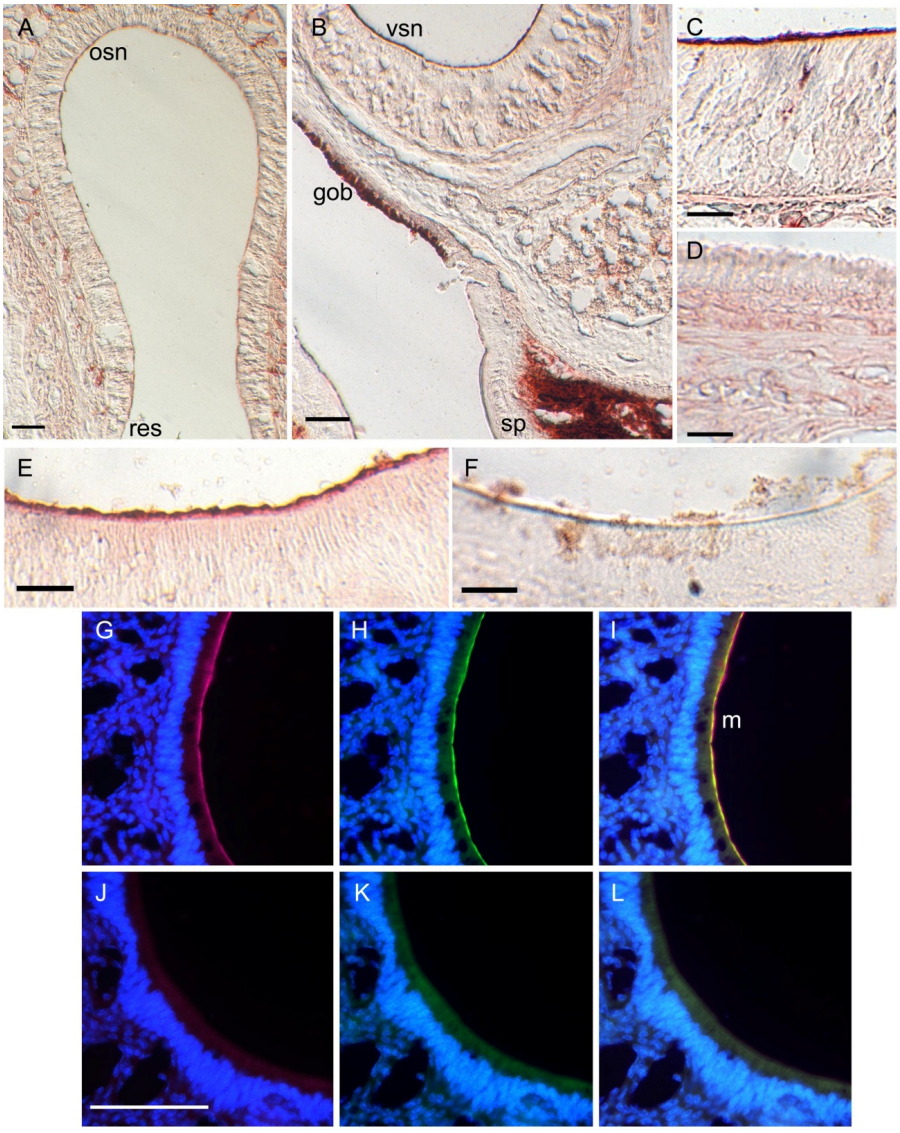

Figure 2.2 TRPC2/ RTP1 co-localization in the rat nasal cavity. Coronal sections were processed for αRTP1 immunocytochemistry using an avidin-peroxidase chromagen method (A-F) or dual-colored immunocytochemistry with fluorescent secondary antisera (G-L). Low-power magnification of the (A) main olfactory epithelium (MOE) and (B) vomeronasal epithelium. osn = olfactory sensory neuron, res = respiratory epithelium, vsn = vomeronasal sensory neuron, gob = goblet cells, sp = soft palate. Higher-power magnification reveals αRTP1 labeling in the cilia layer of the MOE (inset C) and microvilli layer of the VNO (inset E) but absence of label in the respiratory cilia (inset D). Control VNO section with primary antiserum omitted (F). Higher-power magnification of the VNO (G-L), αRTP1 (G), αTRPC2 (H), merged image (I). Control sequential sections to that of G-I with omission of the primary antisera (J-L). Scale bar = 25 μm (C-F) or 100 μm (A, B, G-L). Scale bar in J is the same for G-L. Italicized lettering in boxes is linked to enlarged image sub-panel. m = microvillar layer.

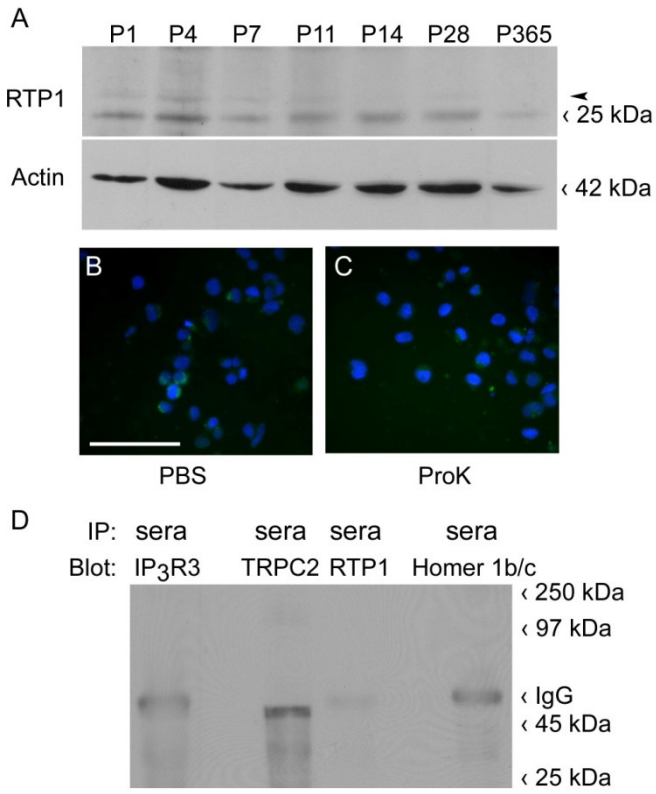

Figure 2.3 RTP1 Antiserum Characterization. (A) NP40 solubilized samples of mouse main olfactory epithelia, collected at noted postnatal (P) stages, were separated by SDS-PAGE and electro-transferred to nitrocellulose. RTP1 antiserum recognized the appropriate band (expected M_r = 25 kDa). The faint band at the arrowhead may be an RTP1 variant described previously (Zhuang and Matsunami 2007). The top blot probed for the RTP1 chaperone (RTP1) was stripped and reprobed for β-actin (actin)(M_r = 42 kDa). (B-C) HEK293 cells transfected with the RTP1 expression vector. 36 hrs following the transfection were incubated at 37° with either PBS (B) or 200 µg/µl proteinase K (C), were immunolabled with αRTP1 without any detergents, and processed for RTP1 immunoreactivity. Note the loss of RTP1 immunoreactivity in C. (D) VNO lysates were used in immunoprecipitation experiments as in Figure 2.4, except a non-immune rabbit sera was used as the source of the first immunoglobulin. Note the loss of bands at the expected M_r for TRPC2 97, IP_3R3 >220, Homer 1b/c 45, and RTP1 25 kDa as indicated. IgG = the heavy chain of the immunoglobin G.

with both $IP3R_3$ (Figure 2.4A and 2.4B) and TRPC2. Protein-interactions with REEP1 could not be investigated due a lack of available antiserum.

TRPC2 transfection efficiency in a heterologous expression system

Due to the reported increased surface expression of olfactory receptors by the chaperone RTP1 (Saito *et al.* 2004) and our discovery of its interaction and cellular co-localization with TRPC2, we hypothesized that the chaperone would increase the surface expression of TRPC2. To test this, TRPC2 was expressed with or without either RTP1 or REEP1 in HEK293 cells. Transfected cells were incubated with an antiserum for the myc-epitope tag on the plasmid-encoded TRPC2 and then visualized using a species-specific FITC-conjugated secondary antiserum. A representative field of view used to calculate the transfection efficiency for various transfection conditions is shown in Figure 2.5. The ratio of fluorescent cells (left column, Figures 2.5A, 2.5C, 2.5E, and 2.5G) over that of all cells (right column, Figures 2.5B, 2.5D, 2.5F, and 2.5H; DAPI nuclear stain) was used to calculate transfection efficiency for each condition, respectively (Figure 2.5I). TRPC2 transfection by itself (Figure 2.5A and2.5 B) and in conjunction with either RTP1 (Figure 2.5C and 2.5D) or REEP1 (Figure 2.5E and 2.5F) resulted in an efficiency near 30% (Figure 2.5I). Transfection with another myc-epitope tagged six transmembrane spanning ion channel (Kv1.3) was used as a positive control (Figure 2.5G-H). The TRPC2 transfection condition efficiencies were significantly below that of the positive control as measured by a one-way ANOVA followed by a Student Newman-Keuls (*snk*) post-hoc test ($F= 4.01$, $p< 0.05$). Neither cells transfected with empty vector nor those labeled without the primary antiserum were immunoreactive (data not shown).

RTP1 alters the subcellular localization of TRPC2 *in vitro*

RTP1 and REEP1 are able to induce membrane expression of olfactory receptors in HEK293 (Saito *et al.* 2004). Therefore, we sought to visualize the effect of these chaperones on the subcellular distribution of TRPC2 in the HEK293 cells. The identical transfection scheme as in Figure 2.5 was repeated but high-resolution images of the labelled cells were acquired using confocal microscopy. The results of three such experiments are shown in Figure 2.6. When expressed alone, TRPC2 immunoreactivity is visualized either near the nucleus (light blue; Figure 2.6A) or in dense patches seemingly away from the surface membrane (bright green) and more easilyviewed in an unstacked image (Figure 2.6A'). In contrast, Kv1.3 immunoreactivity

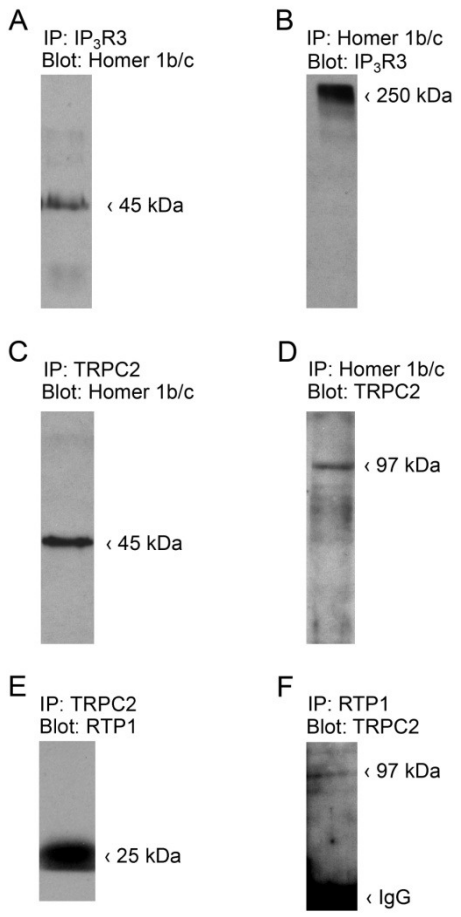

Figure 2.4 TRPC2 co-immunoprecipitates with IP_3R_3, Homer 1b/c, and RTP1 in the VNO. For each condition the antiserum used for immunoprecipitation (IP) was added to the VNO lysates, proteins were separated by SDS-PAGE and then probed (Blot) with an antiserum against the suspected protein partner. Expected M_r = TRPC2 97, IP_3R_3 >220, Homer 1b/c 45 kDa, as indicated. (A) Homer 1b/c co-immunoprecipitated with IP_3R_3. (B) Procedure reversed from A. (C) Homer 1b/c co-immunoprecipitated with TRPC2. (D) Procedure reversed from C. (E) RTP1 co-immunoprecipitated with TRPC2. (F) T Procedure reversed from E. IgG = the heavy chain of the immunoglobin G.

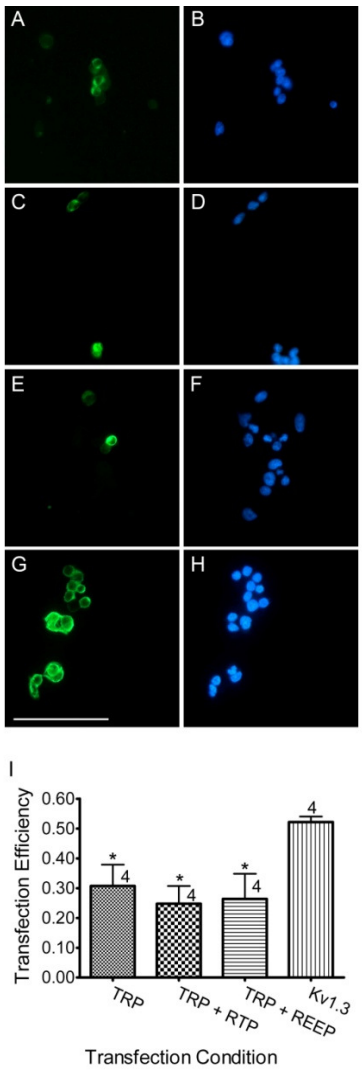

Figure 2.5 TRPC2 transfection efficiency in HEK293 cells. (A-H) Representative micrographs of cells grown on glass-coverslips, transfected as in text, incubated with an antiserum to the c-myc epitope and labeled with FITC-conjugated secondary antiserum. (A, C, E, and G) Representative fields of view for antiserum specific fluorescence (green). (B, D, F, and H) The same fields of view as in images B, D, F, and H with DAPI nuclear stain (blue). Note the low percentage of cells transfected in (A, B) TRPC2, (C, D) TRPC2 + RTP1, (E, F) TRPC2 + REEP1, as compared to (G, H) Kv1.3. The scale bar = 100 μm. (I) Histogram plot of the percentage of transfected cells from four transfections. * = denotes significant difference from Kv1.3 transfection; one-way ANOVA followed by a *snk* post-hoc test ($p \leq 0.05$).

is visualized primarily at the surface membrane (Figure 2.6D-6D') and is known to insert into the surface membrane in large numbers in HEK293 cells. Interestingly, co-expression with RTP1 (Figure 2.6B-6B') results in immunoreactivity that is more typical of surface expression, with less immunoreactivity near the nucleus (ie less light blue), than that observed for the TRPC2 alone condition. Co-transfection with REEP1 results in an intermediate distribution (Figure 2.6C-6C'). Transfection of HEK293 cells with TRPC2 and both chaperones did not appear different than that of cells using transfection conditions with only one chaperone in conjunction with TRPC2 (data not shown). Cells labelled without the primary antiserum were not immunoreactive (Figure 2.6E-6E'). Line plots of each transfection condition in Figure 2.6A-E demonstrate the α-myc immunoreactivity distribution.

To biochemically confirm the suggested increase in surface expression of TRPC2 by RTP1 and REEP1, a set of cell-surface biotinylation experiments were conducted on HEK293 cells transfected as in Figure 2.5. The biotinylated surface proteins were collected and processed by SDS-PAGE and visualized via Western analysis using an antiserum to the myc-epitope. Cell lysates were also processed by SDS-PAGE and visualized via Western analysis for β-actin to confirm equivalent protein loading. A representative Western blot of biotinylated TRPC2 channel were quantified 48 hrs following transfection as reported in Figure 2.7. RTP1, but not REEP1, significantly increased TRPC2 surface biotinylation (Significantly-different mean pixel density; one-way ANOVA followed by a Dunnett's post-hoc test $F= 4.1$, $p<0.05$; Figure 2.7B). When transfected alone, surface TRPC2 was detected in only 2 out of 7 trials; while when transfected with RTP1, surface TRPC2 was detected in 7 out of 7 trials. Comparatively, myc-tagged Kv1.3 was strongly detected under either condition (Figure 2.7A).

Cell-surface TRPC2 is functionally detected

To confirm that the cell-surface expressed TRPC2 was functional, a set of whole-cell electrophysiological experiments were conducted on HEK293 cells transfected as in Figure 2.5. Dynabead technology using co-transfection of the channel with CD8 was employed to pan for transfected cells appropriate for whole-cell patch-clamp (see methods for details). Transfected HEK293 cells that were lightly beaded (2-4 beads) and apparently exiting mitosis were targeted in order to facilitate the generation of consistent, comparable recordings across several transfections. Cells were stimulated with a voltage-ramp protocol as described in (Lucas *et al.* 2003) and graphically displayed in Figure 2.8A. The total duration of the ramp was 140 ms with

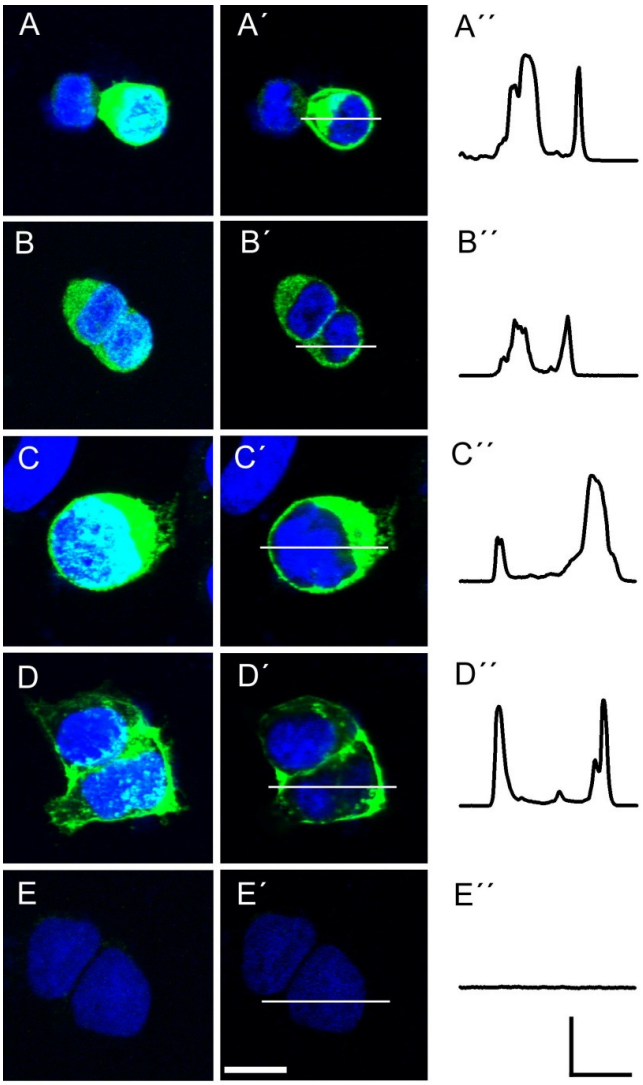

Figure 2.6 Subcellular localization of TRPC2 in HEK293 cells. (A-E) Representative two-photon confocal micrographs of cells grown, transfected, and immunolabeled as in Figure 4. Note that TRPC2 immunoreactivity in (A) appears subcellular while that of Kv1.3 immunoreactivity (D) is localized to or compartmentalized near the membrane. The presence of RTP1 (B) or REEP1 (B-C) appears to shift some TRPC2 immunoreactivity to, or near, the membrane while that in the presenece of REEP1 (C) remains more cytosolic or intermediate. Immunoreactivity is abolished in a vector-only transfection in E ($pcDNA_3$). (A-E) = Z-series stacked confocal image; (A`-E`) = Representative single optical slice in the midline; (A``-E``) = Intensity profiles quantified as a line scan taken at the horizontal bar in A`-E`. Horizontal scale bar = 10 µm. Vertical scale bar = 50 arbitrary units.

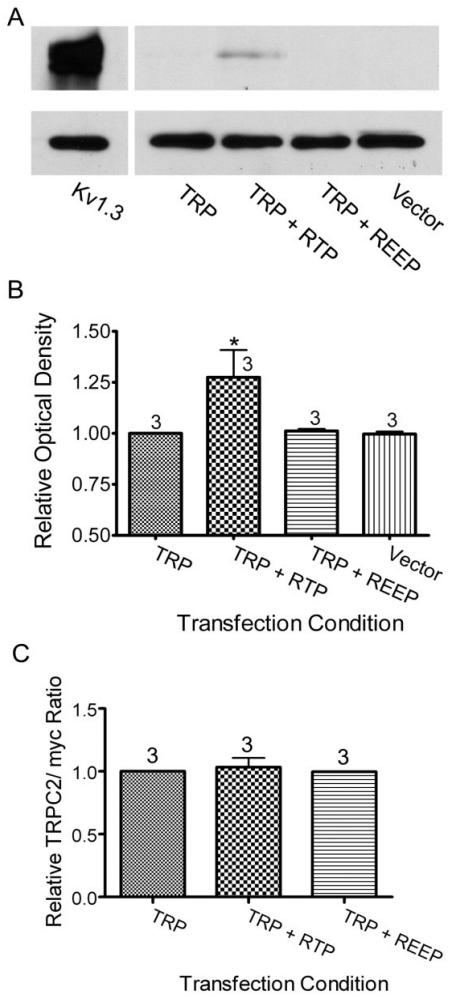

Figure 2.7 TRPC2 cell-surface biotinylation. Representative Western blot of TRPC2-biotinylated protein following 48 hours after transfection of indicated cDNAs in HEK293s. (A) (Top panel) Biotinylated protein products (see methods) were precipitated with streptavidin agarose beads, subjected to SDS-PAGE, and then probed with α-c-myc (1:400) to visualize myc-Kv1.3 expression (far left lane) versus that of mycTRPC2 expression under various transfection conditions. (Bottom panel) Lysate input probed with α-β-actin. (B) Histogram plot of the mean ± s.e.m. pixel immunodensity normalized to that of the TRP alone condition. Transfection sample size noted. *= Mean pixel density is statistically-different from channel only transfection; Dunnett's post-hoc test, $p \leq 0.05$. (C) Ratio of the expression levels of mycTRPC2 and the internal standard, myc. Values are normalized against the channel only condition.

an interpulse interval of 60 s. Three to five ramp pulses were applied to determine baseline current and then the recording bath was changed (see methods) to yield a final ATP concentration of 166 μM. Although diacylglycerol (DAG) has been reported to activate endogenous TRPC2 channels in mouse VSNs (Lucas *et al.* 2003), in our hands neither DAG nor a synthetic analogue, OAG, was effective in gating TRPC2 current in vertebrate VSNs (Brann and Fadool 2006). We therefore relied upon reported augmentation of TRPC2 via activation of purinergic current (Jungnickel *et al.* 2001) as the metric of a functional assay of our *in vitro* system. Current at the end of the voltage-ramp protocol (-80 mV) was used as a measure of response to ATP stimulation. As shown in Figure 8C, cells transfected with both TRPC2 and RTP1 elicited an increase in ATP-evoked whole-cell current compared to that of control cells that were transfected, but beadles (Figure 2.8A) or TRPC2-transfected only cells (Figure 2.8B) (Significantly-different mean current; one-way ANOVA followed by a *snk* post-hoc test $F= 7.68$, $p<0.05$; Figure 2.8E). Additionally, a different population of heavily-beaded cells (N= 7) were observed, which had much larger voltage-activated current amplitudes that ranged from 400 to 4400 pA (mean= 1550 pA). These cells were minimally responsive to ATP (Figure 2.8D-E) and were only observed in dishes transfected with both TRPC2 and RTP1.

Discussion

These experiments demonstrate that the putative olfactory receptor chaperone RTP1 interacts with not only proteins of the GPCR superfamily, but also with ion channels. This novel finding was demonstrated *in vivo* by a protein-protein interaction between TRPC2 and RTP1, and *in vitro* by a RTP1- dependent increase in TRPC2 surface expression. An ion channel complex consisting of TRPC2, Homer, and IP_3R_3 may exist *in vivo*. Our biochemical experiments indicate that TRPC2, the scaffold protein Homer 1b/c, and the ion channel IP_3R_3 form protein-protein interactions in the native VNO. To the best of our knowledge, an interaction between Homer and TRPC2 has not been demonstrated in any sensory system. Lastly, our data represent the first characterization of Homer expression in the rat VNO.

Homers are widely expressed in both the male and female rat including, but not limited to, many brain regions and the testes. Although these biochemical data cannot exclusively rule out the possibility of Homer expression in non-sensory regions, Homers are typically associated

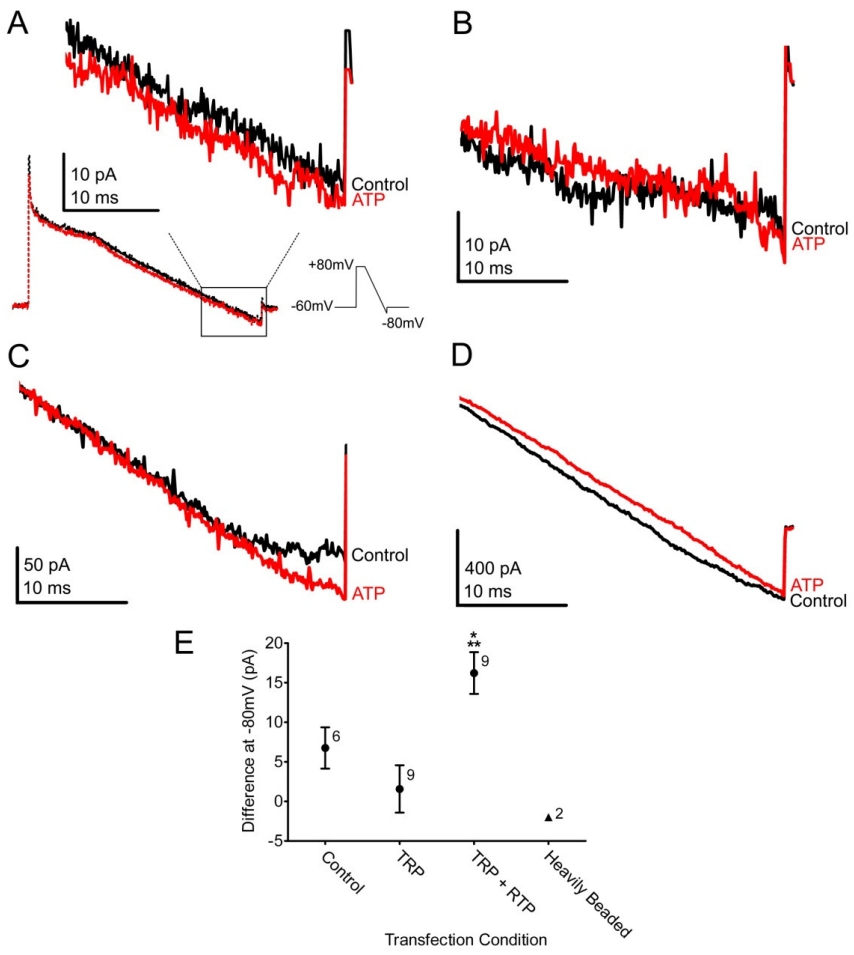

Figure 2.8 Whole-cell electrophysiology. (A-D) Human embryonic kidney 293 (HEK293) cells were transiently transfected with cDNAs encoding the TRPC2 channel, hCD8 and with or without RTP1 as noted. HEK293 cells were voltage-clamped at –60mV in the whole-cell configuration and then a ramp was applied (+80 to –80mV; see methods) under control (black) and subsequent to ATP bath application (red). (A) Representative control (beadless) whole-cell recording. The bottom recordings are of the entire voltage protocol. The box outlines the portions of these recordings shown in greater detail in the inset above the dashed lines and used in C-D. Representative recordings from the TRPC2 alone (B), TRPC2+ RTP1+ (C), and the heavily beaded TRPC2+ RTP1+ (D) conditions. (E) Graph of the change in mean (± s.e.m) current at -80mV following ATP stimulation as compared to a previous stimulation under various transfection conditions as in (A-C). ▲= denotes the mean response to ATP stimulation by heavily beaded cells as in (D). Transfection sample size as noted. * = denotes significant difference from control transfection; ** = denotes significant difference from TRPC2 transfection; one-way ANOVA followed by a *snk* post-hoc test ($p \leq 0.05$). The voltage-ramp protocol is described graphically in (A).

with either post-synaptic membranes (Brakeman *et al.* 1997; Gasperini and Foa 2004; Kaja *et al.* 2003; Kammermeier and Worley 2007; Lu *et al.* 2007; Tu *et al.* 1999; Xiao *et al.* 1998) or membranes involved in calcium signalling (Worley *et al.* 2007a). The VNO lysates used in these experiments contained both of these subcellular elements, consistent with previous expression patterns for Homer. The non-sensory portions of the VNO are densely innervated by the autonomic nervous system (Meredith and O'Connell 1979; Soler and Suburo 1998) and the sensory microvilli contain a well-explored calcium-signalling pathway (Figure 2.9) (Brann *et al.* 2002; Brann and Fadool 2006; Halpern and Martinez-Marcos 2003). Homer isoforms expressed in the VNO could function similarly in smooth muscle cells and in chemosensory signal transduction. Unlike mouse data reported by (Shiraishi *et al.* 2004), we do not find Homer 2 expression in the rat VNO. Overall, we detected neither a sex difference in VNO expression of Homer 1b/c and 3 isforms nor an appreciable amount of the Homer 2 isoform.

Our data demonstrating transcription of RTP1 and REEP1 in the rat VNO support the previous finding of these transcripts in the mouse VNO (Saito *et al.* 2004). The immunocytochemical detection of RTP1 protein in olfactory sensory neuron cilia, VSN microvilli, goblet cells and in the soft-palate, and not in the non-sensory respiratory epithelium, may provide important clues as to function. *In vitro* experiments support RTP1 interactions with GPCRs associated with either odorant (Saito *et al.* 2004) or taste receptor families (Behrens *et al.* 2006). Similar protein-protein interactions have not been found, however, with VRs (Saito *et al.* 2004). Alternatively, MHC class 1b proteins have been found to associate with the V2Rs and thus may not function with TRPC2 (Loconto *et al.* 2003; Olson *et al.* 2005). Allowing for several different protein associations including M10-VR, RTP1-TRPC2, and Homer-TRPC2-IP_3R_3 provides the pheromone transduction cascade with multiple regulatory sites (Figure 2.9).

The immunoprecipitation data indicate that Homer is not expressed in the non-sensory areas of the VNO, rather it is expressed in VSN microvilli. Other data have indicated that TRPC channels can interact with Homer proteins (Yuan *et al.* 2003). For example, TRP (the *drosophila* homologue of TRPC (Venkatachalam and Montell 2007)) is involved in such interactions in the invertebrate photoreceptor (Huber 2001). Functionally, Homer expression in the VSN would allow for receptor and channel modulation. Linking TRPC2 and IP_3R_3 via Homer 1 would ensure high-fidelity transmission of the calcium signal that flows through the open TRPC2 channel during chemosignal detection. Homer 3 does not form protein-protein interactions with

TRPC2 (Yuan *et al.* 2003). The inducible form of Homer (1a isoform) was not detected in the rat VNO. This short form lacks the coiled-coiled domain and would oppositely be predicted to disassemble a TRPC2-Homer 1-IP_3R_3 complex (see Figure 2.9).

Disruption of the TRPC2-Homer 1-IP_3R_3 complex by Homer 1a could alter TRPC2 activity in a manner similar to Homer 1a modulation of mGluR activity (Kammermeier and Worley 2007). In previous VSN recordings, disruption of the interaction between TRPC2 and IP_3R_3 resulted in a diminished chemosignal response (Brann and Fadool 2006). On the other hand, TRPC1 mutants lacking Homer binding sites formed spontaneously active channels when expressed *in vitro* (Yuan *et al.* 2003) and gene-targeted deletion of Homer 1 increased TRPC1 activity *in vivo* (Stiber *et al.* 2008; Yuan *et al.* 2003). Thus, Homer 1 could subserve to provide the VSN signalling apparatus more flexibility in responding to and adapting to chemosignals. The interaction between TRPC2 and RTP1 could provide further regulation of TRPC2 and the response of VSNs to chemosignals, by modulation of total TRPC2 activity dependent upon surface expression driven by the chaperone. The recognition sequence for RTP1 binding will need to be investigated in future experiments.

The plasmid containing TRPC2-C14 had a low transfection efficiency in HEK293 cells. Transient transfection of a plasmid containing Kv1.3 produces an efficiency percentage of approximately 60% (Fadool *et al.* 1997), whereas TRPC2 efficiency is only about 30%. Poor transfection efficiencies have been noted of some constructs using polycationic transfection reagents (Yamamoto *et al.* 1999); however, other researchers have tried alternative transient transfection methods with TRPC2 and reported comparably low efficiencies (Hofmann *et al.* 2000; Hofmann *et al.* 2002). It is interesting to speculate that the low transfection efficiency might be a result of apoptosis due to calcium cytotoxicity associated with spontaneously active TRPC2 channels. At least one other TRPC channel, TRPC4, has been demonstrated to be spontaneously active in HEK293 cells (McKay *et al.* 2000). In light of the facts that neither chaperone increased TRPC2 transfection efficiency nor did this efficiency match that of Kv1.3, a structurally similar channel (Lepage and Boulay 2007), suggests that proper TRPC2 cellular distribution and function may require binding partners not present in our experiments. Lastly, RTP1 and REEP1 do not appear to be toxic to the HEK293 cells, as transfection efficiency did not decrease with their expression.

RTP1 and REEP1 appear to alter the sub-cellular distribution of TRPC2 *in vitro*. In HEK293 cells, TRPC2 immunolabeling is predominately in large deposits that are presumably vesicles, as imaged with laser confocal microscopy. Although every transfection condition with TRPC2 led to vesicular immunolabeling, the presence of either RTP1 or REEP1 seemed to shift expression of the channel toward the surface membrane. These data indicate a functional relationship for the RTP1-TRPC2 co-immunoprecipitation found in VNO tissue. Our data cannot distinguish the mechanism of TRPC2 surface expression, which could be the result of either increased TRPC2 inserted or inhibition of TRPC2 internalization.

Demonstration of robust Kv1.3 surface expression leads credence to the assumptions made earlier when comparing sub-cellular localization of TRPC2 in different transfection conditions. Namely, when transfected with chaperone, the TRPC2 immunolabeling signal was similar to the Kv1.3 immunolabeling in terms of subcellular distribution. A similar shift in the immunolabeling signal of olfactory receptors occurs when these receptors are expressed *in vitro* with RTP or REEP (Saito *et al.* 2004) and with unrelated GPCRs (Bush *et al.* 2007). It then follows that with the addition of chaperone, more TRPC2 is in the surface membrane. In support of this notion, in each transfection condition where TRPC2 and RTP1 were transfected together, TRPC2 was detected in the surface membrane. When expressed alone, TRPC2 was infrequently detected in the surface membrane. Increased TRPC2 surface expression was detected with both cell-surface biotinylation and with whole-cell electrophysiology.

The endogenous metabotropic ATP receptor pathway utilized in our experiments to investigate *in vitro* TRPC2 current is similar to the VNO sensory transduction pathway as each activates PLC (Figure 2.9) (Jungnickel *et al.* 2001; Schachter *et al.* 1997; Van Kolen and Slegers 2006). The electrophysiological data indicate that the surface expressed TRPC2 is functional and able to respond to a signal transduction pathway similar to that present in the VNO. That heavily-beaded, and presumably highly expressing, TRPC2+ RTP1+ cells were minimally responsive to purinergic stimulation is not unexpected. TRPC3, another TRPC channel, gains and loses agonist-induced activity based on expression level (Vazquez *et al.* 2003). Alternatively, the TRPC2 protein level may have been high enough and the purinergic receptor protein level low enough, that any interaction between the two might be negligible due to stoichiometric limitations.

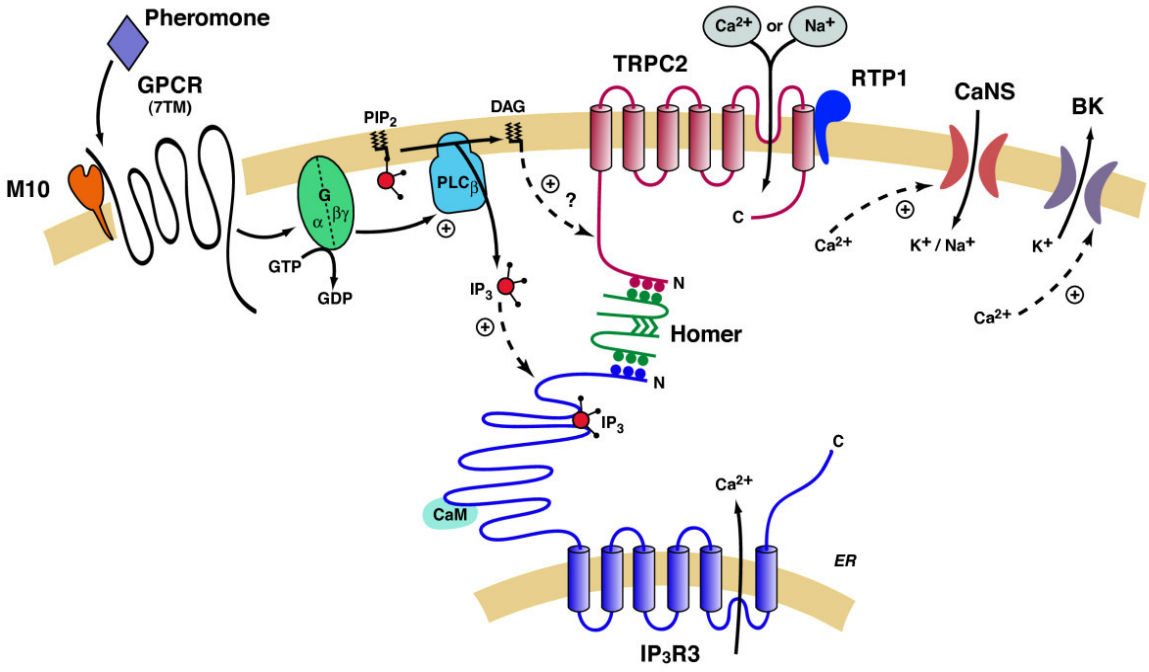

Figure 2.9 Schematic of the hypothetical vomeronasal organ transduction model. The vomeronasal organ (VNO) signal transduction pathway begins at either a type 1 vomeronasal (V1R) or type 2 vomeronasal (V2R) G-protein coupled receptor (GPCR); V2Rs may be associated with a member of the M10 major histocompatibility protein family. Upon pheromone binding, the V1R/ V2R activates a guanidine trisphosphate-binding protein (G-protein). The activated G-protein stimulates the cleavage of phosphatidylinositol 4,5-bisphosphate (PIP_2) into 1,4,5-inositol trisphosphate (IP_3) and diacylglycerol (DAG) via phospholipase C (PLC). DAG has been reported to gate the non-specific cation current through the type 2 canonical transient receptor potential channel (TRPC2). Although binding of IP_3 to the IP_3 receptor (IP_3R) is not supported to yield a transduction current alone, two isoforms of IP_3R (IP_3R_2 and IP_3R_3) are expressed in the VNO, and IP_3R_3 forms a complex with TRPC2. Whether or not ligand occupancy is required, inhibition of complex formation blocks chemosignal-activated current. TRPC2 expression is increased in the VSN microvillar membrane with the assistance of the chaperone receptor transporting protein 1 (RTP1), whereby the channel associates with both Homer 1b/c and IP_3R_3. A calcium-activated non-selective ion channel (CaNS) can amplify the chemosignal-induced current following the rise in intracellular calcium. This rise in intracellular calcium also actives calcium-activated big conductance potassium ion channels (BK) as well as calmodulin (CaM), which may bind to both IP_3R_3 and TRPC2.

Regardless of the mechanism, these data suggest that the half-life residence of TRPC2 in the membrane is increased in the presence of RTP1. These results may indicate that the functional interaction between RTP1 and TRPC2 is one of membrane stabilization rather than trafficking. This is a different functional role for RTP1 from previously described (Saito *et al.* 2004) and is speculative. With both olfactory and gustatory GPCRs, RTP1 is presumed to traffic its target to the surface membrane (Behrens *et al.* 2006; Saito *et al.* 2004).

Based upon our current results in the context of current knowledge (Halpern and Martinez-Marcos 2003; Tirindelli *et al.* 2009; Zufall *et al.* 2005), we propose the following model (Figure 2.9). A chemosignal binds to either VR-type GPCR, activation of which ultimately results in a TRPC2-dependent calcium influx across the surface membrane. Calcium can also enter the cytosol from the endoplasmic reticulum via IP_3R_3. Homer 1 binding at either TRPC2 terminus (Stamboulian *et al.* 2005) (residues 303PPTLL and 953LPVPF) may alter the channel function. TRPC2 and mGluRs are both integral transmembrane proteins and, therefore, the known interactions of mGluR/ IP_3R (Tu *et al.* 1999) could be replaced by TRPC2/ IP_3R complex formation in the VNO. For example, Homer 1 may cluster IP_3R_3 to TRPC2 using Homer binding motifs (PPXF, PPXXF and LPSSP) on both channels in a similar fashion that Homers cluster IP_3R_3 to mGluR (Worley *et al.* 2007b). This would be advantageous for at least two reasons. First, the products of phospholipase C hydrolysis of PIP_2, IP_3 and DAG, gate both $IP3R_3$ and TRPC2. Maintaining close proximity of the second-messenger targets would increase the speed of the signalling cascade and decrease the amount of second-messenger lost due to errant diffusion. Second, as IP_3R_3 may adopt a conformation that favors opening upon calcium binding (Hamada *et al.* 2003), tethering IP_3R_3 next to the calcium source would increase the speed of the signalling cascade. By tethering IP_3R_3 underneath TRPC2, Homer would be expected to increase the open probability of IP_3R_3 using calcium influx contributed through the surface channel TRPC2. Thus, Homer could both increase the speed and the efficiency of the TRPC2 signalling cascade as it does for mGluR cascades. Signal adaptation is likely to come from calcium-calmodulin inhibition of both IP_3R_3 (Taylor and Laude 2002) and TRPC2 (Spehr *et al.* 2009), calcium-activated big conductance potassium channels (BK) (Ukhanov *et al.* 2007; Zhang *et al.* 2008) and metabolism of DAG into the lipid arachidonic acid (Spehr *et al.* 2002; Zhang *et al.* 2008).

Although complexes of channels and adaptors have been found in the visual system, Homer is a relatively newly discovered protein, and appears to be involved in scaffolding, targeting, and localization. Our previous finding of a direct protein-protein interaction between IP_3R_3 and TRPC2 in the VNO neither ruled out an additional role for scaffolding proteins, such as the Homer family, nor a role for chaperones, such as REEP1 and RTP1. In fact, the addition of chaperones and the formation of an adaptor complex may be critical to channel function and eagerly warrants future experimentation.

Conclusion

The VNO expresses members of the Homer protein family. Within the VSN microvillus, Homer1b/c complexes with both TRPC2 and IP_3R_3. RTP1 is expressed in the VNO, co-localizes with other members of the VNO transduction pathway and may be a member of the transduction pathway as it forms a protein-protein interaction with TRPC2 *in vivo*. *In vitro,* RTP1 appears to function as a chaperone of TRPC2, increasing the amount of functional channel in the surface membrane.

CHAPTER THREE

HUMAN PHEROMONE DETECTION BY THE VOMERONASAL ORGAN: UNNECESSARY FOR MATE SELECTION?[2]

Introduction

A recent paper proposes the hypothesis that the human vomeronasal organ (VNO) provides crucial inhibitory chemosensory information that discourages mating between 'inappropriate' partners (Foltan and Sedy 2009). New information about human chemical communication would be exciting; unfortunately, the authors provide no data to support their hypothesis aside from an anecdotal personal observation. The authors also poorly cite research articles. For example, the section titled 'How the VNO influences human behaviour' presents only rodent data without any accompanying comparisons to human behavior. The authors discuss the crucial role that an ion channel, TRPC2, plays in rodent VNO function without mentioning that the human TRPC2 gene is a non-protein producing pseudogene (Liman and Innan 2003; Wes *et al.* 1995). Although significant, these points alone do not invalidate the hypothesis. We argue that this hypothesis is critically flawed due to the following: firstly, the authors disregard data that suggest that the adult human VNO is non-functional; secondly, the authors assume that every 'scent[s] of a pheromone nature' is detected by the VNO; thirdly, they argue that every human pheromone triggers an 'inhibitory feedback mechanism' crucial for the 'involuntary ability to exclude inappropriate mates' and therefore encouraging commitment to an existing mate.

Review and Analysis

The Le Forte I surgery performed by the authors is a surgery of the mid-face that repositions the maxilla for proper alignment with the mandible (Perciaccante and Bays 2004). The surgery involves separating the maxilla from the surrounding bones and some of the

[2] Portions of this chapter were duplicated from the original article Mast TG, Samuelsen CL. (2009) Human pheromone detection by the vomeronasal organ: unnecessary for mate selection? *Chem Senses*. 34(6):529-31. The authors retain copyright.

associated soft tissues, including removing a portion of the nasal septum and mucosa (Perciaccante and Bays 2004). It is during this step that Foltan and Sedy (2009) claim to damage the VNO and the 'supplying nerve'. The authors then contradict this statement by acknowledging that the human VNO does not look like a 'classical' sensory organ and that there is no VNO nerve.

The adult human VNO has been repeatedly reviewed as non-functional (Keverne 1999; Meredith 2001; Wysocki and Preti 2004). Physical and histological examination of the human VNO suggests that this organ contains few neurons, consists mostly of epithelial cells and has no sensory function (Johnson *et al.* 1985). Specifically, most cells within the adult human VNO express keratin proteins, markers of epithelial cells (Trotier *et al.* 2000; Witt *et al.* 2002). No cells express olfactory marker protein, a hallmark of mature olfactory neurons (Monti-Graziadei *et al.* 1977; Trotier *et al.* 2000; Witt *et al.* 2002). No cells have synaptic contacts (Trotier *et al.* 2000), and few if any cells express S-100, a marker of glia and nerve bundles (Trotier *et al.* 2000; Witt *et al.* 2002). Additionally, there is no evidence for a nerve connecting to or from the VNO (Trotier *et al.* 2000; Witt *et al.* 2002).

Chemosensory cues that meet the authors' definition of a pheromone are not detected exclusively by the VNO. The mouse's main olfactory system does not receive sensory input from the VNO, yet it responds to social signals (Kang *et al.* 2009; Lin *et al.* 2005). Multiple signaling pathways within the main olfactory epithelium (MOE) mediate this sensitivity (Leinders-Zufall *et al.* 2007; Lin *et al.* 2007; Wang *et al.* 2006). Importantly, human perception of the putative pheromone androstadienone does not require VNO stimulation (Knecht *et al.* 2003), though brain activation by androstadieone and another putative human pheromone, estratetraenol, is dependent upon access to the MOE (Savic *et al.* 2009). Therefore, the authors' assumption of total loss of chemosensory communication by putative pheromones following VNO ablation is not supported in the literature.

The VNO-independent mechanism by which these steroidal compounds stimulate the central nervous system is undefined. The possibilities include diffusion into the blood stream via nasal capillaries, direct access to the cerebral spinal fluid via movement across the cribiform plate (Hanson and Frey 2008), and receptor activation in the MOE. Receptor activation in the MOE is supported by a brain imaging study that demonstrates a short latency between sniffing and brain activation and the requirement of an accessible MOE (Savic *et al.* 2009). Additionally,

a putative human homologue to the rodent vomeronasal receptors is expressed in the MOE (Rodriguez *et al.* 2000) and can be activated by odorants *in vitro* (Shirokova *et al.* 2008). These data are not conclusive, and more studies are needed on the role of the MOE in human pheromone sensation.

Our last concern centers on the pheromone's presumed effect on human behavior. The authors suggest that human pheromones exclusively provide 'negative stimuli' that provoke 'an involuntary response'. As to the first point, we are unsure as to the conceptual framework in which mating stimuli that eventually block mating would be produced, released and conserved within a population. In this hypothesis, how are the senders of such stimuli able to mate and thus raise their own fitness level? That is, the pheromone producers must successfully mate-- - apparently against great odds-- in order for this communication system to be maintained. Secondly, the authors provide no evidence that human pheromones are 'negative stimuli'. Putative human pheromones do not appear to stimulate a 'negative' response. On the contrary, published evidence suggests that putative human pheromones inhibit decreases in positive mood (Jacob *et al.* 2002; Jacob and McClintock 2000; Wyart *et al.* 2007). Therefore, the authors' assumption that all pheromonal communication produces a negative effect during mate selection is not supported.

Conclusion

In our view, the hypothesis proposed by Foltan and Sedy (2009) that the human VNO provides crucial inhibitory chemosensory information preventing inappropriate mating is unsound. They provide no data to support their claim and the cited research literature is mischaracterized. They acknowledge that it is generally agreed that the human VNO is nonfunctional, but contend it is crucial for normal human social behavior. They assume that all putative pheromonal communication requires the VNO; where the research literature clearly demonstrates that suspected pheromones can activate both the main and accessory olfactory systems. The authors assert that human pheromonal communication provides negative information and in doing so, they disregard the data on human pheromonal function that suggests human pheromones have positive effects.

CHAPTER FOUR

OLFACTORY SENSORY DEPRIVATION INCREASES THE NUMBER OF PROBDNF-IMMUNOREACTIVE MITRAL CELLS IN THE OLFACTORY BULB OF MICE[3]

Introduction

Sensory activity shapes the structure and function of the developing olfactory system (Brunjes 1994; McLean *et al.* 2001; Najbauer and Leon 1995). When olfactory cues are deprived by unilateral-naris occlusion in neonatal rats, the olfactory bulb (OB) ipsilateral to the occlusion is ~ 25% smaller than that of the contralateral OB (Cao *et al.* 2007; Meisami 1976). This reduction is principally attributed to apoptotic cell death of interneurons in the glomerular and granule cell layers (Najbauer and Leon 1995). The number of mitral cells, the major projection neuron, is practically unaffected by unilateral-naris occlusion (Najbauer and Leon 1995).

Brain-derived neurotrophic factor (BDNF), a member of the neurotrophin family, regulates neuronal survival, growth, synaptic plasticity, and modulates ion channel activity (Blum and Konnerth 2005). TrkB, the preferred high-affinity receptor for BDNF, is expressed in the OB (Tucker and Fadool 2002). There is a time-dependent modulation of potassium current in mitral cell neurons in response to acute or chronic BDNF stimulation (Tucker and Fadool 2002). BDNF-activation of TrkB receptors causes phosphorylation of tyrosine residues on the *Shake*r family member, Kv1.3, which is highly expressed in mitral cells (Colley *et al.* 2004). Moreover, juxtaposition of unstimulated TrkB receptors with Kv1.3 channels modulates the resident half-life of the channel in the plasma membrane (Colley *et al.* 2007). Thus, BDNF modulation of mitral cell excitability is well known, while BDNF regulation of mitral cell survival is not. This study monitored the BDNF immunoreactive (ir) profile of OB neurons in order to understand the role of BDNF following sensory deprivation. Special attention was

[3] Portions of this chapter were duplicated from the original article Biju KC, Mast TG, Fadool DA. (2008) Olfactory sensory deprivation increases the number of proBDNF-immunoreactive mitral cells in the olfactory bulb of mice. *Neurosci Lett*. 447(1):42-7. The authors retain copyright.

directed to mitral cells because 1) these neurons do not undergo apoptosis following unilateral-naris occlusion and 2) we know these neurons express TrkB receptors and undergo changes in excitability upon stimulation by BDNF.

Materials and Methods

Solutions and antibodies

Solutions used for protein samples or tissue preparation, namely, nonidet-P40 protease and phosphatase inhibitor (NP40 PPI), homogenization buffer (HB), and phosphate-buffered saline (PBS), were made as previously (Tucker and Fadool 2002). The BDNF antiserum was from Santa Cruz Biotechnology, (Santa Cruz, CA, cat # sc-546). BDNF antiserum recognizes both the proneurotrophin (M_r= 27 kDa) as well as the mature neurotrophin (M_r= 13 kDa). Monoclonal actin antiserum (cat # A-2066) was from Sigma-Aldrich (St. Louis, MO) and used at 1:1000 for Western blots. All electrophoresis reagents were from Sigma-Aldrich.

Unilateral-naris occlusion procedures

C57BL/6 mice (Jackson Laboratories, Jacksonville, FL, USA) were anesthetized by hypothermia and the left naris was cauterized using a heated metal probe inserted 1-2 mm into the nostril at postnatal day one (P1) as described previously (Meisami 1976; Tucker and Fadool 2002). The animals were then warmed to 37˚C and returned to the dam. Scar formation resulted in permanent unilateral-naris closure. To facilitate the study of morphological changes in mitral cells that might accompany the unilateral-naris occlusion, *thy1*–yellow fluorescent protein transgenic mice (YFP mice) (Feng *et al.* 2000) were handled as above. Previously, we used this mouse to identify mitral cells and their dendritic processes (Marks and Fadool 2007). All procedures were carried out as approved by the Florida State University Laboratory Animal Resources and the National Institutes of Health.

At postnatal day (P) 20, 30 and 40, complete closure of the cauterized nostril was confirmed by visual examination under a dissecting microscope. Animals were perfused using paraformaldehyde dissolved in phosphate-buffered saline (4%PFA/PBS); the olfactory bulbs (OBs) were removed and post-fixed in 4% PFA/PBS for 4 hours (h). OBs were cryoprotected in 30% sucrose and 16 µm coronal sections were placed onto gelatin-coated slides, and stored at -20^{o}C until use.

Anatomical analysis

Avidin–biotin–peroxidase (ABC) methods were employed to localize BDNF (anti-BDNF 1:1000 dilution) in OB tissue sections as per manufacturer's protocols (ABC Elite Kit, Vector Laboratories, Burlingame, CA). Fifteen animals of each treatment condition (control = C, naris occluded = O) per occlusion duration (20, 30, or 40 days) were sampled. An investigator blind to the deprivation condition counted BDNF-ir mitral or juxtaglomerular cells within 12 fields of view using 93,500 μm^2 areas and sampling equally (3 sections each) from the dorsal, ventral, medial, and lateral aspects of the OB. The counts from these 12 sampled areas were then averaged for the analysis. Statistical significance was determined at the 95% confidence level by mixed block factorial design analysis of variance (ANOVA) with a *Bonferoni's* post-hoc test to compare the multiple factors of naris-occlusion and duration.

Confocal Microscopy

Olfactory bulb sections from YFP mice were prepared as above, except a 4^0C overnight incubation with anti-BDNF was followed by 2 h incubation in Alexa Fluor 546-conjugated anti-rabbit IgG (1:100; Invitrogen, Carlsbad, CA) and a five min incubation with DAPI (1:5000). Sections were rinsed, mounted with Vectashield (Vector Laboratories, Burlingame, CA), and viewed using a Zeiss LSM510 two-photon confocal system (Thornwood, NY). Image brightness and contrast were adjusted with Adobe Photoshop CS (Adobe Systems Inc., San Jose, CA) for maximal clarity.

Biohemistry

Twenty days after unilateral-naris or sham (probe to shank of nose) occlusion, the OBs were harvested following euthanasia with CO_2. Tissues from 3 animals were pooled and homogenized in Nonidet-P40 protease and phosphatase inhibitor (NP40 PPI) buffer and detergent-soluble proteins were extracted as previously described (Cook and Fadool 2002). Cytoplasmic proteins (50 µg/lane) were separated on 15% bis-acrylamide gels by SDS-PAGE and electro-transferred to nitrocellulose as previously described (Cook and Fadool 2002). Membranes were blocked for 30 min with 5% nonfat milk and incubated overnight at 4^oC in anti-BDNF (1:200). The nitrocellulose was then incubated with horseradish peroxidase-conjugated donkey anti-rabbit IgG (1:5000, GE Healthcare, Piscataway, NJ) for 90 min at room temperature. Enhanced chemiluminescence (GE Healthcare) exposure on Classic Blue film

(Midwest Scientific; St. Louis, MO) was used to visualize labeled proteins. Paired treatments (sham, contralateral, and ipsilateral) were compared on the same film to standardize differences in exposure between films.

Results

Prior to the preparation of histological samples, animals were visually confirmed to have complete naris closure and reduced OB size ipsilateral to the naris-occlusion as anticipated (Meisami 1976) and shown in Figure 4.1A. Independent of postnatal age, the OB contralateral (open) to the naris closure consistently revealed BDNF-ir in mitral cells, juxtaglomerular cells, and in the fibers contained in the external plexiform layer (EPL) (Figure 4.1C). Strongly labeled fibers were evident along the superficial (outer) layer of the EPL (oEPL) and glomerular layer (GL) (Figure 4.1C). All BDNF-ir profiles were abolished when the antiserum was preadsorbed with rhBDNF (Figure 4.1D) or when the primary antiserum was omitted (Figure 4.1E). Ipsilateral to the naris-occlusion, the glomeruli (data not shown) as well as the EPL were reduced in size (Figure 4.1B). BDNF-ir fibers in the oEPL and in the GL were markedly reduced (Figure 4.1B). Moreover, as early as P20 an increase in the number of BDNF-ir mitral cells per unit area (see methods) was observed (Figure 4.1B).

Quantification of mitral cell BDNF-ir was made (see methods) comparing the OB contralateral (open) and ipsilateral (closed) to the occlusion in animals in which deprivation ranged from 20 to 40 days (Figure 4.2A). We did not observe changes in BDNF-ir labeling intensity of individual mitral cells as a result of the naris-occlusion procedure. The number of BDNF-ir mitral cells per unit area, however, was significantly increased at all sampled time points (ANOVA, *Bonferoni's*, $\alpha \leq 0.05$). Interestingly, a similar tabulation for juxtaglomerular cells indicated the opposite effect; a significant decrease in BDNF-ir for juxtaglomerular cells per unit area at all sampled time points of sensory deprivation (Figure 4.2B). In a separate set of controls, sham animals (heated probe applied to shank of nose, n = 3) had BDNFir profiles (numbers of mitral and juxtaglomerular neurons per unit area) that were not different in numbers per unit area in comparison to that of the contralateral OB (open) from naris-occluded animals following 20 days of treatment (Student's t-test, $\alpha \leq 0.05$).

We performed naris-occlusion on YFP mice so that BDNF-ir could be followed as a double label with YFP-positive mitral cells. A representative confocal micrograph

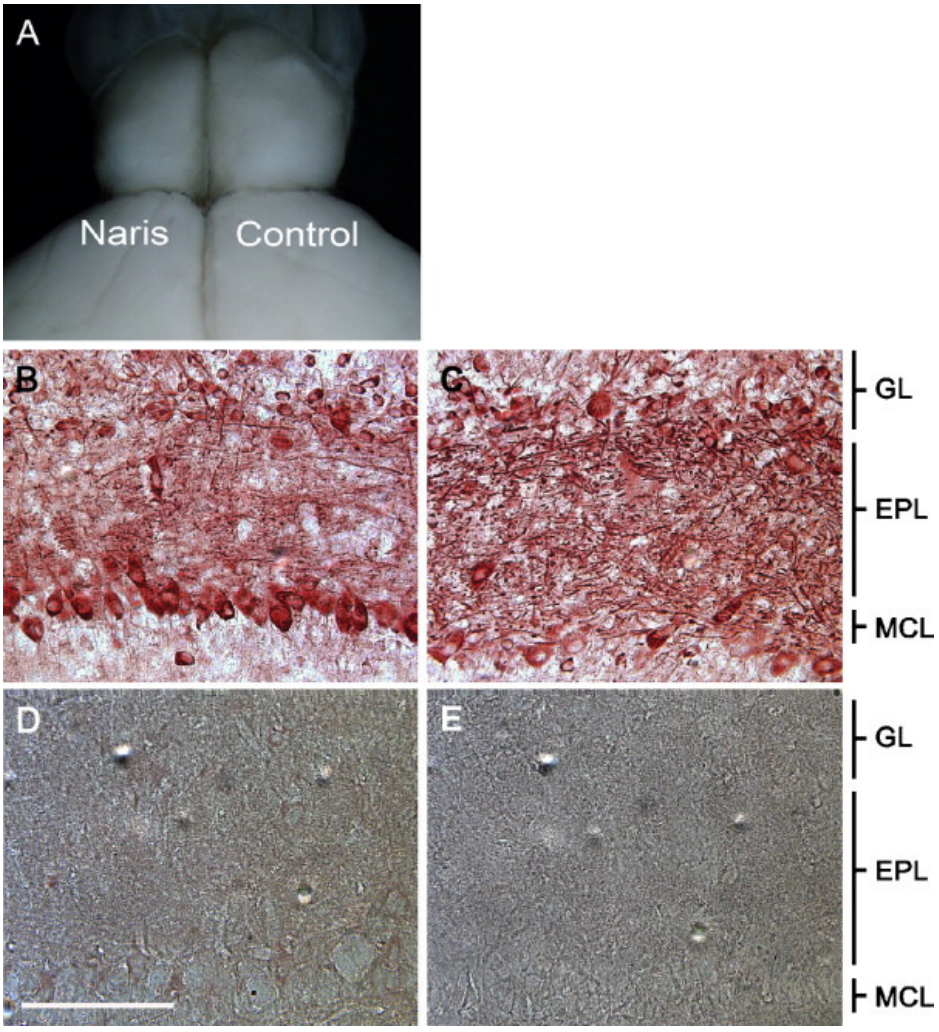

Figure 4.1 Unilateral-naris occlusion induces anatomical changes in the mouse OB. (A) This representative mouse was naris occluded within 24 hours of birth and photographed on postnatal day twenty (P20). Olfactory bulb (OB) ipsilateral to the occluded nostril (Naris) versus that of the contralateral control (Control). Representative photomicrographs at P20 comparing BDNF immunoreactivity (BDNF-ir) in the (B) olfactory bulb ipsilateral to the naris-occlusion and the (C) control olfactory bulb. (D) Preadsorption control with rhBDNF. (E) No primary control. EPL, external plexiform layer; GL, glomerular layer; MCL, mitral cell layer. Scale bar = 100 µm.

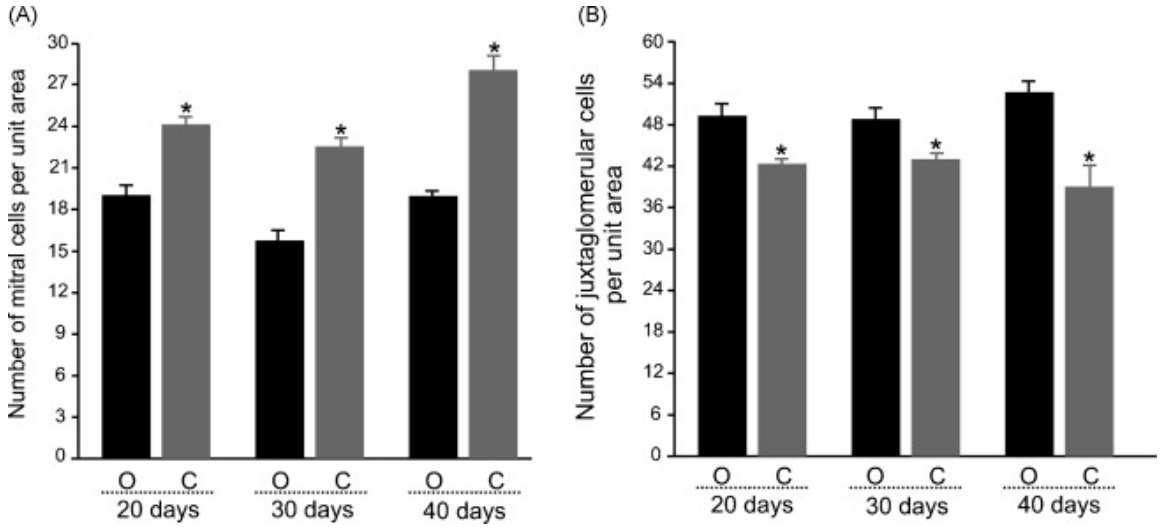

Figure 4.2 Bar plot of olfactory bulb neurons following sensory deprivation. Plotted are the mean number (per 93,500 μm^2) of (A) mitral cells and (B) juxtaglomerular cells in a population of OBs contralateral to the naris-occlusion (O, open) versus that for OBs ipsilateral to the naris-occlusion (C, closed). Data represent mean +/- standard error of the mean for three sections analyzed across quadrants (dorsal, ventral, medial, lateral) acquired from 15 animals in each of three occlusion durations. * denotes significant difference by mixed-block factorial design ANOVA, *Bonferoni's*, $\alpha \leq 0.05$.

demonstrating increased mitral cell BDNF-ir per unit area following 30 days sensory deprivation is reported in Figure 4.3. The secondary dendrites of mitral/tufted cells were restricted to the inner layer of the EPL (EPL) indicating (1) an anatomical subdivision within the EPL and (2) that BDNF-ir fibers in the oEPL do not arise from mitral cells. In a subset of control YFP animals (n = 3), we additionally confirmed that absolute numbers of YFP+ mitral cells per unit area were not significantly different following 20 days of sensory deprivation, however, numbers of DAPI-nuclear stained juxtaglomerular cells decreased by approximately 20% per unit area (paired t-test, $\alpha \leq 0.05$).

Biochemical confirmation of increased expression of mature BDNF at P20 was not evident. In fact, labeling consistent with the mobility of proBDNF (M_r = 27 kDa) and a pro-BDNF dimer (M_r = 54 kDa) was observed at uniform pixel density independent of the sensory deprivation condition (Figure 4.4). Since mature BDNF could be detected in control tissue (rat hippocampus, M_r = 13 kDa), the level of mature BDNF in the OB may be at or beyond the limits of detection by traditional protein biochemical techniques using this antiserum and our conditions despite our efforts to pool animals, load high concentrations of protein (50 µg), and incubate with a greater titer of antiserum (1:200).

Discussion

Our study monitors the BDNF-ir profile of OB neurons following unilateral sensory occlusion and demonstrates that the number of immunopositive mitral cells per unit area increases while that of juxtaglomerular cells decreases, independent of period of sensory deprivation ranging 20 to 40 days. Decrease in bulb size ipsilateral to the naris closure (Meisami 1976) is attributed mainly to apoptotic cell death in glomerular and granule cell layers, however, the number of mitral cells has been reported to be practically unaffected (Najbauer and Leon 1995). It is possible that sensory deprivation may stimulate mitral cells to synthesize BDNF leading to immunolabeling of cells that would typically escape detection under normal conditions. Because mitral cells have high expression of the *bcl-2* gene that suppresses apoptosis (Allsopp *et al.* 1993; Garcia *et al.* 1992; Hockenbery *et al.* 1993; Najbauer *et al.* 1995), the susceptibility of mitral cells to apoptotic death could be lower than that for other OB cell-types. It is also known that trophic factors and other survival signals in the developing nervous system may suppress an intrinsic suicide program of cells to regulate cell numbers in response to

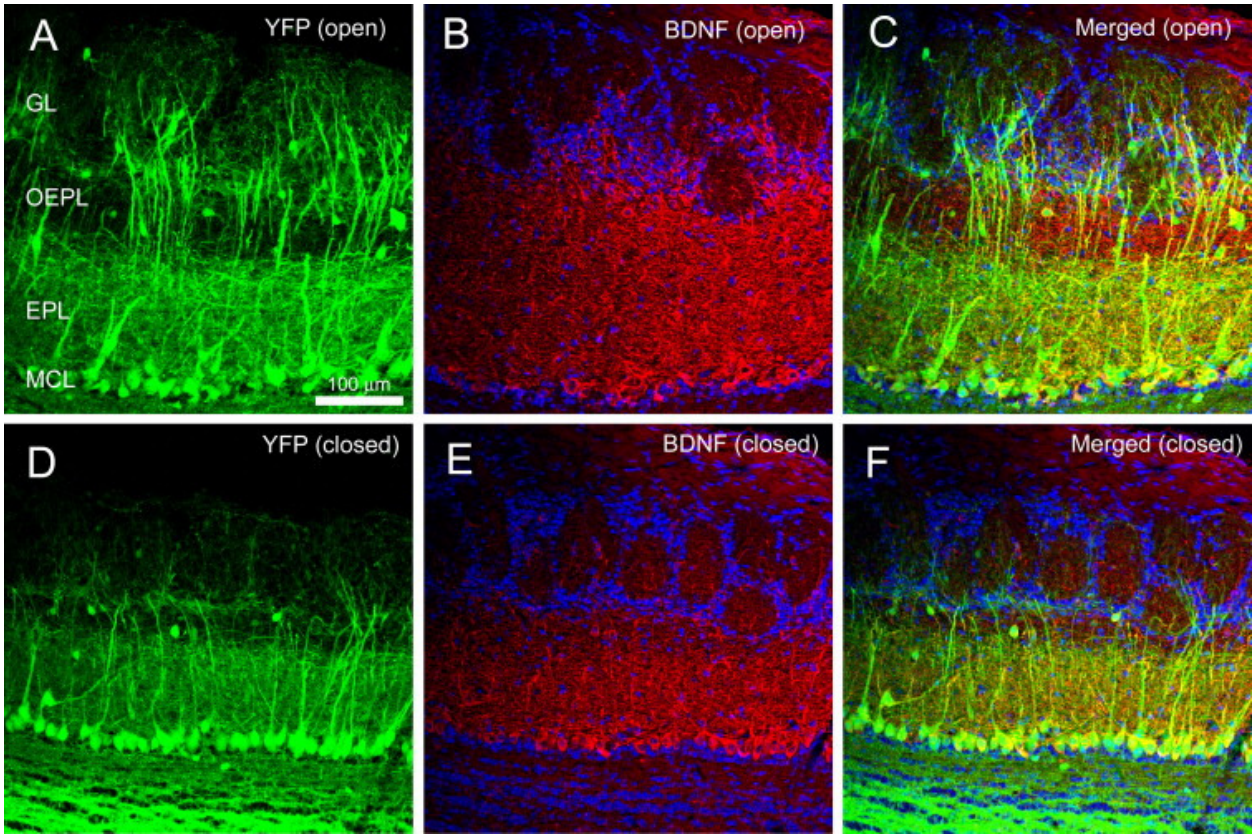

Figure 4.3 BDNF immunoreactive fibers are lost following sensory deprivation.
Representative double-color BDNF immunocytochemistry of the olfactory bulb of *thy1* YFP transgenic mice (YFP) following 30 days of sensory deprivation as imaged on a confocal system. (A) Contralateral control OB (YFP (open)). (B) Same, but demonstrating BDNF-ir (BDNF (open)), and (C) merged image. (D-F) Same as (A-C) but for the OB ipsilateral to the naris-occlusion. EPL, external plexiform layer; GL, glomerular layer; MCL, mitral cell layer; Scale bar = 100 µm.

sensory stimuli (Raff *et al.* 1993). Our correlational biochemistry data may suggest that proBDNF could possibly function as a trophic factor to prevent apoptosis of mitral cells induced by olfactory sensory deprivation. Future experiments would have to be pursued to test this interesting correlation.

Previous studies have revealed that the EPL undergoes the greatest reduction in laminar volume following naris-occlusion (Meisami 1976). Our study using YFP mice may infer that the reduction in EPL thickness following sensory deprivation is due the absence of BDNF-ir fibers in the superficial layer of EPL (oEPL). Although loss of BDNF-ir fibers may not be the sole loss of EPL thickness, genetic deletion of BDNF has been shown to lead to cell and fiber loss in this area of the OB (Berghuis *et al.* 2006). The origin of the oEPL BDNF-ir fibers described here is not clear, but may belong to secondary dendrites of middle-tufted cells since these dendrites ramify into the superficial EPL (Shepherd and Greer 1998). Indeed, Hamilton et al. (2008) have recently shown that middle-tufted cells may undergo trophic changes after adult olfactory-sensory deprivation induced by deafferentation (Hamilton *et al.* 2008). Our data may, therefore, provide preliminary evidence for a functional segregation within the EPL. Recently Clevenger et al. (Clevenger *et al.* 2008) generated mice in which the BDNF promoter drove expression of β-galactosidase in order to effectively map BDNF transcription across the bulb and epithelium. Their data suggest a BDNF transcript signal in the EPL that parallels that of our protein level detection by ICC, but curiously they report no transcript detected in mitral cells (Clevenger *et al.* 2008)-Galactosidase Expression in the Olfactory Epithelium and Bulb}. Since proBDNF is secreted (Blum and Konnerth 2005; Lee *et al.* 2001; Mowla *et al.* 2001) and our biochemistry data support the idea that our ICC is labeling pro and not mature BDNF (as discussed below), absence of transcript in the mitral cells would not be inconsistent with our BDNF-ir specific expression patterns. Although there are reported inconsistencies in mitral cell transcription of BDNF (Clevenger *et al.* 2008)-Galactosidase Expression in the Olfactory Epithelium and Bulb;Conner, 1997, Distribution of brain-derived neurotrophic factor (BDNF) protein and mRNA in the normal adult rat CNS: evidence for anterograde axonal transport.} the majority of studies utilize adult rat, rather than postnatal mice as did our study, and none observed BDNF levels in mice following naris cauterization from birth (McLean *et al.* 2001).

The high affinity receptor for mature BDNF, TrkB, is present in various cell types within the rat OB (Fryer *et al.* 1996) and is predominantly expressed as a full-length receptor

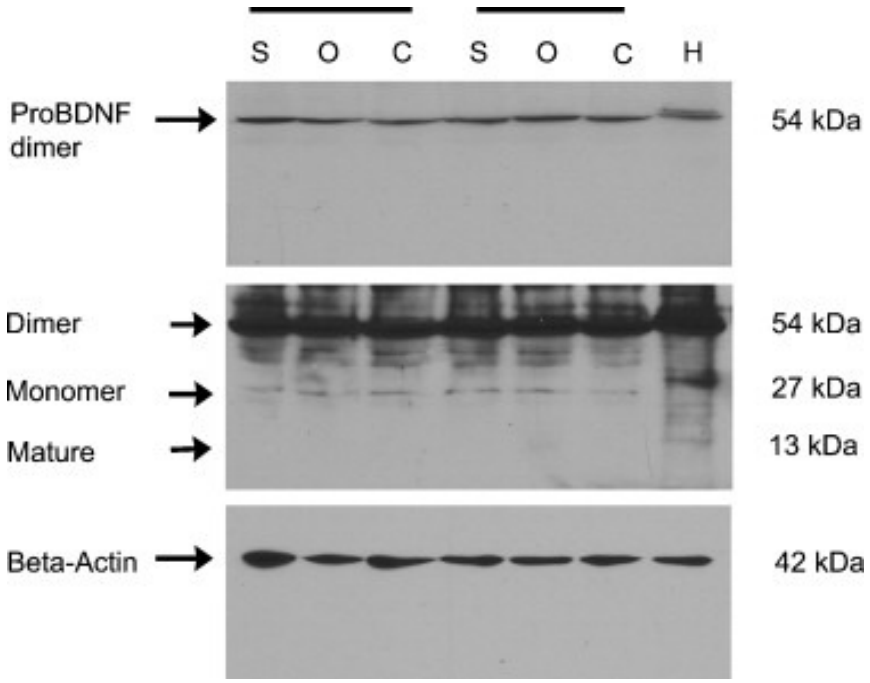

Figure 4.4 Confirmation of antiserum specificity by Western blot analysis. Shown are detergent-solubilized (NP-40) protein fractions electrophoretically separated using 15% SDS PAGE. Two representative trial blocks are shown (horizontal bars) for sham treatment (S), contralateral control OB (O, open), and ipsilateral naris-occluded OB (C, closed). H, rat hippocampus. Top blot: proBDNF dimer is observed following a short exposure (30 s) of the film. Middle blot: Same blot, but a longer exposure (5 min) was used to visualize the pro-BDNF monomer (Monomer) and mature BDNF (Mature). Bottom blot: Nitrocellulose was stripped and reprobed for beta-actin to demonstrate equal protein loading across treatments.

(Tucker and Fadool 2002). Consequently it was surprising that we did not find a mature form of the receptor's preferred ligand, BDNF, but rather could only resolve the precursor, proBDNF. It is possible that there exists a species difference across rodents, given that biochemical, immunocytochemical and *in situ* hybridization studies have independently revealed the presence of both pro- and mature BDNF in the rat OB (Conner *et al.* 1997; McLean *et al.* 2001). Cao et al. (Cao *et al.* 2007), however, detect slight amounts of mature BDNF from crude mouse OB extracts, therefore it is likely that the detection limits of mature BDNF by SDS-PAGE in mouse OB has been reached. In fact, the mouse OB has little BDNF (0.5 ng/g wet weight) that could be detected at P30 using an ELISA method (Katoh-Semba *et al.* 1998). ELISA cannot distinguish between the two forms of BDNF (Michalski and Fahnestock 2003), so presumably this quantity represents both forms.

Our Western analysis indicated a minor band of 27 kDa and a major band of 54 kDa representing proBDNF and proBDNF dimer, respectively. The control, rat hippocampus, revealed an additional band at 13 kDa representing mature BDNF and a cluster of high molecular weight bands presumably corresponding to the glycosylated forms of the mature BDNF(Mowla *et al.* 2001). Preadsorption of the same antiserum used in our study with BDNF has been shown by Western analysis to quench the proBDNF, but not the mature BDNF, band observed in human cortex (Michalski and Fahnestock 2003), which strongly infers that our immunocytochemical signal is proBDNF. If the signal is predominantly proBDNF and not mature BDNF, and two different BDNF-ir cell populations within the bulb are oppositely affected by naris-occlusion (mitral cell BDNF-ir is elevated while juxtaglomerular cell BDNF-ir is decreased), then it follows that no net change in pixel density of proBDNF might be expected due to a cross-nulling effect.

ProBDNF has been considered an inactive precursor prior to cleavage by the serine protease plasmin and selective matrix metalloproteinases (Blum and Konnerth 2005; Lee *et al.* 2001; Mowla *et al.* 2001). The cleaved (mature) BDNF can activate TrkB receptors and promote cell survival and synaptic plasticity. Alternatively, proBDNF may directly bind to and activate TrkB receptors to promote mitral cell survival. In support of this idea, furin-resistant proBDNF, secreted from COS-7 cells, is known to bind to the extracellular domains of both TrkB and p75NTR (Fayard *et al.* 2005). Fayard et al. (Fayard *et al.* 2005) demonstrate that proBDNF

binds to and activates TrkB and could be involved in TrkB-mediated neurotrophic activity *in vivo*. In human Alzheimer's disease, a pathological condition of extreme apoptosis, it is quite intriguing that proBDNF levels decrease in the parietal cortex (Michalski and Fahnestock 2003).

Conclusion

In summary, our data provide evidence for a neurotrophic role of proBDNF in the mouse olfactory system. Most OB neurons are interneurons that have short life spans and are replaced by neurons migrating from the subventricular zone (Whitman and Greer 2007). ProBDNF may provide the neurotrophic environment necessary for a continuous degenerative/regenerative process inherent in the olfactory system (Graziadei and Monti Graziadei 1985). In fact, BDNF signaling has recently been shown to affect olfactory terminal-arbor pruning under competitive environments (Cao *et al.* 2007).

CHAPTER FIVE

BDNF AND PROBDNF HAVE SEPARATE ROLES IN THE MOUSE OLFACTORY BULB[4]

Introduction

The loss of sensory afferents (i.e. inputs) induces cell death in target brain regions or nuclei (Bush *et al.* 2008; Leon 1998; Najbauer and Leon 1995; Nucci *et al.* 2003; Scholz *et al.* 2005). The type of neuron that will die following sensory deprivation is different across modalities and is tissue specific. Visual (Nucci *et al.* 2003) and auditory (Bush *et al.* 2008) nuclei affected by sensory loss respond by losing relay or projection neurons. Interneurons die following loss of sensory input to the spinal cord dorsal horn (Scholz *et al.* 2005) and to the OB (Kim *et al.* 2006a; Leon 1998; Najbauer and Leon 1995; Yamaguchi and Mori 2005). OB interneuron death can be induced by both deafferentation (direct insult to the peripheral neuron) (Kim *et al.* 2006a; Margolis *et al.* 1974) and by sensory deprivation (indirect insult by loss of odorant stimulation) (Brunjes *et al.* 1985; Kelsch *et al.* 2009; Najbauer and Leon 1995; Yamaguchi and Mori 2005). Although olfactory sensory deprivation was originally developed as a model to study neonatal olfactory bulb development (Brunjes *et al.* 1985; Meisami 1976), this model of neuronal insult works well in the adult mouse OB (Baker *et al.* 1993; Biju *et al.* 2008; Kelsch *et al.* 2009; Kim *et al.* 2006a; Yamaguchi and Mori 2005).

Mouse OB interneurons are differentially sensitive to sensory deprivation. Catecholamine interneurons, in the glomerular layer, have been shown to be particularly sensitive to sensory-deprivation. In the deprived OB relative to control OB, catecholamine loss has been measured by lower OB dopamine concentrations (Baker *et al.* 1993; Baker *et al.* 1988; Brunjes *et al.* 1985), lower TH expression and activity (Baker *et al.* 1993), loss of tyrosine hydroxylase immunoreactive neurons (Kelsch *et al.* 2009; Kim *et al.* 2006a; Yamaguchi and Mori 2005), and increased DNA fragmentation in the glomerular layer (Najbauer and Leon 1995). The mechanism underlying interneuron cell loss in the mouse OB is not yet known. After sensory deprivation granule cells, the other major class of OB interneurons, express the

[4] Portions of this chapter are to be submitted to *Neuroscience* and are formatted accordingly.

apoptotic enzyme activated-caspase 3 (Yamaguchi and Mori 2005) whereas catecholamine neurons express activated-caspase 3 prior to methamphetamine-induced apoptosis (Deng *et al.* 2007).

Previously we investigated the role of brain-derived neurotrophic factor (BDNF) following OB sensory deprivation. BDNF immunohistochemistry revealed a selective loss of BDNF-immunoreactive fibers from the external plexiform layer (Biju *et al.* 2008). This layer is known to shrink in size following naris-occlusion (Cao *et al.* 2007; Meisami 1976) and contains processes of glomerular interneurons (Shepherd and Greer 1998). At the same time, mitral cells, an olfactory bulb output neuron, appeared to gain BDNF immunoreactivity. We also found that the major BDNF isoform was unprocessed proBDNF (Biju *et al.* 2008). Neurotrophins are secreted as a 'pro' isoform (i.e. proBDNF, proNGF) (Lee *et al.* 2001) that requires processing by an extracellular protease that will cleave the pro domain from the mature neurotrophin. ProBDNF has been considered an inactive precursor prior to cleavage by the serine protease plasmin and selective matrix metalloproteinases (Blum and Konnerth 2005; Lee *et al.* 2001; Mowla *et al.* 2001; Pang *et al.* 2004). The mature BDNF can activate tyrosine receptor kinase B (TrkB) receptors and promote cell survival and synaptic plasticity (Blum and Konnerth 2005). ProBDNF can also directly bind to and activate TrkB receptors (Fayard *et al.* 2005). Proneurotrophins have a higher affinity for the p75 neurotrophin receptor (p75NTR) than for Trk receptors (Kalb 2005; Lee *et al.* 2001; Reichardt 2006) and proneurotrophin activation of the p75NTR can induce cell death (Beattie *et al.* 2002; Kalb 2005; Lee *et al.* 2001; Reichardt 2006; Teng *et al.* 2005). Interestingly, mouse mitral cells express TrkB (Colley *et al.* 2007; Imamura and Greer 2009), do not express p75NTR (Cao *et al.* 2007; Imamura and Greer 2009) and respond to BDNF stimulation with a reduction in voltage-gated potassium current *in vitro* (Colley *et al.* 2004; Tucker and Fadool 2002). Glomerular layer interneurons express p75NTR (Cao *et al.* 2007; Imamura and Greer 2009) and not TrkB (Imamura and Greer 2009). Our goal, therefore, was to investigate a direct action of proBDNF on mitral cells via the TrkB receptor kinase.

In the present study we tested the hypothesis that proBDNF alters adult mouse OB function both acutely and chronically by action on two different neurotrophin receptors expressed by different neuron types. Acute affects by proBDNF were predicted to be mediated by the mitral cell TrkB receptor and could be measured by changes in electrical excitability.

Conversely, proBDNF chronic affects were predicted to be mediated by the glomerular interneuron p75NTR and could be measured by an increase in activated-caspase 3 expression and a loss of tyrosine hydroxylase expression.

Materials and Methods

Unilateral-naris occlusion procedures

Postnatal day (P) 30-35 C57BL/6 mice (Jax Laboratories, Jacksonville, FL, USA) were anesthetized with isoflurane and the left naris was cauterized using a heated metal probe inserted 1-2 mm into the nostril as described previously (Biju *et al.* 2008; Meisami 1976; Tucker and Fadool 2002). Scar formation resulted in permanent unilateral-naris closure. Five days later complete closure of the cauterized nostril was confirmed by visual examination under a dissecting microscope. Sham animals had the heated metal probe placed on the tip of the snout. Naris-occlusions were performed at 2 pm (circadian time), a time at which the mice in our colony briefly awaken for a meal (personal communication, Dr. Kristal Tucker). All procedures were carried out as approved by the Florida State University Laboratory Animal Resources and the National Institutes of Health.

Antisera and neurotrophins

The anitserum for activated caspase-3 was used at a final dilution of 1:100 (Promega, Madison, WI, USA) and antiserum for tyrosine hydroxylase was used at 1:4,000 (ImmunoStar, Hudson, WI, USA). Neurotrophins were made as a 1µM stock solution in 0.1% bovine serum albumin (BSA) in phosphate-buffered saline (PBS) and frozen as individual aliquots at -80ºC until use. Recombinant cleavage-resistant, mouse probrain-derived neurotrophic factor (proBDNF, B-243) and recombinant human BDNF (B-250) were from Alomone (Alomone, Jerusalem, IL). PBS was made as previously (Tucker and Fadool 2002). All other reagents were from Sigma-Aldrich or Fisher Scientific (Suwannee, GA, USA).

Intranasal delivery

Neurotrophin intranasal delivery (IND) was performed as described before (Marks *et al.* 2009). Briefly, P 30-35 mice were hand-restrained, placed in a supine position, and given three, ten microliter drops of 10 ng/µl BDNF or proBDNF into both nares simultaneously. The 0.01% BSA/PBS neurotrophin diluent was used as a vehicle control (PBS). Following IND mice were

held supine for 5–10 sec after delivery to ensure all fluid was inhaled. Ninety µl was delivered to each mouse per day for 5 days. The IND protocol was conducted at 2 pm (circadian time). Intranasally delivered insulin-like growth factor reaches the OB with an efficiency of 0.11% (Thorne *et al.* 2004). Based on this efficiency, the molecular weight of BDNF, and the mass of the mouse brain (Williams *et al.* 2001), the effective dose reaching the OB was calaculated to be between 0.2 to 4 nM BDNF, which is close to the reported concentration of OB BDNF (Katoh-Semba *et al.* 1998; Schulte-Herbrüggen *et al.* 2008). Five days after performing naris-occlusion and one day after the fifth day of IND, animals were perfused using paraformaldehyde dissolved in phosphate-buffered saline (4%PFA/PBS). The OBs were then dissected and post-fixed in 4% PFA/PBS for 4 hours (h). OBs were cryoprotected by incubation in 30% sucrose/PBS overnight at 4ºC and then stored in optimal cutting temperature medium (Sakura, Torrance, CA, USA) at -80 ºC until further use. Sixteen µm coronal sections were cut on a crytostat, placed onto pre-treated slides (superfrost plus, Fisher) and stored at -20^{o}C until use with immunofluorescence.

Immunofluorescence

Sections were air-dried on the bench for 60 minutes, re-hydrated with PBS, and then incubated for 60-minute in blocking solution (5% normal goat serum/2.5% BSA/0.3% triton in PBS). After the block, sections were rinsed with 0.3% triton/PBS and incubated with antiserum in blocking solution overnight at 4ºC in a darkened, humidified chamber. Immunofluorescence was detected with either goat anti-rabbit Cy3 or goat anti-mouse Cy3 in PBS (1:400; Jackson Immunoresearch, PA, USA). Following three washes in PBS, cells were counter-stained with a five-minute incubation in diamidino-phenyindole (DAPI, Fisher) in PBS (1:20,000), washed again in PBS and coverslipped with Fluoromount G (SouthernBiotech, Birmingham, AL, USA) to prevent photobleaching. Image brightness and contrast were adjusted with Adobe Photoshop CS (Adobe Systems Inc., San Jose, CA) for maximal clarity.

Anatomical analysis

Three animals of each treatment condition (sham and naris occluded; intranasal delivery of PBS, proBDNF or matureBDNF) were sampled. Immunoreactive glomerular cells (including both peri- and juxtaglomerular cells) within 12 fields of view (each 93,500 µm^2) per animal were counted using Neurolucida (MicroBrightField, Colchester, VT, USA). Immunoreactive-TH cells had clearly defined soma and perinuclear labeling. Activated-caspase 3 immunoreactive cells

had punctate labeling near the nucleus as defined by DAPI. These 12 fields of view were from representative sections evenly distributed from the rostral to caudal aspects of the OB (3 sections total). On each section, a field of view was taken from the dorsal, ventral, medial, and lateral glomerular layers of the OB. The counts from these 12 fields of view were then averaged for the analysis. To calculate the total area for the counted OB sections (i.e. the entire OB including both the counted and uncounted fields of view) Neurolucida was used to trace the entire section and then the three sections per animal and per treatment were summed. Using Prizm software (version 4, GraphPad, San Diego, CA, USA) statistical significance was determined at the 95% confidence level via an one-way analysis of variance (ANOVA) with a Student-Newman-Kewls post-hoc test to separately compare the cell counts across treatment groups.

Slice preparation

Postnatal day 15-35 (P15-35) mice were anesthetized to a surgical plane using gaseous isoflurane in a bell jar (Aerrane; Baxter, Deerfield, IL). The animals were rapidly decapitated and the OBs exposed by removing the dorsal and lateral portions of the cranium between the cribriform plate and the lambda suture (De Saint Jan and Westbrook 2007). After removing the dura, the OBs were quickly removed, glued down to a sectioning block with Superglue and submerged in oxygenated, ice-cold, sucrose-modified artificial cerebrospinal fluid (ACSF). Sucrose-modified ACSF contained (in mM): 83 NaCl, 26.2 $NaHCO_3$, 1 NaH_2PO_4, 3.3 $MgCl_2$,0.5 CaCl2, 72 sucrose, and 20 D-glucose; 310-320 mOsm, pH 7.3. Horizontal sections (275- 350 µm) were cut in oxygenated, ice-cold, sucrose-modified ACSF using a Series 1000 Vibratome. Sections were then incubated in oxygenated, sucrose-modified ACSF at 33ºC for 30 minutes and then maintained at room temperature in normal ACSF until needed (Nickell *et al.* 1996). ACSF contained (in mM): 119 NaCl, 26.2 $NaHCO_3$, 1 NaH_2PO_4, 2.5 KCl, 1.3 $MgCl_2$, 2.5 $CaCl_2$ and 20 D-glucose; 300-310 mOsm, pH 7.3. OB slices were continuously perfused with standard ACSF plus synaptic blockers (5 µM NBQX and 25 µM APV; Ascent Scientific, Princeton, NJ) (Ismatec; 2 ml/min).

Electrophysiology

Membrane voltage was measured in the whole-cell configuration and controlled by pClamp 9 software coupled with an Axopatch 200B amplifier (Molecular Devices, Sunnyvale, CA, USA). The analog signal was filtered at either 2 or 5 kHz and minimally digitally sampled

every 100 µs. OB slices were visualized at 10X and 40X using an Axioskop 2FS Plus microscope (Carl Zeiss, Thornwood, NY, USA) equipped with infrared, differential interference contrast detection capabilities (Dage MT1, CCD100). The patch pipettes were fabricated from borosilicate glass (Hilgenberg #1405002, Malsfeld, Germany). The OB pipette solution contained (in mM): 135 potassium gluconate, 10 KCl, 10 HEPES, 10 EGTA, 1 $MgCl_2$, 0.3 Tris GTP, and 4 MgATP; 285-295 mOsm, pH 7.3. Pipette resistance ranged from 5-8 MΩ. Mitral cell bodies were confirmed by soma size (15-30 µm) in the mitral cell layer (Balu *et al.* 2004; Chen and Shepherd 1997). Cells that failed to have a resting membrane potential of at least -50 mV, a stable input resistance of at least 150 MOhms, and repetitive spiking in response to current injection were discarded from analysis due to biophysical indicators of poor health. Resting membrane potential was recorded, and adjusted to -65 mV for consistency between cells (Balu *et al.* 2004; Chen and Shepherd 1997). The presented values were not adjusted for the 14 mV calculated junction potential. Cells were injected with a series of 10 current steps ranging from -50 to +175 pA for 1000 ms. After establishing baseline evoked responses the bath solution was changed to one containing: cleavage resistant BDNF (10 ng/ml), proBDNF (10 ng/ml) or Margatoxin (MgTX) (1 nM; EMD Chemicals, San Diego, CA, USA). After approximately ten minutes of neurotrophin or toxin bath application, the cells were again injected with the series of current steps. The evoked firing frequency and burst analysis (three or more spikes with an interval less than 100 ms) at each current step before and after bath application was analyzed in Clampfit9 (Molecular Devices). Prizm software (version 4, GraphPad, San Diego, CA, USA) was used to determine statistical significance at the 95% confidence level with a two-way analysis of variance (ANOVA) for neurotrophin or toxin effect and a *Bonferoni* post-hoc test to separately compare current steps.

Results

BDNF increases mitral cell excitability

The mouse OB contains little mature BDNF, but does express proBDNF, the precursor to mature BDNF (Biju *et al.* 2008). We have also demonstrated that BDNF stimulation of mitral cells *in vitro* reduces the total potassium current (Colley *et al.* 2004). This current reduction is dependent upon TrkB phosphorylation of the *Shaker* voltage-gated potassium channel (Kv), Kv1.3 (Colley *et al.* 2009; Colley *et al.* 2004; Colley *et al.* 2007; Tucker and Fadool 2002).

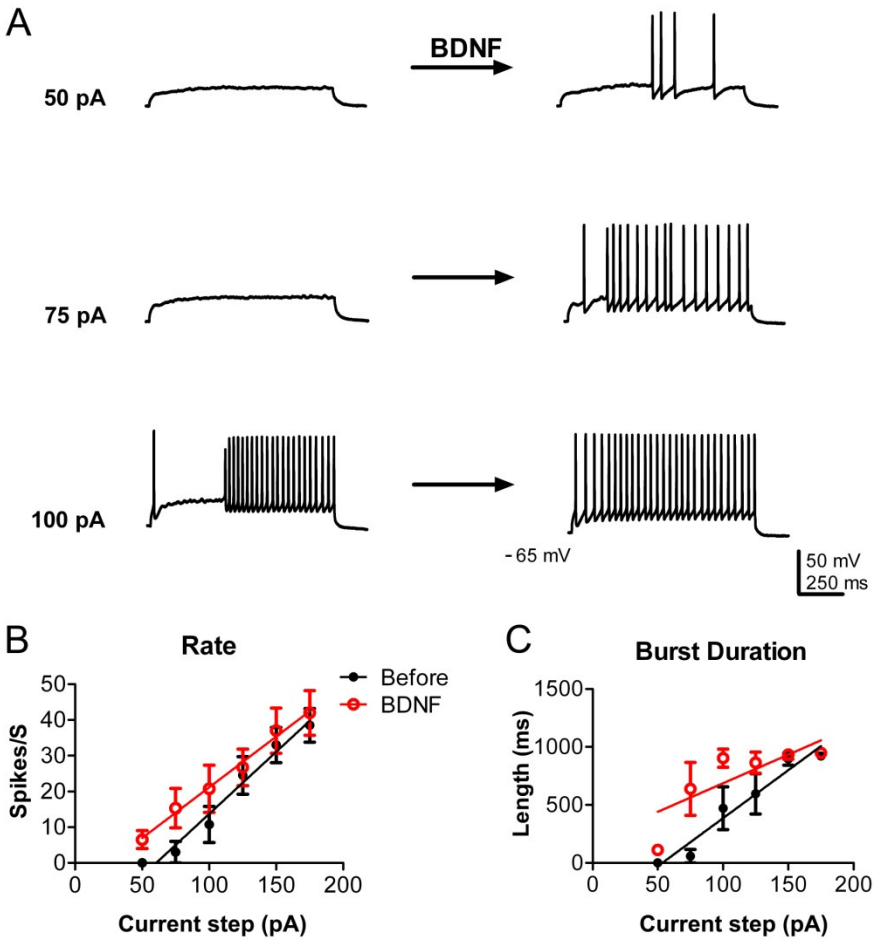

Figure 5.1 BDNF increases mitral cell excitability. (A) Representative current-clamp recordings from a single mitral cell in the whole-cell configuration. Responses are shown to 1000 ms current injections of: 50, 75, 100 pA before (left) and approximately 10 min after 10 ng/ml BDNF bath application (right). (B) Graph of the mean number of spikes (± s.e.m) evoked at each current injection. (C) Graph of mean burst duration (± s.e.m) at each current injection. BDNF has a significant treatment effect for both parameters; two-way ANOVA (N= 4; $p \leq 0.05$). Holding potential (-65 mV) and scale bars shown in the last recording in (A) apply to all traces.

Therefore, we hypothesized that both proBDNF and BDNF are active ligands in the mouse OB. We first sought to establish that BDNF increases mitral cell excitability, as measured by action potential generation in an OB slice preparation. Mitral cells were identified in OB slices as large, pyramidal cells in a discreet layer when viewed with infrared optics and continuously perfused with ACSF containing fast synaptic blockers (see Methods). Cells were stimulated with series of ten 1000 ms current injections ranging from -50 to 175 pA. After establishing a baseline response the bath solution was then changed to ACSF plus 10 ng/ml BDNF. Ten to fifteen minutes later, cells were again stimulated with the same series of current injections. After BDNF bath application mitral cells tended to fire action potentials at lower current injections than before (Figure 5.1A). Overall, mitral cells fired significantly more action potentials after BDNF bath application (N= 4, BDNF treatment effect, two-way ANOVA, $\alpha \leq 0.05$) (Figure 5.1B). Additionally, bursts of action potentials were significantly longer after BDNF (N= 4, BDNF treatment effect, two-way ANOVA, $\alpha \leq 0.05$) (Figure 5.1C). Although proBDNF has been reported to bind to and activate TrkB (Fayard *et al.* 2005), unlike BDNF, bath application of cleavage-resistant proBDNF did not induce mitral cells to fire more action potentials at lower current injections (Figure 5.2A). Denatured BDNF (BDNF heated to 95ºC for 10 minutes) served as a protein control and also had no effect on mitral cell excitability (Figure 5.2B). Neither proBDNF nor the denatured BDNF negative control significantly altered mitral cell excitability as measured by frequency (N= 4, proBDNF treatment effect, two-way ANOVA, $\alpha \geq 0.05$) (Figures 5.2C and E) and burst duration (N= 4, denatured BDNF treatment effect, two-way ANOVA, $\alpha \geq 0.05$) (Figures 5.2D and F). None of the treatments (BDNF, proBDNF, and denatured BDNF) significantly altered the latency to first spike (data not shown).

Margatoxin increases mitral cell excitability

BDNF has been demonstrated to induce TrkB-dependent phosphorylation of Kv1.3 (Colley *et al.* 2009; Colley *et al.* 2004; Colley *et al.* 2007; Tucker and Fadool 2002) resulting in a reduced mitral cell Kv1.3 current (Colley *et al.* 2004; Tucker and Fadool 2002). BDNF modulation of the Kv1.3 current can be prevented with pre-incubation the selective Kv1.3 pore blocker margatoxin (MgTX) (Colley *et al.* 2004). There are no reports demonstrating MgTX block of mitral cell Kv1.3 currents or any reports on MgTX-induced increases in action potential production in a slice preparation. Mitral cells were therefore stimulated with the same series of current injections before and after bath application of 1 nM MgTX. MgTX at this concentration

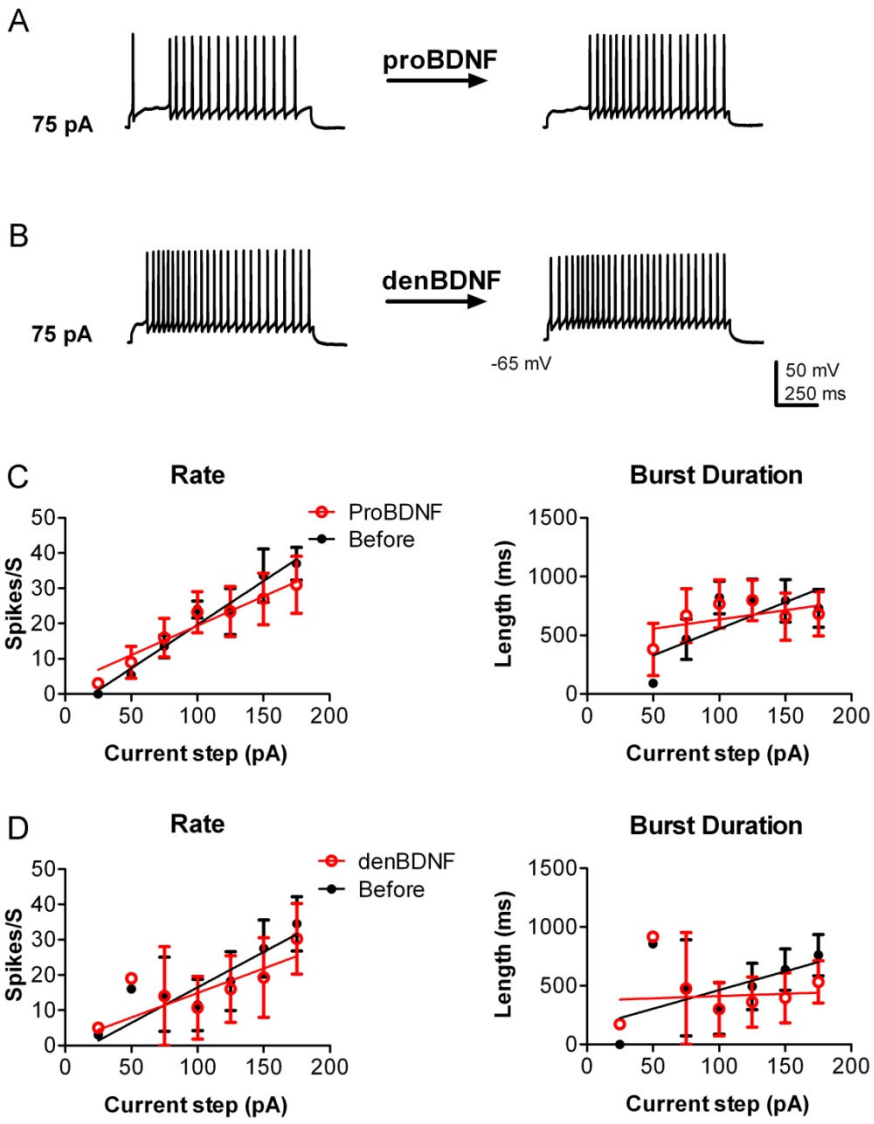

Figure 5.2 Neither proBDNF nor denatured BDNF increase mitral cell excitability. (A-B) Representative current-clamp recordings from two mitral cells in the whole-cell configuration. Responses are shown to a 75 pA, 1000 ms current injection before (left) and approximately 10 min after (right) bath application of either 10 ng/ml proBDNF (A) or 10 ng/ml denatured BDNF (B, denBDNF). (C) Graphs of the mean number of spikes (± s.e.m) and of the mean burst duration (± s.e.m) at each current injection before and after proBDNF. (D) Same as C except with denatured BDNF (dBDNF). Neither treatment has a significant effect upon either parameter; two-way ANOVA (N= 4; $p \geqq 0.05$). Holding potential (-65 mV) and scale bars shown in the last recording in (B) apply to all traces.

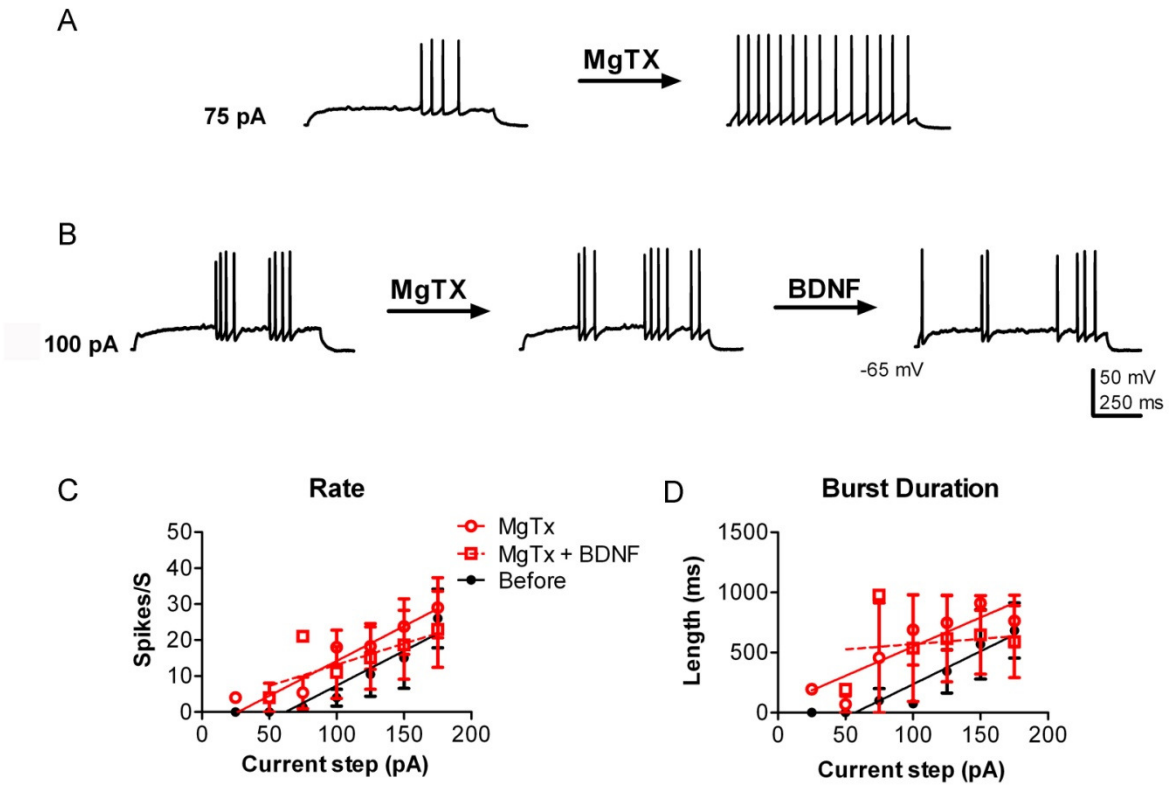

Figure 5.3 Margatoxin increases mitral cell excitability. (A-B) Representative current-clamp recordings from two mitral cell in the whole-cell configuration. (A) Reponses are shown to a 75 pA, 1000 ms current injection before (left) and approximately 10 min after (right) bath application of 1 nM Margatoxin (MgTX). (B) Pretreatment with MgTX blocks BDNF effect (N=3). (C) Graph of the mean number of spikes evoked (± s.e.m) at each current injection. (D) Graph of the mean burst duration (± s.e.m) at each current injection. MgTX has a significant treatment effect for both parameters; two-way ANOVA (N= 5; $p \leq 0.05$). Holding potential (-65 mV) and scale bars shown in the last recording in (A) apply to all traces.

partially blocks homomeric Kv1.3 channels, but not heteromeric Kv1.3 channels in non-neuronal cell types (Menteyne *et al.* 2009; Vicente *et al.* 2006). Similar to the effect of BDNF, mitral cells treated with MgTX tended to fire action potentials at lower current injections than before the bath application (Figure 5.3A). Importantly, the effect of BDNF was completely blocked in neurons that were pre-incubated with MgTX(Figure 5.3B). Equally as important, MgTX significantly increased mitral cell excitability as measured by frequency (N= 5, MgTX treatment effect, two-way ANOVA, $\alpha \leq 0.05$) (Figure 5.3C) and by burst duration (N= 5, MgTX treatment effect, two-way ANOVA, $\alpha \leq 0.05$) (Figure 5.3D). MgTX did not significantly alter the latency to first spike (data not shown).

Intranasal delivery of proBDNF mimics naris-occlusion

With proBDNF failing to alter mitral cell excitability in the acute slice preparation, we surmised that it may have a chronic effect. We decided to investigate the p75NTR, through which proBDNF induces apoptosis *in vitro* (Koshimizu *et al.* 2009; Teng *et al.* 2005). *In vivo*, adult mouse OB glomerular layer cells express p75NTR (Cao *et al.* 2007; Imamura and Greer 2009) and are prone to sensory deprivation-induced cell death (Najbauer and Leon 1995). We tested whether intranasal delivery (IND) of proBDNF could induce cell loss in the mouse OB glomerular layer *in vivo*. Adult mice were given intranasal PBS, BDNF, or proBDNF once a day for five days and then were sacrificed 24hrs after the last treatment (Weise *et al.* 2005). The mice were fix perfused and the OBs were processed for immunofluorescence (see Methods). Few activated caspase 3 immunoreactive cells were visible in the either PBS (Figure 5.4A) or mature BDNF (Figure 5.4B) treatment groups. In contrast, activated caspase 3 immunoreactive cells was approximately 3-fold more abundant in the proBDNF (Figure 5.4C) treatment group. The effect of proBDNF treatment was significant as compared to either PBS or mature BDNF treatment (N= 3, one-way ANOVA, *snk*, $\alpha \leq 0.05$) (Figure 5.4D). The number of activated-caspase 3 positive neurons is not different between the PBS and mature BDNF treatment groups (Figure 5.4D) (N= 3, one-way ANOVA, *snk*, $\alpha \geq 0.05$). Next we immunolabeled for TH (a marker of glomerular interneurons) following treatment with: PBS (Figure 5.5A), BDNF (Figure 5.5B), or proBDNF (Figure 5.5C). Compared to both PBS and mature BDNF, proBDNF induced a significant reduction in TH immunoreactivity (N= 3, one-way ANOVA, *snk*, $\alpha \leq 0.05$) (Figure 5.5D). Thus, proBDNF simultaneously reduces TH immunoreactivity and enhances activated-caspase 3 immunoreactivity.

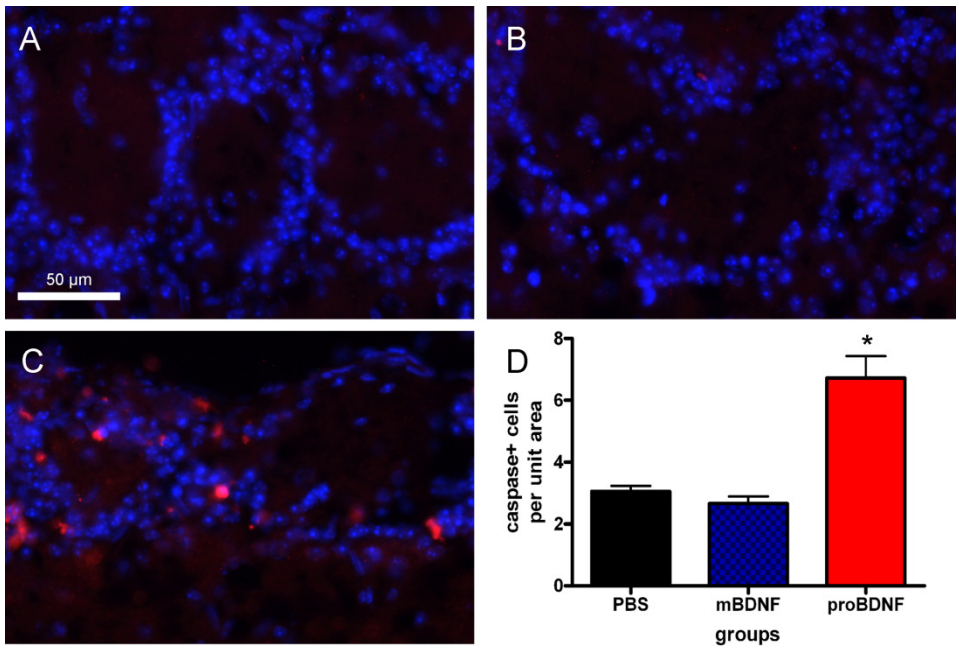

Figure 5.4 ProBDNF intranasal delivery (IND) induces activated-caspase 3 expression. Representative photomicrographs taken of the mouse glomerular layer following a five day treatment of: (A) PBS, (B) mature BDNF, and (C) proBDNF as administered by IND. Cryosections were incubated with activated-caspase 3 antiserum (1:100) (red) and DAPI nuclear stain (blue) to visualize immunoreactive glomerular cells. (D) Bar plot of the mean number (± s.e.m) of activated-caspase 3 immunoreactive glomerular cells per treatment condition per 93,500 μm^2 field of view. * = Significantly-different by a one-way ANOVA, *snk* (N=3, $\alpha \leq 0.05$).

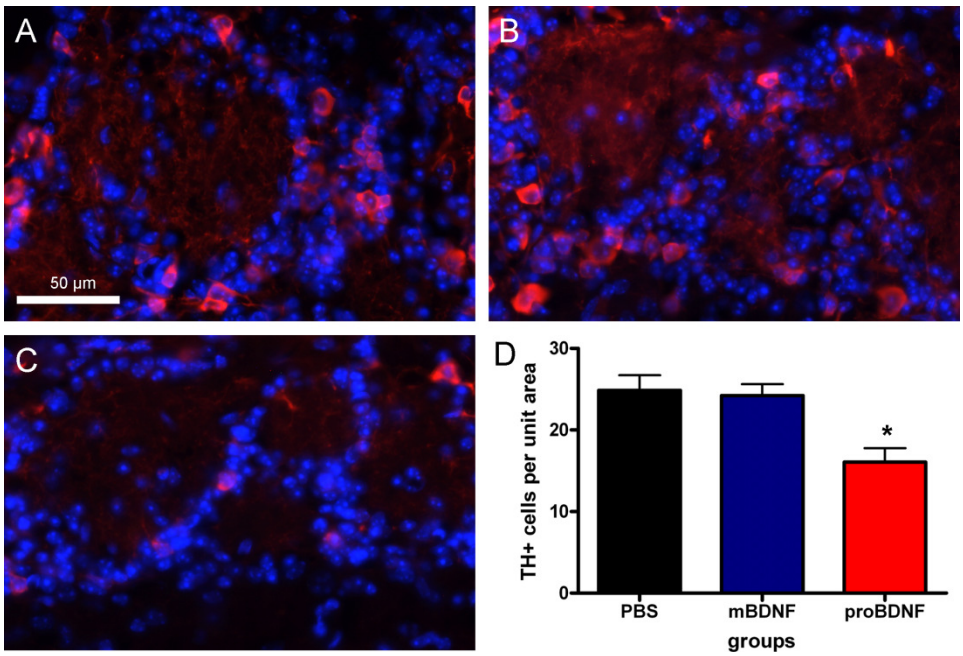

Figure 5.5 ProBDNF intranasal delivery (IND) reduces tyrosine hydroxylase expression. Representative photomicrographs taken of the mouse glomerular layer following a five day treatment of: (A) PBS, (B) mature BDNF, and (C) proBDNF as administered by IND. Cryosections were incubated with tyrosine hydroxylase (TH) antiserum (1:4,000) (red) and DAPI nuclear stain (blue) to visualize immunoreactive glomerular cells. (D) Bar plot of the mean number (± s.e.m) of TH immunoreactive glomerular cells per treatment condition per 93,500 μm^2 field of view. * = Significantly-different by a one-way ANOVA, *snk* (N=3, $\alpha \leq 0.05$).

Next we sought to compare the activated caspase 3 and TH immunoreactivity following olfactory sensory deprivation. Adult mice underwent 5 days of naris-occlusion. Prior to sacrifice, animals were visually confirmed to have complete naris-closure (Biju *et al.* 2008; Meisami 1976). As before, we first investigated activated-caspase 3 immunoreactivity (Figure 5.6). Here the treatment groups consisted of sham (control) (Figure 5.6A), contralateral to the naris-occlusion (open) (Figure 5.6B), and ipsilateral to the naris-occlusion (occluded) (Figure 5.6C). Activated-caspase 3 immunoreactive neurons were significantly more abundant in the glomerular layer following naris-occlusion as compared to either the control or open treatment (one-way ANOVA, *snk,* N=3, $\alpha < 0.05$) (Figure 5.6D). TH immunoreactivity (Figure 5.7) was robust following control (Figure 5.7A) and open (Figure 5.7B) treatment, but weak following naris-occlusion (Figure 5.7C). Naris-occlusion significantly reduced TH immunoreactivity in the OB glomerular layer (N= 3, one-way ANOVA, *snk*, $\alpha < 0.05$) (Figure 5.7D). To control for OB shrinkage following naris-occlusion (Meisami 1976) and possible shrinkage following IND, the total area of each entire OB section was measured (Figure 5.8). Neither 5 days of naris-occlusion did not (N= 3, one-way ANOVA, *snk*, $\alpha \geq 0.05$) (Figure 5.8A) nor 5 days of IND treatment (N= 3, one-way ANOVA, *snk*, $\alpha \geq 0.05$) (Figure 5.8B) significantly altered OB area.

Discussion

ProBDNF is an active ligand in the mouse olfactory bulb. This novel finding was demonstrated when proBDNF IND mimicked adult naris-occlusion. Both treatments resulted in decreased TH and increased activated-caspase 3 immunolabeling in the glomerular layer. This is the first demonstration of a proneurotrophin inducing a marker of apoptosis *in vivo*. ProBDNF did not increase mitral cell excitability. In the OB slice preparation, mitral cells were electrically stimulated via a whole-cell patch-clamp electrode. Bath application of BDNF, but not proBDNF, increased mitral cell spike frequency and initiated spike firing at lower amplitude current injections. Similarly, MgTX also increased mitral cell spike frequency and initiated spike firing at lower amplitude current injections. These are the first data to demonstrate that BDNF modulation of action potential firing n mitral cells mimics the effect of MgTX. Given that MgTX selectively blocks Kv1.3 channels, the mechanism of BDNF modulation of mitral cell excitability is likely via Kv1.3 current suppression.

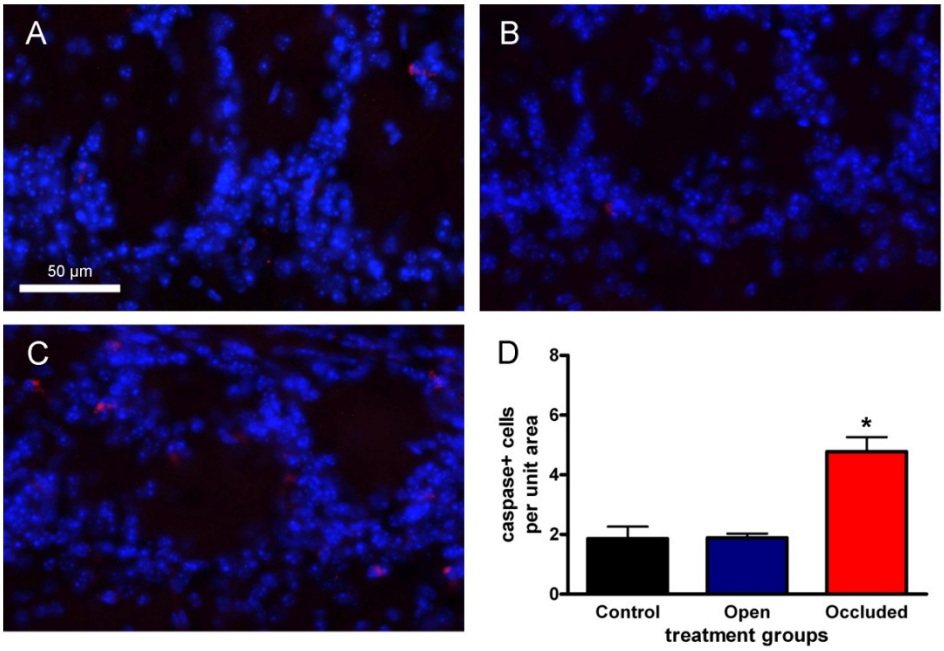

Figure 5.6 Five days of naris occlusion induces activated-caspase 3 expression. Representative photomicrographs taken of the mouse glomerular layer following five days of (A) sham (control), (B) contralateral to the naris occlusion (open), and (C) ipsilateral to the naris occlusion (occluded) treatment. Cryosections were incubated with activated-caspase 3 antiserum (1:100) (red) and DAPI nuclear stain to visualize immunoreactive glomerular cells. (D) Bar plot of the mean number (± s.e.m) of activated-caspase 3 immunoreactive glomerular cells per treatment condition per 93,500 μm^2 field of view. * = Significantly-different by a one-way ANOVA, *snk* (N=3, $\alpha \leq 0.05$).

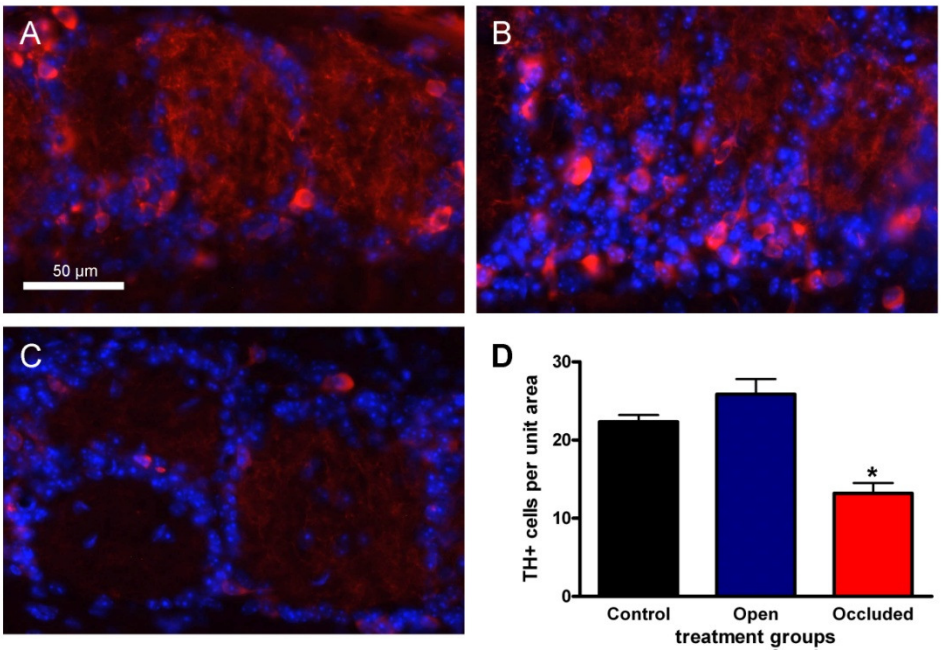

Figure 5.7 Five days of naris occlusion reduces tyrosine hydroxylase expression. Representative photomicrographs taken of the mouse glomerular layer following five days of (A) sham (control), (B) contralateral to the naris occlusion (open), and (C) ipsilateral to the naris occlusion (occluded) treatment. Cryosections were incubated with tyrosine hydroxylase (TH) antiserum (1:100) (red) and DAPI nuclear stain to visualize immunoreactive glomerular cells. (D) Bar plot of the mean number (± s.e.m) of tyrosine hydroxylase immunoreactive glomerular cells per treatment condition per 93,500 μm^2 field of view. * = Significantly-different by a one-way ANOVA, *snk* (N=3, $\alpha \leq 0.05$).

The present data support our previous findings that BDNF inhibits Kv1.3 channels via TrkB induced phosphorylation. Evoked potassium currents in cultured mouse and rat mitral cells are reduced by ~35% after BDNF application (Colley *et al.* 2004; Tucker and Fadool 2002). Cultured mitral cells preteated with MgTX fail to respond to subsequent BDNF stimulation. (Colley *et al.* 2004; Tucker and Fadool 2002). Biochemically, BDNF induces Kv1.3 tyrosine phosphorylation by activating TrkB (Colley *et al.* 2007; Tucker and Fadool 2002). TrkB phosphorylation of and subsequent current reduction of Kv1.3 requires specific tyrosine residues in the channel (Colley *et al.* 2004; Colley *et al.* 2007).

Here we measured the effect of BDNF isoforms on mitral cells in a slice preparation. A physiological concentration of BDNF (10 ng/ml) (Katoh-Semba *et al.* 1998; Schulte-Herbrüggen *et al.* 2008) increased mitral cell frequency at low amplitude current injections but not larger amplitude current injections. It is interesting that BDNF had a stronger effect at lower amplitude current injections. Activation of the insulin receptor, another receptor tyrosine kinase, allows mitral cells to increase spike frequency and spike adaptation at higher amplitude current injections (Tucker *et. al*., submitted). The fact that the unprocessed BDNF isoform, proBDNF (Lee *et al.* 2001), which is also more abundant in the mouse OB (Biju *et al.* 2008; Cao *et al.* 2007) did not alter mitral excitability at any amplitude current injection indicates that mitral cells *in vivo* are likely to be surrounded by suitable concentrations of mature BDNF. Even though the total amount of OB BDNF is still low (Cao *et al.* 2007; Conner *et al.* 1997; Katoh-Semba *et al.* 1998). We conjecture that plasminogen and tissue plasminogen activator—the enzymatic system that cleaves proBDNF in the hippocampus (Pang *et al.* 2004)—are expressed in the extracellular space around mitral cells creating local gradients for both proBDNF and mature BDNF.

Our pharmacological results compare well with data showing that low concentrations of 4-aminopyridine (4-AP), a broad potassium channel blocker (Choquet and Korn 1992; Yeh *et al.* 1976), increased mitral cell firing frequency and burst length (Balu *et al.* 2004). Electrically-stimulated mitral cells generate sub-threshold oscillations that involve the slow-inactivating potassium current (Balu *et al.* 2004; Chen and Shepherd 1997). The slow-inactivating potassium current I_D is associated with Kv1.3 (Balu *et al.* 2004; Bean 2007; Fadool and Levitan 1998). 4-AP is thought to increase mitral cell evoked activity and burst length through channels containing Kv1.3 and other *Shaker* subunits (Balu *et al.* 2004). The 1.0 nM MgTX concentration used in the present studies partially blocks Kv1.3 homomeric channels and

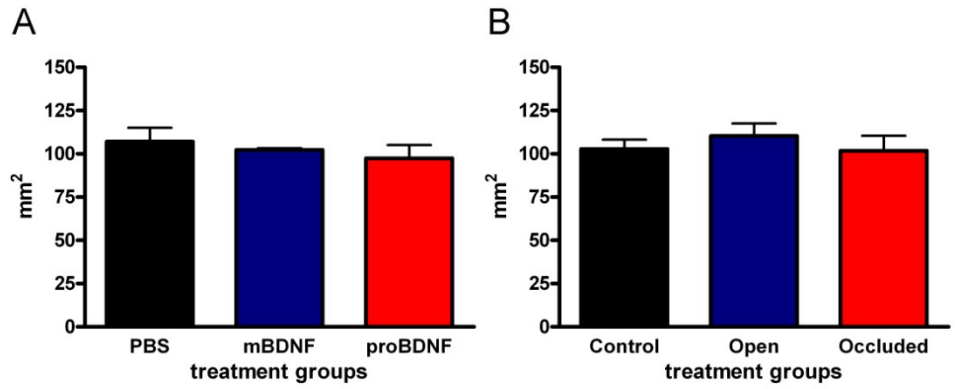

Figure 5.8 Neither naris-occlusion nor intranasal delivery (IND) reduces OB size. Bar plots of the mean area (± s.e.m) of the OB sections used for the quadrant counts analyzed in Figures 5.4-5.7. (A) Bar plot comparing mean OB area (± s.e.m) in the PBS, mature BDNF (mBDNF) and proBDNF treatment groups. (B) Bar plot comparing mean OB area (± s.e.m) in the sham (control), contralateral (open) and ipsilateral (occluded) to the naris-occlusion treatment groups. Not significantly different means by a one-way ANOVA, *snk* (N=3, $\alpha \leq 0.05$).

not heteromeric Kv1.3 channels in non-neuronal cells (Menteyne *et al.* 2009; Vicente *et al.* 2006). Thus, the specific *Shaker* alpha subunits present in mitral cells is not known, but the MgTX concentration used here reveals a role for Kv1.3. MgTX was cloned from scorpion venom and was originally found to maximally inhibit Kv1.3 currents at 110 pM (Garcia-Calvo *et al.* 1993). At 1.0 nM MgTX may inhibit Kv1.1 currents (Koch *et al.* 1997), but it has no effect on Kv1.2 (Gutman *et al.* 2005), Kv1.4 (Gutman *et al.* 2005), Kv1.5 (Gutman *et al.* 2005; Vicente *et al.* 2006), Kv1.6 (Garcia-Calvo *et al.* 1993; Gutman *et al.* 2005), and Kv1.7 and Kv1.8 (Gutman *et al.* 2005). Furthermore in tissue preparations, 1.0 nM MgTX has been used to separate Kv1.3 currents in choroid plexus (Speake *et al.* 2004), 5 nM MgTX has been used on aspiny forebrain neurons (Deng *et al.* 2005), and 10 nM MgTX has used to increase presynaptic excitability in the calyx of Held (Nakamura and Takahashi 2007). Thus, the MgTX concentration used here is likely specific to Kv1.3 homomers. It is interesting to speculate that cells that gave weak response to our low MgTX concentration might respond more vigorously to a higher concentration that also blocks heteromeric Kv1.3 channels, providing evidence for multiple *Shaker* currents. Other work in our laboratory suggests that Kv1.3 forms heteromers with other *Shaker* subunits in the OB, which are potentially modulated by adaptor proteins and phosphorylation (Marks and Fadool 2007). Heterogeneity in mitral cells might exist based upon Kv subunit stoichiometry and channel interactions with adaptor proteins. Lastly, it has been recently proposed the heterogeneous responses of mitral cells to current injections may add to neural coding of odors (Padmanabhan and Urban 2010).

Unlike biophysical data previously reported in rat mitral cells, we did not see any changes in the latency to first evoked action potential (Balu *et al.* 2004). This is likely due to differences in experimental design. In those experiments, mitral cells were stimulated with longer current injections (5s). The resulting latencies (800 to 1200 ms) were nearly as long as our pulse duration (1s) and were highly variable (± 150 ms) (Balu *et al.* 2004). Therefore, it is not surprising that no effect on the latency to first evoked action potential was detected.

When proBDNF failed to increase mitral cell excitability we explored an alternative function in the glomerular layer. Sensory deprivation via naris-occlusion reduces the number of proBDNF immunoreactive glomerular cells (Biju *et al.* 2008) and induces cell death in the OB glomerular layer (Najbauer and Leon 1995). Glomerular interneurons express p75NTR (Cao *et al.* 2007; Imamura and Greer 2009) that can induce apoptosis (Kalb 2005). Both proBDNF and

pro-nerve growth factor (proNGF) have a higher affinity for the p75NTR than for their respective Trk receptor (Kalb 2005; Lee *et al.* 2001; Reichardt 2006). The increased affinity for p75NTR by proneurotrophins is likely due to binding to the p75NTR co-receptor sortilin (Beattie *et al.* 2002; Kalb 2005; Reichardt 2006; Teng *et al.* 2005). Regardless of the ligand-receptor interaction, both proBDNF and proNGF have been shown to induce p75NTR dependent cell-death. ProNGF has been shown to induce p75NTR-dependent apoptosis in smooth muscle cells, sympathetic neurons, and in a pheochromocytoma cell line (Lee *et al.* 2001) *in vitro*. ProNGF stimulates cell death in oligodendrocytes in an *in vivo* model of nerve damage (Beattie *et al.* 2002). Examining the glia in the dying nerve at multiple time points reveals that the oligodendrocytes first upregulate p75NTR and caspase 3 before succumbing to apoptosis (Beattie *et al.* 2002). Our data indicates that proBDNF, but not BDNF, induced activated caspase 3, a proteolytic enzyme in the apoptosis pathway (Beattie *et al.* 2002; Cowan and Roskams 2004; D'Amelio *et al.* 2010; Deng *et al.* 2007; Kalb 2005; Weise *et al.* 2005; Yamaguchi and Mori 2005) in the glomerular layer. Interestingly, proBDNF reduced the number of TH immunoreactive cells in the glomerular layer in a manner reminiscent of adult naris-occlusion (Baker *et al.* 1993; Kim *et al.* 2006a; Parrish-Aungst *et al.* 2011). The same effective proBDNF dose (10 ng/ml; 0.2 nM) used in our studies, also induced apoptosis in sympathetic ganglion neurons (Teng *et al.* 2005) and cerebellar granule neurons (Koshimizu *et al.* 2009). Our current data, however, are the first to demonstrate proBDNF inducing a marker of apoptosis *in vivo*.

Previous studies have also demonstrated a reduction in the number of TH immunoreactive glomerular interneurons in response to adult naris-occlusion. (Baker *et al.* 1993; Kim *et al.* 2006a; Parrish-Aungst *et al.* 2011); additionally, we report that short-term naris-occlusion enhanced activated-caspase 3 immunoreactivity. Thus, both short-term naris-occlusion and proBDNF administration reduces TH and enhances activated-caspase 3 immunoreactivity. Activated-caspase 3 expression following naris-occlusion supports previous studies demonstrating neuronal degeneration (Kim *et al.* 2006a) and DNA fragmentation (Najbauer and Leon 1995) in the glomerular layer following deafferentation and sensory deprivation, respectively. In contrast, naris-occlusion has been reported to only reduce TH expression and not cell loss (Baker *et al.* 1993). Recently, deafferentation was reported to reduce the number of TH immunoreactive neurons, but not the total number of glomerular interneurons

(Parrish-Aungst *et al.* 2011). This conflict may be due to differences in the age of mice. We used young adult mice in the IND experiments in order to keep the age difference between the animals used in the physiology and histology experiments at a minimum. The result was that our animals were about 3 weeks younger than those used by the other groups (Baker *et al.* 1993; Parrish-Aungst *et al.* 2011). Alternatively, activated-caspase 3 may be activated as a mechanism of synapse and dendrite pruning (D'Amelio *et al.* 2010). Indeed, after sensory input loss the OB undergoes extensive synaptic remodeling as measured at the histological, receptor and physiological level (Biju *et al.* 2008; Brunjes 1994; Hamilton *et al.* 2008; Kim *et al.* 2006a; Maher *et al.* 2009; Tucker and Fadool 2002).

In summary our data provide a role for proBDNF in the mouse olfactory bulb and have potentially important implications for therapies that target diseases of neuronal death. Multiple studies have shown that BDNF improves locomotor ability in rodents following experimental ischemia-induced neuronal loss (Schäbitz *et al.* 2007; Shi *et al.* 2009; Yamashita *et al.* 1997). ProBDNF levels are reduced in the cortices of human patients that are developing and living with Alzheimer's disease, a condition of massive neuronal loss (Longo *et al.* 2007; Michalski and Fahnestock 2003; Peng *et al.* 2005). Strikingly, in another human disease of progressive neuronal death, amyotrophic lateral sclerosis, intravenous infusions of BDNF were shown to improve the respiratory capabilities of late-stage patients (Bradley 1999). Intravenous application of BDNF, nonetheless, is inefficient due to the poor blood brain barrier permeability of BDNF and to deleterious side effects (Bradley 1999). As a result, small molecule ligands for p75NTR and TrkB are being developed as therapeutic agents for diseases of neuronal death (Jang *et al.* 2010; Longo *et al.* 2007). The mouse OB promises to be retained as an interesting model to study the actions of BDNF and proBDNF on easily identifiable, central nervous system neurons that express either p75NTR or TrkB, but not both *in vivo*.

CHAPTER SIX

CONCLUSIONS

In this dissertation, I sought to find novel combinations and applications of proteins in chemosensory neurons. By doing so, I personally re-discovered the utility of the vomeronasal organ (VNO) as a model for neuronal and protein function. The VNO has a number of calcium-producing proteins that tethered together by 'scaffolding' proteins. Supporting proteins play this role in other calcium-sensitive tissues. I also found a novel function for a recently discovered chaperon protein. The findings broaden the putative binding partners of the chaperone from only olfactory receptor proteins to include at least some ion channels. In the main olfactory bulb (MOB), I sought to define a role for a neurotrophin, a protein that supports neuronal growth, in a process of cell death. Taking advantage of different neurotrophin receptors expressed by interneurons and output neurons, I used the MOB as a model to study differential receptor activation by different neurotrophin isoforms. Here, I describe the first *in vivo* evidence that neurotrophins may induce cell death.

Chapter 2 demonstrates two novel protein-protein interactions in the rodent VNO. First, receptor transporting protein 1 (RTP1), an olfactory receptor chaperone, interacts with not only members of this superfamily, but also with ion channels. The first novel finding was demonstrated *in vivo* by a protein-protein interaction between the type 2 canonical transient receptor potential channel (TRPC2) and RTP1, and *in vitro* by a RTP1- dependent increase in TRPC2 surface expression. Secondly, TRPC2, the scaffold protein Homer 1b/c, and the ion channel IP_3R_3 form protein-protein interactions in the native VNO. This is the first description of Homer expression in the VNO and the first demonstration of an interaction between Homer and TRPC2 in any sensory system.

Homers are located to synapses (Brakeman *et al.* 1997; Gasperini and Foa 2004; Kaja *et al.* 2003; Kammermeier and Worley 2007; Lu *et al.* 2007; Tu *et al.* 1999; Xiao *et al.* 1998) and to calcium signalling complexes (Worley *et al.* 2007a) (Figure 2.9). Immunoprecipitation experiments support a TRPC2-Homer 1-IP_3R_3 complex in the VNO (Figure 2.4). The VNO lysates used in these experiments contained both synapses from autonomic nervous system (Meredith and O'Connell 1979; Soler and Suburo 1998) and a calcium-signalling pathway

located to the vomeronasal sensory neuron dendrite (Brann *et al.* 2002; Brann and Fadool 2006; Halpern and Martinez-Marcos 2003). TRPC2 immunolabeling was found only in the vomeronasal sensory neuron (VSN) microvilli (Figure 2.2) strongly supporting Homer 1 function chemosensory signal transduction. The functional consequence of Homer linking these ion channels would be to ensure high-fidelity transmission of the calcium signal that flows through the open TRPC2 channel during chemosensory detection.

RTP1 expression in the rat VNO supports the previous finding of RTP1 mRNA in the mouse VNO (Saito *et al.* 2004) (Figure 2.2). The immunocytochemical detection of RTP1 protein to olfactory sensory neuron cilia, and VSN microvilli provides an important clue to a function in chemosensory signal transduction. RTP1 interacts with G-protein coupled-receptors (GPCRs) associated with either odorant (Saito *et al.* 2004) or taste receptor families (Behrens *et al.* 2006) *in vitro*, but does not interact with vomeronasal receptors (Saito *et al.* 2004). This lead me to speculate that RTP1 could interact with TRPC2 *in vitro*. TRPC2 had a low transfection efficiency in HEK293 cells as compared with that of a voltage-gated ion channel, Kv1.3 (30% vs. 60%; Figure 2.5) (Fadool *et al.* 1997). This low transfection efficiency may be due to calcium cytotoxicity associated with spontaneously active TRPC2 channels such as TRPC4 that has been demonstrated to be spontaneously active in HEK293 cells (McKay *et al.* 2000). That being said, RTP1 did manage to increase the amount TRPC2 present in the surface membrane. Increased TRPC2 surface expression was detected with both cell-surface biotinylation (Figure 2.7) and with whole-cell electrophysiology (Figure 2.8). The electrophysiological data indicate that the surface-expressed TRPC2 is functional and is responsive to a signal transduction pathway similar to the one present in the VNO (Jungnickel *et al.* 2001; Schachter *et al.* 1997; Van Kolen and Slegers 2006). The biochemical and electrophysiological data suggest that the TRPC2 surface membrane half-life residence is increased in the presence of RTP1. RTP1 and TRPC2 form a functional interaction, but it is unclear whether it is one of membrane stabilization or one of trafficking.

In Chapter 3, Dr. Chad Samuelsen and I addressed a recently published work on the function of the human VNO. We felt that the authors of the paper did not address the published data on the human VNO fairly. In our critique we briefly reviewed human VNO function and compared it to their published assertions. In short, humans do not have a functional VNO and may not respond to chemical signals (chemosignals) that are 'pheromones'(Doty 2003; Meredith

2001; Wysocki and Preti 2004) . This does not mean that humans do not respond to certain chemical signals (chemosignals) (Jacob *et al.* 2002; Jacob and McClintock 2000; Wyart *et al.* 2007), including, possibly, compounds found in sweat (Knecht *et al.* 2003; Wyart *et al.* 2007) and tears (Gelstein *et al.* 2011). It does mean that human chemosignal detection does not require a VNO (Hummel *et al.* 2011; Knecht *et al.* 2003).

Chapter 4 investigated neurotrophin expression following unilateral sensory occlusion, a model of sensory deprivation and cell death. Naris-occlusion reduces the OB volume ipsilateral to the naris closure (Meisami 1976). This effect has been attributed to apoptotic cell death in glomerular and granule cell layers, however, the number of mitral cells has been reported to be practically unaffected (Najbauer and Leon 1995). The high affinity receptor for brain-derived neurotrophic factor (BDNF), tyrosine receptor kinase B (TrkB), is present in various cell types within the MOB, including the mitral cells (Fryer *et al.* 1996) and is predominantly expressed as a full-length receptor (Imamura and Greer 2009; Tucker and Fadool 2002). Consequently, I looked for brain-derived neurotrophic factor (BDNF), the receptor's preferred ligand, to increase following naris-occlusion.

My experiments in Chapter 4 monitored the BDNF-immunoreactive profile of OB neurons following unilateral sensory occlusion. The number of immunoreactive mitral cells per unit area increased while that of glomerular layer interneurons cells decreased, independent of period of sensory deprivation ranging from 20 to 40 days (Figures 4.1 and 4.2). The mechanism behind the changing BDNF-immunoreactive cells is unknown. In one scenario, the increased number of BDNF-immunoreactive mitral cells may be driven by increased mitral cell BDNF expression. It is unclear, however, if mitral cells express BDNF (Clevenger *et al.* 2008). Since BDNF is secreted, absence of a BDNF transcript in mitral cells would not be inconsistent with my BDNF-immunoreactivity patterns (Blum and Konnerth 2005; Lee *et al.* 2001; Mowla *et al.* 2001). Because mitral cells have high expression of the *bcl-2* gene that suppresses apoptosis (Allsopp *et al.* 1993; Garcia *et al.* 1992; Hockenbery *et al.* 1993; Najbauer *et al.* 1995), the susceptibility of mitral cells to apoptotic death could be lower than that for other OB cell-types. What is the source of the loss of volume in the external plexiform layer (EPL)? In mice that express yellow fluorescent protein in mitral cells (Feng *et al.* 2000) the reduction in EPL thickness following sensory deprivation is clearly due to the absence of BDNF-immunoreactive fibers in the superficial layer of EPL (oEPL) (Figure 4.3). Genetic deletion of BDNF leads to

cell and fiber loss in this area of the OB (Berghuis *et al.* 2006). The origin of the oEPL BDNF-immunoreactive fibers described here is not clear, but they may belong to secondary dendrites of middle-tufted cells since these dendrites ramify into the superficial EPL (Shepherd and Greer 1998). Indeed, Hamilton et al. (2008) have recently shown that middle-tufted cells may undergo trophic changes after adult olfactory-sensory deprivation induced by deafferentation (Hamilton *et al.* 2008).

My biochemistry data presented in Chapter 4 suggests that the OB has little mature BDNF (Figure 4.4). In Figure 4.4 a minor band at 27 kDa and a major band at 54 kDa are clearly visible and represent proBDNF and a proBDNF dimer, respectively. A mature BDNF band could not be resolved from the OB but could be from the rat hippocampus (Figure 4.4). Preadsorption of the antiserum used in our study with BDNF quenches the proBDNF, but not the mature BDNF, band on an immunoblot (Michalski and Fahnestock 2003), which strongly infers that the immunocytochemical signal is proBDNF. ProBDNF has been considered an inactive precursor prior to cleavage by the serine protease plasmin and selective matrix metalloproteinases (Blum and Konnerth 2005; Lee *et al.* 2001; Mowla *et al.* 2001). The cleaved (mature) BDNF can activate TrkB receptors and promote cell survival and synaptic plasticity. Alternatively, proBDNF may directly bind to and activate TrkB receptors to promote mitral cell survival. In support of this idea, furin-resistant proBDNF, secreted from COS-7 cells, is known to bind to the extracellular domains of both TrkB and p75NTR (Fayard *et al.* 2005). Fayard *et al.* (2005) demonstrated that proBDNF can activate TrkB and could be involved in TrkB-mediated neurotrophic activity *in vivo*. In human Alzheimer's disease, a pathological condition of extreme apoptosis, it is quite intriguing that proBDNF levels decrease in the parietal cortex (Michalski and Fahnestock 2003). Another possibility is that proBDNF induces cell death through the P75NTR (Lee *et al.* 2001; Pang *et al.* 2004; Teng *et al.* 2005; Woo *et al.* 2005) located in oEPL (Cao *et al.* 2007; Imamura and Greer 2009).

Chapter 5 investigated the effect of proBDNF on both short-term and long-term plasticity in the mouse OB. Long-term plasticity was measured with histological techniques and short-term plasticity was measured with electrophysiological techniques. These experiments were conducted to measure the effect of the P75NTR neurotrophin receptor (p75NTR) on interneurons in the OB and the mechanism of the tyrosine receptor kinase B (TrkB) activation on OB mitral

cells. P75NTR activation initiates cell remodeling and possibly apoptosis; while TrkB activation inhibits a *Shaker* family voltage-gated potassium channel, Kv1.3.

I measured the effect of both BDNF isoforms—mature and proBDNF— on mitral cells in an OB slice preparation in a whole-cell current clamp configuration. I recorded mitral cell action potentials and, thus, mitral cell excitability. BDNF, but not proBDNF, increased mitral cell excitability following low amplitude current injections (compare Figures 5.1 and 5.2). Additionally, I also investigated the effect of margatoxin (MgTX), a Kv1.3 channel blocker (Garcia-Calvo *et al.* 1993; Gutman *et al.* 2005), on mitral cell excitability. MgTX and BDNF had similar effects on mitral cell excitability. Thus, both MgTX and BDNF likely inhibit Kv1.3-dependent potassium currents in mouse OB mitral cells.

While proBDNF failed to increase mitral cell excitability, it did alter glomerular interneuron immunoreactivity for activated-caspase 3 and tyrosine hydroxylase (TH). Following intranasal delivery (IND) of neurotrophins, I looked for a proBDNF function in the glomerular layer because glomerular interneurons express p75NTR (Cao *et al.* 2007; Imamura and Greer 2009) which can induce apoptosis (Kalb 2005). It has also been shown that proBDNF concentrations similar to those found in the bulb (10 ng/ml; 0.2 nM) (Katoh-Semba *et al.* 1998; Schulte-Herbrüggen *et al.* 2008) initiate apoptosis (Koshimizu *et al.* 2009; Teng *et al.* 2005), inhibit neurite growth , and decreased spine density in cultured neurons (Koshimizu *et al.* 2009). My data indicate that proBDNF, but not BDNF, can induced the apoptosis marker activated-caspase 3 (Beattie *et al.* 2002; Cowan and Roskams 2004; D'Amelio *et al.* 2010; Deng *et al.* 2007; Kalb 2005; Weise *et al.* 2005; Yamaguchi and Mori 2005) in the glomerular layer (Figure 5.4D), concomitant with a reduced number of TH immunoreactive cells in the glomerular layer (Figure 5.5D). Importantly, proBDNF administration produces histological results parallel to those found after sensory deprivation by naris-occlusion—both treatments reduced TH expression and increased activated caspase 3 expression. These results are the first *in vivo* demonstration of proBDNF induction of an apoptosis marker.

There are conflicting reports on apoptosis following sensory deprivation. Naris-occlusion can induce neuronal degeneration (Kim *et al.* 2006a) and DNA fragmentation (Najbauer and Leon 1995) in the glomerular layer following deafferentation and sensory deprivation, respectively. In contrast, naris-occlusion has been reported to only reduce TH expression and not cell loss (Baker *et al.* 1993; Parrish-Aungst *et al.* 2011). Activated-caspase 3

does not always induce apoptosis and can be involved in neurite remodeling (D'Amelio *et al.* 2010). It may be that activated-caspase 3 is part of a mechanism of neurite pruning whereby sensory reduces the number of proBDNF immunoreactive fibers in the EPL (Biju *et al.* 2008).

Summary

The chemosensory pathways are complex, beautiful structures that are not as yet fully described. The experiments that I conducted again confirm that the chemosensory pathways are excellent models for exploring neuronal and protein function. I describe a novel complex of TRPC2, a chaperone, a scaffolding protein, and IP_3R_3. These ion channels and proteins function in many cell types and disease states. The VNO may be a superior model to investigate the function of these protein function in the awake, behaving animal, considering the VNO role in rodent behavior. My investigation of the OB provided preliminary evidence for a functional segregation within the EPL, a layer of the OB. This result may inform new studies on sensory function and neural circuits. I also found mechanistic interactions between BDNF and neurotrophin receptors underlying neural plasticity in the adult OB. BDNF signaling has the potential to rescue dying neurons and any data that describes this process has the potential to be insightful.

Future Directions

There are always more questions to ask. Below are a few questions for the VNO and OB.

Vomeronasal future directions

What is the nature of the TRPC2-RTP1 interaction? This can be studied at the molecular level by describing the residues within each that are necessary for the interaction. This can also be studied at the cellular level. Does RTP1 stabilize TRPC2 in a 'closed' conformation in the surface membrane and that is why it appears to increase surface expression? Or does RTP1 act like a traditional chaperone? Lastly, what is the ligand for TRPC2? This should be examined *in vitro* using the heterologous expression of TRPC2.

OB future directions

Which cell type(s) are lost following naris-occlusion? The first follow-up should look for p75NTR expression in TH-positive glomerular neurons. The second should utilize other cellular markers to define the cells according to long-standing glomerular layer cell types (i.e. short-axon

cells). Following naris-occlusion, what is the signalling cascade downstream of activated-caspase 3? The goal of this question is to describe how activated-caspase 3 drives plasticity in these cells. Lastly, where does OB BDNF come from? What cell(s) produce BDNF? What enzymatic cleavage system exists in the OB to produce BDNF from proBDNF?

APPENDIX A

ACUC APPROVAL LETTER

Animal Care and Use Committee (ACUC)
101 Biomedical Research Facility
P.O. Box 3064341
Tallahassee, FL 32306-4341
Telephone: 644-4262 Fax: 644-5570
Mail Code: 4341 Email: acucsecretary@mailer.(su.edu

MEMORANDUM

TO: Dr. Debra Fadool
Department of Biological Science

FROM: Dr. Elaine M. Hull, Chairt>m[71]
Animal Care and Use Committee

SUBJECT: Protocol #9912

DATE: October 30,2008

"YOUR REWRITE IS APPROVED"

The Animal Care and Use Committee (ACUC) approved the rewrite of Protocol #9912, *"Modulation of Olfactory Bulb Neuron Current Properties"*, as stated in the attached ACUC Review Comments form at its September 24, 2008 meeting. You are approved for the following species and numbers for the proposed protocol approval period.

Species	*Approved Number of Animals*	*Next Rewrite Due*	*Protocol Expiration Date*
Mice	10140	08/01/11	09/31/11

Enclosed for your records are:
- ./ The original Committee Comments
- ./ A copy of your Protocol Rewrite
- ./ The original of page one for signature and return in the enclosed envelope

Please remember to convey the ACUC number to LAR at 644-4262, when ordering animals on this protocol. Let us know if we can be of further assistance. We appreciate your contribution to assuring that animal research at Florida State University complies with federal guidelines and regulations.

EMH/sc
Enclosures

REFERENCES

Allsopp TE, Wyatt S, Paterson HF, Davies AM. 1993. The proto-oncogene bcl-2 can selectively rescue neurotrophic factor-dependent neurons from apoptosis. Cell 73: 295-307.

Baker H, Morel K, Stone DM, Maruniak JA. 1993. Adult naris closure profoundly reduces tyrosine hydroxylase expression in mouse olfactory bulb. Brain Res 614: 109-116.

Baker H, Towle A, Margolis F. 1988. Differential afferent regulation of dopaminergic and GABAergic neurons in the mouse main olfactory bulb. Brain Res 450: 69-80

Balu R, Larimer P, Strowbridge B. 2004. Phasic stimuli evoke precisely timed spikes in intermittently discharging mitral cells. J Neurophysiol 92: 743-753.

Bamji S, Majdan M, Pozniak C, Belliveau D, Aloyz R, Kohn J, Causing C, Miller F. 1998. The p75 neurotrophin receptor mediates neuronal apoptosis and is essential for naturally occurring sympathetic neuron death. J Cell Biol 140: 911-923.

Barde YA, Edgar D, Thoenen H. 1982. Purification of a new neurotrophic factor from mammalian brain. EMBO J 1: 549-553.

Barker PA. 2009. Whither proBDNF? Nat Neurosci 12: 105-106.

Bean B. 2007. The action potential in mammalian central neurons. Nat Rev Neurosci 8: 451-465.

Beattie M, Harrington A, Lee R, Kim J, Boyce S, Longo F, Bresnahan J, Hempstead B, Yoon S. 2002. ProNGF induces p75-mediated death of oligodendrocytes following spinal cord injury. Neuron 36: 375-386.

Behrens M, Bartelt J, Reichling C, Winnig M, Kuhn C, Meyerhof W. 2006. Members of RTP and REEP gene families influence functional bitter taste receptor expression. J Biol Chem 281: 20650-20659.

Ben-Shaul Y, Katz LC, Mooney R, Dulac C. 2010. In vivo vomeronasal stimulation reveals sensory encoding of conspecific and allospecific cues by the mouse accessory olfactory bulb. Proc Natl Acad Sci USA 107: 5172-5177.

Berghard A, Buck LB, Liman ER. 1996. Evidence for distinct signaling mechanisms in two mammalian olfactory sense organs. Proc Natl Acad Sci USA 93: 2365-2369.

Berghuis P, Agerman K, Dobszay MB, Minichiello L, Harkany T, Ernfors P. 2006. Brain-derived neurotrophic factor selectively regulates dendritogenesis of parvalbumin-containing interneurons in the main olfactory bulb through the PLCgamma pathway. J Neurobiol 66: 1437-1451.

Berkowicz DA, Trombley PQ, Shepherd GM. 1994. Evidence for glutamate as the olfactory receptor cell neurotransmitter. J Neurophysiol 71: 2557-2561.

Biju K, Mast T, Fadool D. 2008. Olfactory sensory deprivation increases the number of proBDNF-immunoreactive mitral cells in the olfactory bulb of mice. Neurosci Lett 447: 42-47.

Blum R, Konnerth A. 2005. Neurotrophin-mediated rapid signaling in the central nervous system: mechanisms and functions. Physiol 20: 70-78.

Boschat C PC, Randin O, Roppolo D, Lüscher C, Broillet MC, Rodriguez I. 2002. Pheromone detection mediated by a V1R vomeronasal receptor. Nat Neurosci 5: 1261-1262.

Boughman JW. 2002. How sensory drive can promote speciation. Trends Ecol Evol 17: 571-577.

Bradley W. 1999. A controlled trial of recombinant methionyl human BDNF in ALS: the BDNF study group (phase III). Neurol 52: 1427-1433.

Brakeman PR, Lanahan AA, O'Brien R, Roche K, Barnes CA, Huganir RL, Worley PF. 1997. Homer: a protein that selectively binds metabotropic glutamate receptors. Nature 386: 284-288.

Brann JH, Dennis JC, Morrison EE, Fadool DA. 2002. Type-specific inositol 1,4,5-trisphosphate receptor localization in the vomeronasal organ and its interaction with a transient receptor potential channel, TRPC2. J Neurochem 83: 1452-1460.

Brann JH, Fadool DA. 2006. Vomeronasal sensory neurons from sternotherus odoratus (stinkpot/musk turtle) respond to chemosignals via the phospholipase C system. J Exp Biol 209: 1914-1927.

Brunjes P, Smith-Crafts L, McCarty R. 1985. Unilateral odor deprivation: effects on the development of olfactory bulb catecholamines and behavior. Brain Res 354: 1-6.

Brunjes PC. 1994. Unilateral naris closure and olfactory system development. Brain Res Brain Res Rev 19: 146-160.

Buck L AR. 1991. A novel multigene family may encode odorant receptors: a molecular basis for odor recognition. Cell 65: 175-187.

Bush A, Carzoli K, Hyson R. 2008. The influence of chronic lithium administration on deafferentation-induced cellular changes in the chick cochlear nucleus. Neurosci 157: 229-237.

Bush CF, Jones SV, Lyle AN, Minneman KP, Ressler KJ, Hall RA. 2007. Specificity of olfactory receptor interactions with other G protein-coupled receptors. J Biol Chem 282: 19042-19051.

Cajal R. 1995. Histologie du Systeme Nerveux de L'homme et des Vertebres. New York, NY: Oxford University Press.

Cao L, Dhilla A, Mukai J, Blazeski R, Lodovichi C, Mason C, Gogos J. 2007. Genetic modulation of BDNF signaling affects the outcome of axonal competition in vivo. Curr Biol 17: 911-921.

Catsch A. 1948. Eine erblich storung des bewegungsmechanismus bei drosophila melanogaster. Zeitschrift Fur Induktive Abstammungs Und Vererbungslehre 82: 64-66.

Chandy K, Gutman G. 1993. Nomenclature for mammalian potassium channel genes. Trends Pharmacol Sci 14: 434.

Chapleau C, Larimore J, Theibert A, Pozzo-Miller L. 2009. Modulation of dendritic spine development and plasticity by BDNF and vesicular trafficking: fundamental roles in neurodevelopmental disorders associated with mental retardation and autism. J Neurodev Disord 1: 185-196.

Chen W, Shepherd G. 1997. Membrane and synaptic properties of mitral cells in slices of rat olfactory bulb. Brain Res 745: 189-196.

Chess A, Simon I, Cedar H, Axel R. 1994. Allelic inactivation regulates olfactory receptor gene expression. Cell 78: 823-834.

Choquet D, Korn H. 1992. Mechanism of 4-aminopyridine action on voltage-gated potassium channels in lymphocytes. J Gen Physiol 99: 217-240.

Clevenger AC, Salcedo E, Jones KR, Restrepo D. 2008. BDNF promoter-mediated {beta}-galactosidase expression in the olfactory epithelium and bulb. Chem Senses 33: 531-539.

Cohen S. 1960. Purification of a nerve-growth promoting protein from the mouse salivary gland and its neuro-cytotoxic antiserum. Proc Natl Acad Sci USA 46: 302-311.

Colley B, Cavallin M, Biju K, Marks D, Fadool D. 2009. Brain-derived neurotrophic factor modulation of Kv1.3 channel is disregulated by adaptor proteins Grb10 and nShc. BMC Neurosci 10: 8.

Colley B, Tucker K, Fadool D. 2004. Comparison of modulation of Kv1.3 channel by two receptor tyrosine kinases in olfactory bulb neurons of rodents. Receptors Channels 10: 25-36.

Colley BS, Biju KC, Visegrady A, Campbell S, Fadool DA. 2007. Neurotrophin B receptor kinase increases Kv subfamily member 1.3 (Kv1.3) ion channel half-life and surface expression. Neurosci 144: 531-546.

Conner JM, Lauterborn JC, Yan Q, Gall CM, Varon S. 1997. Distribution of brain-derived neurotrophic factor (BDNF) protein and mRNA in the normal adult rat CNS: evidence for anterograde axonal transport. J Neurosci 17: 2295-2313.

Cook KK, Fadool DA. 2002. Two adaptor proteins differentially modulate the phosphorylation and biophysics of Kv1.3 ion channel by src kinase. J Biol Chem 277: 13268-13280.

Cowan CM, Roskams AJ. 2004. Caspase-3 and caspase-9 mediate developmental apoptosis in the mouse olfactory system. J Comp Neurol 474: 136-148.

Crowley MP, Reich Z, Mavaddat N, Altman JD, Chien Y-h. 1997. The recognition of the nonclassical major histocompatibility complex (MHC) class I molecule, T10, by the γδ T Cell, G8. J Exp Med 185: 1223-1230.

D'Amelio M, Cavallucci V, Cecconi F. 2010. Neuronal caspase-3 signaling: not only cell death. Cell Death Differ 17: 1104-1114.

De Saint Jan D, Westbrook G. 2007. Disynaptic amplification of metabotropic glutamate receptor 1 responses in the olfactory bulb. J Neurosci 27: 132-140.

De Saint Jan D, Westbrook GL. 2005. Detecting activity in olfactory bulb glomeruli with astrocyte recording. J. Neurosci. 25: 2917-2924.

Del Punta K, Leinders-Zufall T, Rodriguez I, Jukam D, Wysocki CJ, Ogawa S, Zufall F, Mombaerts P. 2002a. Deficient pheromone responses in mice lacking a cluster of vomeronasal receptor genes. Nature 419: 70-74.

Del Punta K, Puche A, Adams NC, Rodriguez I, Mombaerts P. 2002b. A Divergent pattern of sensory axonal projections is rendered convergent by second-order neurons in the accessory olfactory bulb. Neuron 35: 1057-1066.

Deng P, Pang ZP, Zhang Y, Xu ZC. 2005. Increase of delayed rectifier potassium currents in large aspiny neurons in the neostriatum following transient forebrain ischemia. Neurosci 131: 135-146.

Deng X, Ladenheim B, Jayanthi S, Cadet JL. 2007. Methamphetamine administration causes death of dopaminergic neurons in the mouse olfactory bulb. Biol Psychiatry 61: 1235-1243.

Doty RL. 2003. Mammalian Pheromones: Fact or Fiction. In: Doty RL, (ed.), Handbook of Olfaction and Gustation. New York: Marcel Dekker. p. 345-384.

Dulac C, Axel R. 1995. A novel family of genes encoding putative pheromone receptors in mammals. Cell 83: 195-206.

Ernfors P, Ibáñez CF, Ebendal T, Olson L, Persson H. 1990. Molecular cloning and neurotrophic activities of a protein with structural similarities to nerve growth factor: developmental and topographical expression in the brain. Proc Natl Acad Sci USA 87: 5454-5458.

Fadool D, Levitan I. 1998. Modulation of olfactory bulb neuron potassium current by tyrosine phosphorylation. J Neurosci 18: 6126-6137.

Fadool D, Tucker K, Perkins R, Fasciani G, Thompson R, Parsons A, Overton J, Koni P, Flavell R, Kaczmarek L. 2004. Kv1.3 channel gene-targeted deletion produces "Super-Smeller Mice" with altered glomeruli, interacting scaffolding proteins, and biophysics. Neuron 41: 389-404.

Fadool DA. 2005. Mammalian pheromones. eLS. John Wiley & Sons, Ltd.

Fadool DA, Holmes TC, Berman K, Dagan D, Levitan IB. 1997. Tyrosine phosphorylation modulates current amplitude and kinetics of a neuronal voltage-gated potassium channel. J Neurophysiol 78: 1563-1573.

Fadool DA, Tucker K, Phillips JJ, Simmen JA. 2000. Brain insulin receptor causes activity-dependent current suppression in the olfactory bulb through multiple phosphorylation of Kv1.3. J Neurophysiol 83: 2332-2348.

Fadool DA, Wachowiak M, Brann JH. 2001. Patch-clamp analysis of voltage-activated and chemically activated currents in the vomeronasal organ of sternotherus odoratus (stinkpot/musk turtle). J Exp Biol 204: 4199-4212.

Fayard B, Loeffler S, Weis J, Vögelin E, Krüttgen A. 2005. The secreted brain-derived neurotrophic factor precursor pro-BDNF binds to TrkB and p75NTR but not to TrkA or TrkC. J Neurosci Res 80: 18-28.

Feng G, Mellor RH, Bernstein M, Keller-Peck C, Nguyen QT, Wallace M, Nerbonne JM, Lichtman JW, Sanes JR. 2000. Imaging neuronal subsets in transgenic mice expressing multiple spectral variants of GFP. Neuron 28: 41-51.

Foltan R, Sedy J. 2009. Behavioral changes of patients after orthognathic surgery develop on the basis of the loss of vomeronasal organ: a hypothesis. Head Face Med 5: 5.

Fryer RH, Kaplan DR, Feinstein SC, Radeke MJ, Grayson DR, Kromer LF. 1996. Developmental and mature expression of full-length and truncated TrkB receptors in the rat forebrain. J Comp Neurol 374: 21-40.

Fu Y, Subramanya A, Rozansky D, Cohen DM. 2006. WNK kinases influence TRPV4 channel function and localization. Am J Physiol Renal Physiol 290: F1305-F1314.

Garcia I, Martinou I, Tsujimoto Y, Martinou JC. 1992. Prevention of programmed cell death of sympathetic neurons by the bcl-2 proto-oncogene. Science 258: 302-304.

Garcia-Calvo M, Leonard RJ, Novick J, Stevens SP, Schmalhofer W, Kaczorowski GJ, Garcia ML. 1993. Purification, characterization, and biosynthesis of margatoxin, a component of Centruroides margaritatus venom that selectively inhibits voltage-dependent potassium channels. J Biol Chem 268: 18866-18874.

Gasperini R, Foa L. 2004. Homer 1b/c expression correlates with zebrafish olfactory system development. J Neurocytol 33: 671-680.

Gelstein S, Yeshurun Y, Rozenkrantz L, Shushan S, Frumin I, Roth Y, Sobel N. 2011. Human tears contain a chemosignal. Science 331: 226-230.

Gibb SJ, Wolff M, Dalrymple-Alford JC. 2006. Odour-place paired-associate learning and limbic thalamus: Comparison of anterior, lateral and medial thalamic lesions. Behav Brain Res 172: 155-168.

Godfrey PA, Malnic B, Buck LB. 2004. The mouse olfactory receptor gene family. Proc Natl Acad Sci USA 101: 2156-2161.

Graziadei PP, Monti Graziadei GA. 1985. Neurogenesis and plasticity of the olfactory sensory neurons. Ann N Y Acad Sci 457: 127-142.

Griff ER, Mafhouz M, Chaput MA. 2008a. Comparison of identified mitral and tufted cells in freely breathing rats: II odor-evoked responses. Chem Senses 33: 793-802.

Griff ER, Mafhouz M, Perrut A, Chaput MA. 2008b. Comparison of identified mitral and tufted cells in freely breathing rats: I. conduction velocity and spontaneous activity. Chem Senses 33: 779-792.

Gutman GA, Chandy KG, Grissmer S, Lazdunski M, McKinnon D, Pardo LA, Robertson GA, Rudy B, Sanguinetti MC, Stühmer W, Wang X. 2005. International Union of Pharmacology. LIII. Nomenclature and molecular relationships of voltage-gated potassium channels. Pharmacological Rev 57: 473-508.

Haberly LB. 2001. Parallel-distributed processing in olfactory cortex: new insights from morphological and physiological analysis of neuronal circuitry. Chem Senses 26: 551-576.

Hallböök F, Ibáñez CF, Persson H. 1991. Evolutionary studies of the nerve growth factor family reveal a novel member abundantly expressed in xenopus ovary. Neuron 6: 845-858.

Halpern M, Martinez-Marcos A. 2003. Structure and function of the vomeronasal system: an update. Prog Neurobiol 70: 245-318.

Hamada K, Terauchi A, Mikoshiba K. 2003. Three-dimensional rearrangements within inositol 1,4,5-trisphosphate receptor by calcium. J Biol Chem 278: 52881-52889.

Hamilton KA, Parrish-Aungst S, Margolis FL, Erdélyi F, Szabó G, Puche AC. 2008. Sensory deafferentation transsynaptically alters neuronal GluR1 expression in the external plexiform layer of the adult mouse main olfactory bulb. Chem Senses 33: 201-210.

Hanson L, Frey W. 2008. Intranasal delivery bypasses the blood-brain barrier to target therapeutic agents to the central nervous system and treat neurodegenerative disease. BMC Neurosci 9: S5.

He J, Ma L, Kim S, Nakai J, Yu CR. 2008. Encoding gender and individual information in the mouse vomeronasal organ. Science 320: 535-538.

Herrada G, Dulac C. 1997. A novel family of putative pheromone receptors in mammals with a topographically organized and sexually dimorphic distribution. Cell 90: 763-773.

Hockenbery DM, Oltvai ZN, Yin XM, Milliman CL, Korsmeyer SJ. 1993. Bcl-2 functions in an antioxidant pathway to prevent apoptosis. Cell 75: 241-251.

Hofmann T, Schaefer M, Schultz G, Gudermann T. 2000. Cloning, expression and subcellular localization of two novel splice variants of mouse transient receptor potential channel 2. Biochemical Journal 351: 115-122.

Hofmann T, Schaefer M, Schultz G, Gudermann T. 2002. Subunit composition of mammalian transient receptor potential channels in living cells. Proc Natl Acad Sci USA 99: 7461-7466.

Huber A. 2001. Scaffolding proteins organize multimolecular protein complexes for sensory signal transduction. Eur J Neurosci 14: 769-776.

Hummel T, Schultz S, Witt M, Hatt H. 2011. Electrical responses to chemosensory stimulation recorded from the vomeronasal duct and the respiratory epithelium in humans. Int J Physchophysiol 81: 116-120.

Imamura F, Greer C. 2009. Dendritic branching of olfactory bulb mitral and tufted cells: regulation by TrkB. PLoS One 4: e6729.

Inamura K, Kashiwayanagi M. 2000. Inward current responses to urinary substances in rat vomeronasal sensory neurons. Eur J Neurosci 12: 3529.

Inamura K, Kashiwayanagi M, Kurihara K. 1997a. Blockage of urinary responses by inhibitors for IP3-mediated pathway in rat vomeronasal sensory neurons. Neurosci Lett 233: 129-132.

Inamura K, Kashiwayanagi M, Kurihara K. 1997b. Inositol-1,4,5-trisphosphate induces responses in receptor neurons in rat vomeronasal sensory slices. Chem Senses 22: 93-103.

Inamura K, Matsumoto Y, Kashiwayanagi M, Kurihara K. 1999. Laminar distribution of pheromone-receptive neurons in rat vomeronasal epithelium. J Physiol 517: 731-739.

Ip NY, Ibáñez CF, Nye SH, McClain J, Jones PF, Gies DR, Belluscio L, Le Beau MM, Espinosa R, Squinto SP. 1992. Mammalian neurotrophin-4: structure, chromosomal localization, tissue distribution, and receptor specificity. Proc Natl Acad Sci USA 89: 3060-3064.

Ishii T, Hirota J, Mombaerts P. 2003. Combinatorial coexpression of neural and immune multigene families in mouse vomeronasal sensory neurons. Curr Biol 13: 394-400.

Ishii T, Mombaerts P. 2008. Expression of nonclassical class I major histocompatibility genes defines a tripartite organization of the mouse vomeronasal system. J Neurosci 28: 2332-2341.

Ishii T, Mombaerts P. 2011. Coordinated coexpression of two vomeronasal receptor V2R genes per neuron in the mouse. Mol Cell Neurosci 46: 397-408.

Jacob S, Garcia S, Hayreh D, McClintock MK. 2002. Psychological effects of musky compounds: comparison of androstadienone with androstenol and muscone. Horm Behav 42: 274-283.

Jacob S, McClintock MK. 2000. Psychological state and mood effects of steroidal chemosignals in women and men. Horm Behav 37: 57-78.

Jan LY, Jan YN. 1997. Voltage-gated and inwardly rectifying potassium channels. J Physiol 505: 267-282.

Jan YN, Jan LY, Dennis MJ. 1977. Two mutations of synaptic transmission in drosophila. Proc R Soc Lond B Biol Sci 198: 87-108.

Jang S, Liu X, Yepes M, Shepherd K, Miller G, Liu Y, Wilson W, Xiao G, Blanchi B, Sun Y, Ye K. 2010. A selective TrkB agonist with potent neurotrophic activities by 7,8-dihydroxyflavone. Proc Natl Acad Sci U S A 107: 2687-2692.

Jang T SA, O'Connell RJ. 2001. Induction of c-fos in hamster accessory olfactory bulbs by natural and cloned aphrodisin. Neuroreport 12: 449-452.

Jia C, Chen WR, Shepherd GM. 1999. Synaptic organization and neurotransmitters in the rat accessory olfactory bulb. J Neurophysiol 81: 345-355.

Jia C, Halpern M. 1996. Subclasses of vomeronasal receptor neurons: differential expression of G proteins (Gi[alpha]2 and Go[alpha]) and segregated projections to the accessory olfactory bulb. Brain Res 719: 117-128.

Jiao Y, Sun Z, Lee T, Fusco FR, Kimble TD, Meade CA, Cuthbertson S, Reiner A. 1999. A simple and sensitive antigen retrieval method for free-floating and slide-mounted tissue sections. J Neurosci Meth 93: 149-162.

Johnson A, Josepheson R, Hawke M. 1985. Clinical and histological evidence for the presence of the vomeronasal (Jacobson's) organ in adult humans. J Otolaryngol 14: 71-79.

Johnson BA, Ong J, Leon M. 2010. Glomerular activity patterns evoked by natural odor objects in the rat olfactory bulb are related to patterns evoked by major odorant components. J Comp Neurol 518: 1542-1555.

Jungnickel MK, Marrero H, Birnbaumer L, Lemos JR, Florman HM. 2001. Trp2 regulates entry of Ca2+ into mouse sperm triggered by egg ZP3. Nat Cell Biol 3: 499-502.

Jurman ME, Boland LM, Liu Y, Yellen G. 1994. Visual identification of individual transfected cells for electrophysiology using antibody-coated beads. Biotechniques 17: 876-881.

Kaba H, Keverne EB. 1992. Analysis of synaptic events in the mouse accessory olfactory bulb with current source-density techniques. Neurosci 49: 247-254.

Kaja S, Yang SH, Wei J, Fujitani K, Liu R, Brun-Zinkernagel AM, Simpkins JW, Inokuchi K, Koulen P. 2003. Estrogen protects the inner retina from apoptosis and ischemia-induced loss of Vesl-1L/Homer 1c immunoreactive synaptic connections. Invest Ophthalmol Vis Sci 44: 3155-3162.

Kalb R. 2005. The protean actions of neurotrophins and their receptors on the life and death of neurons. Trends Neurosci 28: 5-11.

Kammermeier PJ, Worley PF. 2007. Homer 1a uncouples metabotropic glutamate receptor 5 from postsynaptic effectors. Proc Natl Acad Sci USA 104: 6055-6060.

Kang N, Baum MJ, Cherry JA. 2009. A direct main olfactory bulb projection to the 'vomeronasal' amygdala in female mice selectively responds to volatile pheromones from males. Eur J Neurosci 29: 624-634.

Kang N, Baum MJ, Cherry JA. 2011. Different profiles of main and accessory olfactory bulb mitral/tufted cell projections revealed in mice using an anterograde tracer and a whole-mount, flattened cortex preparation. Chem Senses 36: 251-260.

Kaplan WD, Trout WE. 1969. The behavior of four neurological mutants of drosophila. Genetics 61: 399-409.

Katoh-Semba R, Semba R, Takeuchi IK, Kato K. 1998. Age-related changes in levels of brain-derived neurotrophic factor in selected brain regions of rats, normal mice and senescence-accelerated mice: a comparison to those of nerve growth factor and neurotrophin-3. Neurosci Res 31: 227-234.

Kelsch W, Lin C, Mosley C, Lois C. 2009. A critical period for activity-dependent synaptic development during olfactory bulb adult neurogenesis. J Neurosci 29: 11852-11858.

Keverne EB. 1999. The vomeronasal organ. Science 286: 716-720.

Kim H, Puche A, Margolis F. 2006a. Odorant deprivation reversibly modulates transsynaptic changes in the NR2B-mediated CREB pathway in mouse piriform cortex. J Neurosci 26: 9548-9559.

Kim JY, Zeng W, Kiselyov K, Yuan JP, Dehoff MH, Mikoshiba K, Worley PF, Muallem S. 2006b. Homer 1 mediates store- and inositol 1,4,5-trisphosphate receptor-dependent translocation and retrieval of TRPC3 to the plasma membrane. J Biol Chem 281: 32540-32549.

Kimchi T, Xu J, Dulac C. 2007. A functional circuit underlying male sexual behaviour in the female mouse brain. Nature 448: 1009-1014.

Kiyokage E, Pan Y-Z, Shao Z, Kobayashi K, Szabo G, Yanagawa Y, Obata K, Okano H, Toida K, Puche AC, Shipley MT. 2010. Molecular identity of periglomerular and short axon cells. J Neurosci 30: 1185-1196.

Knecht M, Witt M, Hüttenbrink K-B, Heilmann S, Hummel T. 2003. Assessment of olfactory function and androstenone odor thresholds in humans with or without functional occlusion of the vomeronasal duct. Behav Neurosci 117: 1135-1141.

Koch RO, Wanner SG, Koschak A, Hanner M, Schwarzer C, Kaczorowski GJ, Slaughter RS, Garcia ML, Knaus H-G. 1997. Complex subunit assembly of neuronal voltage-gated K+ channels. J Biol Chem 272: 27577-27581.

Koos DS, Fraser SE. 2005. The Grueneberg ganglion projects to the olfactory bulb. Neuroreport 16: 1929-1932.

Kosaka K, Toida K, Aika Y, Kosaka T. 1998. How simple is the organization of the olfactory glomerulus?: the heterogeneity of so-called periglomerular cells. Neurosci Res 30: 101-110.

Koshimizu H, Kiyosue K, Hara T, Hazama S, Suzuki S, Uegaki K, Nagappan G, Zaitsev E, Hirokawa T, Tatsu Y, Ogura A, Lu B, Kojima M. 2009. Multiple functions of precursor BDNF to CNS neurons: negative regulation of neurite growth, spine formation and cell survival. Mol Brain 2: 27.

Kratskin I. 1995. Functional anatomy, central connections, and neurochemistry of the mammalian olfactory bulb In: Doty R, (ed.), Handbook of Olfaction and Gustation New York, NY: Mercer and Dekker. p. 103-109.

Kues WA, Wunder F. 1992. Heterogeneous expression patterns of mammalian potassium channel genes in developing and adult rat brain. Eur J Neurosci 4: 1296-1308.

Labra A, Brann JH, Fadool DA. 2005. Heterogeneity of voltage- and chemosignal-activated response profiles in vomeronasal sensory neurons. J Neurophysiol 94: 2535-2548.

Lagier S, Panzanelli P, Russo RE, Nissant A, Bathellier B, Sassoè-Pognetto M, Fritschy J-M, Lledo P-M. 2007. GABAergic inhibition at dendrodendritic synapses tunes γ oscillations in the olfactory bulb. Proc Natl Acad Sci USA 104: 7259-7264.

Larriva-Sahd J. 2008. The accessory olfactory bulb in the adult rat: A cytological study of its cell types, neuropil, neuronal modules, and interactions with the main olfactory system. J Comp Neurol 510: 309-350.

Lee R, Kermani P, Teng K, Hempstead B. 2001. Regulation of cell survival by secreted proneurotrophins. Science 294: 1945-1948.

Leinders-Zufall T, Brennan P, Widmayer P, S PC, Maul-Pavicic A, Jäger M, Li XH, Breer H, Zufall F, Boehm T. 2004. MHC class I peptides as chemosensory signals in the vomeronasal organ. Science 306: 1033-1037.

Leinders-Zufall T, Cockerham RE, Michalakis S, Biel M, Garbers DL, Reed RR, Zufall F, Munger SD. 2007. Contribution of the receptor guanylyl cyclase GC-D to chemosensory function in the olfactory epithelium. Proc Natl Acad Sci USA 104: 14507-14512.

Leinders-Zufall T, Lane AP, Puche AC, Ma W, Novotny MV, Shipley MT, Zufall F. 2000. Ultrasensitive pheromone detection by mammalian vomeronasal neurons. Nature 405: 792-796.

Leon M. 1998. Compensatory responses to early olfactory restriction. Ann N Y Acad Sci 855: 104-108.

Lepage PK, Boulay G. 2007. Molecular determinants of TRP channel assembly. Biochem Soc Trans 035: 81-83.

Levi-Montalcini R. 1987. The nerve growth factor 35 years later. Science 237: 1154-1162.

Leypold BG, Yu CR, Leinders-Zufall T, Kim MM, Zufall F, Axel R. 2002. Altered sexual and social behaviors in trp2 mutant mice. Proc Natl Acad Sci USA 99: 6376-6381.

Liman ER. 2003. Regulation by voltage and adenine nucleotides of a Ca2+-activated cation channel from hamster vomeronasal sensory neurons. J Physiol 548: 777-787.

Liman ER, Corey DP. 1996. Electrophysiological characterization of chemosensory neurons from the mouse vomeronasal organ. J Neurosci 16: 4625-4637.

Liman ER, Corey DP, Dulac C. 1999. TRP2: A candidate transduction channel for mammalian pheromone sensory signaling. Proc Natl Acad Sci USA 96: 5791-5796.

Liman ER, Innan H. 2003. Relaxed selective pressure on an essential component of pheromone transduction in primate evolution. Proc Natl Acad Sci USA 100: 3328-3332.

Lin DY, Zhang S-Z, Block E, Katz LC. 2005. Encoding social signals in the mouse main olfactory bulb. Nature 434: 470-477.

Lin W, Margolskee R, Donnert G, Hell SW, Restrepo D. 2007. Olfactory neurons expressing transient receptor potential channel M5 (TRPM5) are involved in sensing semiochemicals. Proc Natl Acad Sci USA 104: 2471-2476.

Lipton PA, Alvarez P, Eichenbaum H. 1999. Crossmodal associative memory representations in rodent orbitofrontal cortex. Neuron 22: 349-359.

Lledo PM, Saghatelyan A, Lemasson M. 2004. Inhibitory interneurons in the olfactory bulb: from development to function. Neuroscientist 10: 292-303.

Loconto J, Papes F, Chang E, Stowers L, Jones EP, Takada T, Kumanovics A, Lindahl KF, Dulac C. 2003. Functional expression of murine V2R pheromone receptors involves selective association with the M10 and M1 families of MHC Class Ib molecules. Cell 112: 607-618.

Longo F, Yang T, Knowles J, Xie Y, Moore L, Massa S. 2007. Small molecule neurotrophin receptor ligands: novel strategies for targeting Alzheimer's disease mechanisms. Curr Alzheimer Res 4: 503-506.

Lu J, Helton TD, Blanpied TA, Racz B, Newpher TM, Weinberg RJ, Ehlers MD. 2007. Postsynaptic positioning of endocytic zones and AMPA receptor cycling by physical coupling of dynamin-3 to homer. Neuron 55: 874-889.

Lucas P, Ukhanov K, Leinders-Zufall T, Zufall F. 2003. A diacylglycerol-gated cation channel in vomeronasal neuron dendrites is impaired in TRPC2 mutant mice: mechanism of pheromone transduction. Neuron 40: 551-561.

Luo Y, Lu S, Chen P, Wang D, Halpern M. 1994. Identification of chemoattractant receptors and G-proteins in the vomeronasal system of garter snakes. J Biol Chem 269: 16867-16877.

Ma M. 2007. Encoding olfactory signals via multiple chemosensory systems. Crit Rev Biochem Mol Biol 42: 463 - 480.

Ma M, Grosmaitre X, Iwema CL, Baker H, Greer CA, Shepherd GM. 2003. Olfactory signal transduction in the mouse septal organ. J. Neurosci. 23: 317-324.

Maher BJ, McGinley MJ, Westbrook GL. 2009. Experience-dependent maturation of the glomerular microcircuit. Proc Natl Acad Sci USA 106: 16865-16870.

Maher BJ, Westbrook GL. 2005. SK Channel regulation of dendritic excitability and dendrodendritic inhibition in the olfactory bulb. J Neurophysiol 94: 3743-3750.

Manganas LN, Trimmer JS. 2000. Subunit composition determines Kv1 potassium channel surface expression. J Biol Chem 275: 29685-29693.

Margolis F, Roberts N, Ferriero D, Feldman J. 1974. Denervation in the primary olfactory pathway of mice: biochemical and morphological effects. Brain Res 81: 469-483.

Margrie TW, Sakmann B, Urban NN. 2001. Action potential propagation in mitral cell lateral dendrites is decremental and controls recurrent and lateral inhibition in the mammalian olfactory bulb. Proce Natl Acad Sci USA 98: 319-324.

Marks D, Tucker K, Cavallin M, Mast T, Fadool D. 2009. Awake intranasal insulin delivery modifies protein complexes and alters memory, anxiety, and olfactory behaviors. J Neurosci 29: 6734-6751.

Marks DR, Fadool DA. 2007. Post-synaptic density perturbs insulin-induced Kv1.3 channel modulation via a clustering mechanism involving the SH3 domain. J Neurochem 103: 1608-1627.

Martínez-Ricós J, Agustín-Pavón C, Lanuza E, Martínez-García F. 2007. Intraspecific communication through chemical signals in female mice: reinforcing properties of involatile male sexual pheromones. Chem Senses 32: 139-148.

Matsunami H, Buck L. 1997. A multigene family encoding a diverse array of putative pheromone receptors in mammals. Cell 90: 775-784.

McClintock TS. 2010. Achieving singularity in mammalian odorant receptor gene choice. Chem Senses 35: 447-457.

McGann JP, Pírez N, Gainey MA, Muratore C, Elias AS, Wachowiak M. 2005. Odorant representations are modulated by intra- but not interglomerular presynaptic inhibition of olfactory sensory neurons. Neuron 48: 1039-1053.

McKay RR, Szymeczek-Seay CL, Lievremont JP, Bird GS, Zitt C, Jungling E, Luckhoff A, Putney JW. 2000. Cloning and expression of the human transient receptor potential 4 (TRP4) gene: localization and functional expression of human TRP4 and TRP3. Biochem J 351: 735-746.

McLean JH, Darby-King A, Bonnell WS. 2001. Neonatal olfactory sensory deprivation decreases BDNF in the olfactory bulb of the rat. Brain Res Dev Brain Res 128: 17-24.

Meisami E. 1976. Effects of olfactory deprivation on postnatal growth of the rat olfactory bulb utilizing a new method for production of neonatal unilateral anosmia. Brain Res 107: 437-444.

Menteyne A, Levavasseur F, Audinat E, Avignone E. 2009. Predominant functional expression of Kv1.3 by activated microglia of the hippocampus after status epilepticus. PLoS ONE 4: e6770.

Meredith M. 1986. Vomeronasal organ removal before sexual experience impairs male hamster mating behavior. Physiol Behav 36: 737-743.

Meredith M. 2001. Human Vomeronasal Organ Function: A critical review of best and worst cases. Chem Senses 26: 433-445.

Meredith M, Marques DM, O'Connell RO, Stern FL. 1980. Vomeronasal pump: significance for male hamster sexual behavior. Science 207: 1224-1226.

Meredith M, O'Connell RJ. 1979. Efferent control of stimulus access to the hamster vomeronasal organ. J Physiol 286: 301-316.

Meredith M, Westberry JM. 2004. Distinctive responses in the medial amygdala to same-species and different-species pheromones. J. Neurosci. 24: 5719-5725.

Michalski B, Fahnestock M. 2003. Pro-brain-derived neurotrophic factor is decreased in parietal cortex in Alzheimer's disease. Brain Res Mol Brain Res 111: 148-154.

Misonou H, Trimmer J. 2004. Determinants of voltage-gated potassium channel surface expression and localization in Mammalian neurons. Crit Rev Biochem Mol Biol 39: 125-145.

Mohedano-Moriano A, Pro-Sistiaga P, Úbeda-Bañón I, Crespo C, Insausti R, Martinez-Marcos A. 2007. Segregated pathways to the vomeronasal amygdala: differential projections from the anterior and posterior divisions of the accessory olfactory bulb. Eur J Neurosci 25: 2065-2080.

Mombaerts P, Wang F, Dulac C, Chao SK, Nemes A, Mendelsohn M, Edmondson J, Axel R. 1996. Visualizing an olfactory sensory map. Cell 87: 675-686.

Monti-Graziadei G, Margolis F, Harding J, Graziadei P. 1977. Immunocytochemistry of the olfactory marker protein. J. Histochem. Cytochem. 25: 1311-1316.

Mowla SJ, Farhadi HF, Pareek S, Atwal JK, Morris SJ, Seidah NG, Murphy RA. 2001. Biosynthesis and post-translational processing of the precursor to brain-derived neurotrophic factor. J Biol Chem 276: 12660-12666.

Murphy FA, Tucker T, Fadool DA. 2001. Sexual dimorphism and developmental expression of signal-transduction machinery in the vomeronasal organ. J Comp Neurol 432: 61-74.

Najbauer J, Ibrahim E, Leon M. 1995. Olfactory experience modulates Bcl-2 expression in the developing olfactory bulb. Neuroreport 7: 197-200.

Najbauer J, Leon M. 1995. Olfactory experience modulated apoptosis in the developing olfactory bulb. Brain Res 674: 245-251.

Nakamura Y, Takahashi T. 2007. Developmental changes in potassium currents at the rat calyx of Held presynaptic terminal. J Physiol 581: 1101-1112.

Nica R, Matter SF, Griff ER. 2010. Physiological evidence for two classes of mitral cells in the rat olfactory bulb. Brain Res 1358: 81-88.

Nickell W, Shipley M, Behbehani M. 1996. Orthodromic synaptic activation of rat olfactory bulb mitral cells in isolated slices. Brain Res Bull 39: 57-62.

Nodari F, Hsu FF, Fu X, Holekamp TF, Kao LF, Turk J, Holy TE. 2008. Sulfated steroids as natural ligands of mouse pheromone-sensing neurons. J Neurosci 28: 6407-6418.

Nucci C, Piccirilli S, Nisticò R, Morrone L, Cerulli L, Bagetta G. 2003. Apoptosis in the mechanisms of neuronal plasticity in the developing visual system. Eur J Ophthalmol 13 Suppl 3: S36-43.

Olsen SR, Wilson RI. 2008. Lateral presynaptic inhibition mediates gain control in an olfactory circuit. Nature 452: 956-960.

Olson R, Huey-Tubman KE, Dulac C, Bjorkman PJ. 2005. Structure of a pheromone receptor-associated MHC molecule with an open and empty groove. PLoS Biol 3: e257.

Padmanabhan K, Urban NN. 2010. Intrinsic biophysical diversity decorrelates neuronal firing while increasing information content. Nat Neurosci 13: 1276-1282.

Pang P, Teng H, Zaitsev E, Woo N, Sakata K, Zhen S, Teng K, Yung W, Hempstead B, Lu B. 2004. Cleavage of proBDNF by tPA/plasmin is essential for long-term hippocampal plasticity. Science 306: 487-491.

Parrish-Aungst S, Kiyokage E, Szabo G, Yanagawa Y, Shipley MT, Puche AC. 2011. Sensory experience selectively regulates transmitter synthesis enzymes in interglomerular circuits. Brain Res 1382: 70-76.

Peng S, Wuu J, Mufson E, Fahnestock M. 2005. Precursor form of brain-derived neurotrophic factor and mature brain-derived neurotrophic factor are decreased in the pre-clinical stages of Alzheimer's disease. J Neurochem 93: 1412-1421.

Perciaccante VJ, Bays RA. 2004. Maxillary Orthognathic Surgery. In: Miloro M, (ed.), Peterson's Principles of Oral and Maxillofacial Surgery. BC Decker. p. 1179-1204.

Price J, Powell T. 1970. The mitral and short axon cells of the olfactory bulb. J Cell Sci 7: 631-651.

Raff MC, Barres BA, Burne JF, Coles HS, Ishizaki Y, Jacobson MD. 1993. Programmed cell death and the control of cell survival: lessons from the nervous system. Science 262: 695-700.

Ramos-Franco J, Caenepeel S, Fill M, Mignery G. 1998. Single channel function of recombinant type-1 inositol 1,4,5-trisphosphate receptor ligand binding domain splice variants. Biophys J 75: 2783-2793.

Reichardt L. 2006. Neurotrophin-regulated signalling pathways. Philos Trans R Soc Lond B Biol Sci 361: 1545-1564.

Rodriguez I. 2007. Odorant and pheromone receptor gene regulation in vertebrates. Curr Opin Gen Dev 17: 465-470.

Rodriguez I, Feinstein P, Mombaerts P. 1999. Variable patterns of axonal projections of sensory neurons in the mouse vomeronasal system. Cell 97: 199-208.

Rodriguez I, Greer CA, Mok MY, Mombaerts P. 2000. A putative pheromone receptor gene expressed in human olfactory mucosa. Nat Genet 26: 18-19.

Rodriguez-Tébar A, Dechant G, Barde YA. 1990. Binding of brain-derived neurotrophic factor to the nerve growth factor receptor. Neuron 4: 487-492.

Rogers AB, Cormier KS, Fox JG. 2006. Thiol-reactive compounds prevent nonspecific antibody binding in immunohistochemistry. Lab Invest 86: 526-533.

Root CM, Masuyama K, Green DS, Enell LE, Nässel DR, Lee C-H, Wang JW. 2008. A presynaptic gain control mechanism fine-tunes olfactory behavior. Neuron 59: 311-321.

Roppolo D, Vollery S, Kan C-D, Luscher C, Broillet M-C, Rodriguez I. 2007. Gene cluster lock after pheromone receptor gene choice. EMBO J 26: 3423-3430.

Ryba NJP, Tirindelli R. 1997. A new multigene family of putative pheromone receptors. Neuron 19: 371-379.

Saito H, Kubota M, Roberts RW, Chi Q, Matsunami H. 2004. RTP family members induce runctional expression of mammalian odorant receptors. Cell 119: 679-691.

Sambrook J, Fitsch EF, Maniatis T. 1989. Molecular Cloning: A Laboratory Manual. Cold Spring Harbor: Cold Spring Harbor Press.

Samuelsen CL, Meredith M. 2009. The vomeronasal organ is required for the male mouse medial amygdala response to chemical-communication signals, as assessed by immediate early gene expression. Neurosci 164: 1468-1476.

Savic I, Hedén-Blomqvist E, Berglund H. 2009. Pheromone signal transduction in humans: What can be learned from olfactory loss. Hum Brain Mapp 30: 3057-3065.

Schachter JB, Sromek SM, Nicholas RA, Harden TK. 1997. HEK293 human embryonic kidney cells endogenously express the P2Y1 and P2Y2 receptors. Neuropharmacol 36: 1181-1187.

Schaefer ML, Yamazaki K, Osada K, Restrepo D, Beauchamp GK. 2002. Olfactory fingerprints for major histocompatibility complex-determined body odors II: relationship among odor maps, genetics, odor composition, and behavior. J Neurosci 22: 9513-9521.

Schild D, Restrepo D. 1998. Transduction mechanisms in vertebrate olfactory receptor cells. Physiological Rev 78: 429-466.

Scholz J, Broom D, Youn D, Mills C, Kohno T, Suter M, Moore K, Decosterd I, Coggeshall R, Woolf C. 2005. Blocking caspase activity prevents transsynaptic neuronal apoptosis and the loss of inhibition in lamina II of the dorsal horn after peripheral nerve injury. J Neurosci 25: 7317-7323.

Schulte-Herbrüggen O, Eckart S, Deicke U, Kühl A, Otten U, Danker-Hopfe H, Abramowski D, Staufenbiel M, Hellweg R. 2008. Age-dependent time course of cerebral brain-derived neurotrophic factor, nerve growth factor, and neurotrophin-3 in APP23 transgenic mice. J Neurosci Res 86: 2774-2783.

Schäbitz W, Steigleder T, Cooper-Kuhn C, Schwab S, Sommer C, Schneider A, Kuhn H. 2007. Intravenous brain-derived neurotrophic factor enhances poststroke sensorimotor recovery and stimulates neurogenesis. Stroke 38: 2165-2172.

Scott JW, Scott-Johnson PE. 2002. The electroolfactogram: A review of its history and uses. Microscopy Res Tech 58: 152-160.

Serizawa S, Miyamichi K, Nakatani H, Suzuki M, Saito M, Yoshihara Y, Sakano H. 2003. Negative feedback regulation ensures the one receptor-one olfactory neuron rule in mouse. Science 302: 2088-2094.

Shepherd GM, Greer CA. 1998. Olfactory bulb. In: Shepherd GM, (ed.), The synaptic organization of the brain. Oxford: Oxford University Press. p. 159-204.

Shi Q, Zhang P, Zhang J, Chen X, Lu H, Tian Y, Parker T, Liu Y. 2009. Adenovirus-mediated brain-derived neurotrophic factor expression regulated by hypoxia response element protects brain from injury of transient middle cerebral artery occlusion in mice. Neurosci Lett 465: 220-225.

Shiraishi Y, Mizutani A, Yuasa S, Mikoshiba K, Furuichi T. 2004. Differential expression of Homer family proteins in the developing mouse brain. J Comp Neurol 473: 582-599.

Shirokova E, Raguse JD, Meyerhof W, Krautwurst D. 2008. The human vomeronasal type-1 receptor family-- detection of volatiles and cAMP signaling in HeLa/Olf cells. FASEB J 22: 1416-1425.

Soler MVC, Suburo AM. 1998. Innervation of blood vessels in the vomeronasal complex of the rat. Brain Res 811: 47-56.

Speake T, Kibble JD, Brown PD. 2004. Kv1.1 and Kv1.3 channels contribute to the delayed-rectifying K+ conductance in rat choroid plexus epithelial cells. AJP - Cell Physiol 286: C611-C620.

Spehr J, Hagendorf S, Weiss J, Spehr M, Leinders-Zufall T, Zufall F. 2009. Ca2+-calmodulin feedback mediates sensory adaptation and inhibits pheromone-sensitive ion channels in the vomeronasal organ. J Neurosci 29: 2125-2135.

Spehr M, Hatt H, Wetzel CH. 2002. Arachidonic acid plays a role in rat vomeronasal signal transduction. J Neurosci 22: 8429-8437.

Spehr M, Kelliher KR, Li XH, Boehm T, Leinders-Zufall T, Zufall F. 2006. Essential role of the main olfactory system in social recognition of major histocompatibility complex Peptide ligands. J Neurosci 26: 1961-1970.

Stamboulian S, Moutin MJ, Treves S, Pochon N, Grunwald D, Zorzato F, De Waard M, Ronjat M, Arnoult C. 2005. Junctate, an inositol 1,4,5-triphosphate receptor associated protein, is present in rodent sperm and binds TRPC2 and TRPC5 but not TRPC1 channels. Dev Biol 286: 326-337.

Stiber JA, Zhang ZS, Burch J, Eu JP, Zhang S, Truskey GA, Seth M, Yamaguchi N, Meissner G, Shah R, Worley PF, Williams RS, Rosenberg PB. 2008. Mice lacking homer 1 exhibit a skeletal myopathy characterized by abnormal TRP channel activity. Mol Cell Biol 28: 2637-2647.

Stowers L, Holy TE, Meister M, Dulac C, Koentges G. 2002. Loss of sex discrimination and male-male aggression in mice deficient for TRP2. Science 295: 1493-1500.

Strausfeld NJ, Hildebrand JG. 1999. Olfactory systems: common design, uncommon origins? Curr Opin Neurobiol 9: 634-639.

Swanson LW. 2000. Cerebral hemisphere regulation of motivated behavior. Brain Res 886: 113-164.

Taylor CW, Laude AJ. 2002. IP3 receptors and their regulation by calmodulin and cytosolic Ca2+. Cell Calcium 32: 321-334.

Teng H, Teng K, Lee R, Wright S, Tevar S, Almeida R, Kermani P, Torkin R, Chen Z, Lee F, Kraemer R, Nykjaer A, Hempstead B. 2005. ProBDNF induces neuronal apoptosis via activation of a receptor complex of p75NTR and sortilin. J Neurosci 25: 5455-5463.

Thorne R, Pronk G, Padmanabhan V, Frey Wn. 2004. Delivery of insulin-like growth factor-I to the rat brain and spinal cord along olfactory and trigeminal pathways following intranasal administration. Neurosci 127: 481-496.

Tirindelli R, Dibattista M, Pifferi S, Menini A. 2009. From pheromones to behavior. Physiological Rev 89: 921-956.

Trombley PQ, Westbrook GL. 1990. Excitatory synaptic transmission in cultures of rat olfactory bulb. J Neurophysiol 64: 598-606.

Trotier D, Døving KB, Ore K, Shalchian-Tabrizi C. 1998. Scanning electron microscopy and gramicidin patch clamp recordings of microvillous receptor neurons dissociated from the rat vomeronasal organ. Chem Senses 23: 49-57.

Trotier D, Eloit C, Wassef M, Talmain G, Bensimon JL, Døving KB, Ferrand J. 2000. The vomeronasal cavity in adult humans. Chem Senses 25: 369-380.

Tu JC, Xiao B, Naisbitt S, Yuan JP, Petralia RS, Brakeman P, Doan A, Aakalu VK, Lanahan AA, Sheng M, Worley PF. 1999. Coupling of mGluR/Homer and PSD-95 complexes by the shank family of postsynaptic density proteins. Neuron 23: 583-592.

Tucker D. 1963. Olfactory, vomeronasal and trigeminal receptor responses to odorants New York: Pergamon Press.

Tucker K, Fadool D. 2002. Neurotrophin modulation of voltage-gated potassium channels in rat through TrkB receptors is time and sensory experience dependent. J Physiol 542: 413-429.

Ukhanov K, Leinders-Zufall T, Zufall F. 2007. Patch-clamp analysis of gene-targeted vomeronasal neurons expressing a defined V1R or V2R receptor: ionic mechanisms underlying persistent firing. J Neurophysiol 98: 2357-2369.

Vaccarezza OL, Sepich LN, Tramezzani JH. 1981. The Vomeronasal organ of the rat. J Anat 132: 167-185.

Van Kolen K, Slegers H. 2006. Integration of P2Y receptor-activated signal transduction pathways in G protein-dependent signalling networks. Purinergic Signal 2: 451-469.

Vannier B, Peyton M, Boulay G, Brown D, Qin N, Jiang M, Zhu X, Birnbaumer L. 1999. Mouse trp2, the homologue of the human trpc2 pseudogene, encodes mTrp2, a store depletion-activated capacitative Ca2+ entry channel. Proc Natl Acad Sci USA 96: 2060-2064.

Vazquez G, Wedel BJ, Trebak M, St John Bird G, Putney JW. 2003. Expression level of the canonical transient receptor potential 3 (TRPC3) channel determines its mechanism of activation. J Biol Chem 278: 21649-21654.

Veh RW, Lichtinghagen R, Sewing S, Wunder F, Grumbach IM, Pongs O. 1995. Immunohistochemical localization of five members of the Kv1 channel subunits: contrasting subcellular locations and neuron-specific co-localizations in rat brain. Eur J Neurosci 7: 2189-2205.

Venkatachalam K, Montell C. 2007. TRP channels. Ann Rev Biochem 76: 387-417.

Vicente R, Escalada A, Villalonga N, Texidó L, Roura-Ferrer M, Martín-Satué M, López-Iglesias C, Soler C, Solsona C, Tamkun MM, Felipe A. 2006. Association of Kv1.5 and Kv1.3 contributes to the major voltage-dependent K+ channel in macrophages. J Biol Chem 281: 37675-37685.

Wang Z, Balet Sindreu C, Li V, Nudelman A, Chan GC-K, Storm DR. 2006. Pheromone detection in male mice depends on signaling through the type 3 adenylyl cyclase in the main olfactory epithelium. J. Neurosci. 26: 7375-7379.

Weise J, Engelhorn T, Dörfler A, Aker S, Bähr M, Hufnagel A. 2005. Expression time course and spatial distribution of activated caspase-3 after experimental status epilepticus: contribution of delayed neuronal cell death to seizure-induced neuronal injury. Neurobiol Dis 18: 582-590.

Wekesa KS, Anholt RRH. 1997. Pheromone regulated production of inositol-(1, 4, 5)-trisphosphate in the mammalian vomeronasal organ. Endocrinol 138: 3497-3504.

Wes PD, Chevesich J, Jeromin A, Rosenberg C, Stetten G, Montell C. 1995. TRPC1, a human homolog of a Drosophila store-operated channel. Proc Natl Acad Sci USA 92: 9652-9656.

Whitman MC, Greer CA. 2007. Synaptic integration of adult-generated olfactory bulb granule cells: basal axodendritic centrifugal input precedes apical dendrodendritic local circuits. J Neurosci 27: 9951-9961.

Williams R, Airey D, Kulkarni A, Zhou G, Lu L. 2001. Genetic dissection of the olfactory bulbs of mice: QTLs on four chromosomes modulate bulb size. Behav Genet 31: 61-77.

Witt M, Georgiewa B, Knecht M, Hummel T. 2002. On the chemosensory nature of the vomeronasal epithelium in adult humans. Histochem Cell Biol 117: 493-509.

Woo N, Teng H, Siao C, Chiaruttini C, Pang P, Milner T, Hempstead B, Lu B. 2005. Activation of p75NTR by proBDNF facilitates hippocampal long-term depression. Nat Neurosci 8: 1069-1077.

Woodley SK, Baum MJ. 2004. Differential activation of glomeruli in the ferret's main olfactory bulb by anal scent gland odours from males and females: an early step in mate identification. Eur J Neurosci 20: 1025-1032.

Worley PF, Zeng W, Huang G, Kim JY, Shin DM, Kim MS, Yuan JP, Kiselyov K, Muallem S. 2007a. Homer proteins in Ca2+ signaling by excitable and non-excitable cells. Cell Calcium 42: 363-371.

Worley PF, Zeng W, Huang GN, Yuan JP, Kim JY, Lee MG, Muallem S. 2007b. TRPC channels as STIM1-regulated store-operated channels. Cell Calcium 42: 205-211.

Wyart C, Webster WW, Chen JH, Wilson SR, McClary A, Khan RM, Sobel N. 2007. Smelling a single component of male sweat alters levels of cortisol in women. J Neurosci 27: 1261-1265.

Wysocki CJ, Preti G. 2004. Facts, fallacies, fears, and frustrations with human pheromones. Anat Rec A Discov Mol Cell Evol Biol 281A: 1201-1211.

Wysocki CJ, Wellington JL, Beauchamp GK. 1980. Access of urinary nonvolatiles to the mammalian vomeronasal organ. Science 207: 781-783.

Xiao B, Tu JC, Petralia RS, Yuan JP, Doan A, Breder CD, Ruggiero A, Lanahan AA, Wenthold RJ, Worley PF. 1998. Homer Regulates the Association of Group 1 Metabotropic Glutamate Receptors with Multivalent Complexes of Homer-Related, Synaptic Proteins. Neuron 21: 707-716.

Yamaguchi M, Mori K. 2005. Critical period for sensory experience-dependent survival of newly generated granule cells in the adult mouse olfactory bulb. Proc Natl Acad Sci USA 102: 9697-9702.

Yamamoto M, Okumura S, Schwencke C, Sadoshima J, Ishikawa Y. 1999. High efficiency gene transfer by multiple transfection protocol. Histocheml J 31: 241-243.

Yamashita K, Wiessner C, Lindholm D, Thoenen H, Hossmann K. 1997. Post-occlusion treatment with BDNF reduces infarct size in a model of permanent occlusion of the middle cerebral artery in rat. Metab Brain Dis 12: 271-280.

Yeh JZ, Oxford GS, Wu CH, Narahashi T. 1976. Dynamics of aminopyridine block of potassium channels in squid axon membrane. J Gen Physiol 68: 519-535.

Yuan JP, Kiselyov K, Shin DM, Chen J, Shcheynikov N, Kang SH, Dehoff MH, Schwarz MK, Seeburg PH, Muallem S, Worley PF. 2003. Homer Binds TRPC Family Channels and Is Required for Gating of TRPC1 by IP3 Receptors. Cell 114: 777-789.

Zhang P, Yang C, Delay RJ. 2008. Urine stimulation activates BK channels in mouse vomeronasal neurons. J Neurophysiol 100: 1824-1834.

Zhuang H, Matsunami H. 2007. Synergism of accessory factors in functional expression of mammalian odorant receptors. J Biol Chem 282: 15284-15293.

Zufall F, Ukhanov K, Lucas P, Leinders-Zufall T. 2005. Neurobiology of TRPC2: from gene to behavior. Pflugers Archiv 451: 61-71.

BIOGRAPHICAL SKETCH

Education:

B.S.	Eastern Michigan University, Biology, 2001.
M.S.	University of Cincinnati, Biology, 2004.
Ph.D.	Florida State University, Program in Neuroscience, 2011.

Professional Experience:

1999-2001	Laboratory Assistant, Eastern Michigan University, Department of Biological Science.
2001-2003	Graduate Student, University of Cincinnati, Department of Biological Science.
2003-2005	Senior Research Assistant, University of Cincinnati, College of Medicine, Department of Molecular Genetics, Biochemistry and Microbiology.
2004 & 2005	Adjunct Assistant Professor, Cincinnati State College, Biology Department.
2005-2011	Graduate Student, Florida State University, Program in Neuroscience.

Support:

2001-2003	Teaching Assistantship, University of Cincinnati, Biological Sciences.
2005 & 2006	Neuroscience Fellowship, Florida State University, Program in Neuroscience.
2007 & 2008	Teaching Assistantship, Florida State University, Biological Sciences.
2009-2011	Pre-Doctoral Fellowship, NIH Chemosensory Training Grant.

Awards and Honors:

1999	Meta Hellwig Special Study Award, Eastern Michigan University, Biological Sciences.
2002	Grant-in-Aid-of-Research, Sigma Xi Scientific Research Society.
2003	Wiemann Summer Fellowship, University of Cincinnati, Biological Sciences.
2006	South East Nerve Net (SENN) Annual Meeting Travel Award.
2007	LEAD Grant, Florida State University, Council on Research and Creativity.
2008	SENN Annual Meeting Travel Award.
2008	Robert B. Short Memorial Award in Zoology, F.S.U., Biological Sciences.
2011	Dissertation Research Grant, Florida State University, Graduate School.

Peer-reviewed Publications:

Qian Y, Baisden JM, Cherezova L, Summy JM, Guaponne-Koay A, Shi XL, **Mast T**, Pastula J, Zot HG, Mazloum N, Lee MY, Flynn DC. 2002. PKC phosphorylation increases the ability of AFAP-110 to cross-link actin filaments. ***Mol. Biol. Cell.*** 13: 2311-2322. PMID: 12134071

Mast TG, ER Griff. 2005. In vivo preparation and identification of mitral cells in the main olfactory bulb of the mouse. ***Brain Res. Brain Res. Prot.*** 15: 105-113. PMID: 17536617
Mast TG, ER Griff. 2007. The effects of analgesic supplements on neural activity in the main olfactory bulb of the mouse. ***Comp. Med.*** 57: 167-174. PMID: 17536617
Biju KC, Marks DR, **Mast TG**, Fadool DA. 2007. Deletion of voltage-gated channel affects glomerular refinement and odor receptor expression in the olfactory system. ***J. Comp. Neurol.*** 506: 161-179. PMID: 18022950
Biju KC, **Mast TG**, and Fadool DA. 2008. Olfactory sensory-deprivation increases the number of proBDNF immunoreactive mitral cells in the olfactory bulb of mice. ***Neurosci. Lett.*** 447: 42-7. PMID: 18834927
Marks DR, K Tucker, MA Cavallin, **TG Mast**, DA Fadool. 2009. Awake intranasal insulin delivery modifies protein complexes and alters memory, anxiety, and olfactory behaviors. ***J. Neurosci.*** 29: 6734-6751. PMID: 19458242
Mast TG, Samuelsen CL. 2009. Human pheromone detection by the vomeronasal organ: unnecessary for mate selection? ***Chem. Senses*** 34: 529-531. PMID: 19477954
Mast TG, Brann JH, and Fadool DA. 2010. The TRPC2 channel forms protein-protein interactions with Homer and RTP in the rat vomeronasal organ. ***BMC Neurosci*** 11:61. PMID: 20492691

Abstracts and Presentations:

Zot HG, **Mast TG**, Pastula J, Atkins S, Liggit P, T Greco. 2000. Transduction of peptides into Chlamydomonous. A*merican Society for Cell Biology (ASCB),* San Francisco, CA.
Nica R, **Mast TG**, ER Griff. 2003. Spontaneous activity of mitral cells in the rat and mouse. *Association for Chemoreception Sciences (AChemS),* Sarasota, FL.
Mast TG, ER Griff. 2004. In vivo preparation for recording antidromically identified mitral cells in the anesthetized mouse. *Association for Chemoreception Sciences (AChemS),* Sarasota, FL. bulb.
Mast TG, Sklenka A, Hassett D, T Doetschman. 2005. Identification of the microflora in the TGFβ-/-mouse colon cancer model. *American Society for Microbiology (ASM),* Atlanta, GA.
Mast TG, ER Griff. 2006. Effects of analgesics on both olfactory bulb single-units and the electroencephalogram in the anesthetized mouse. *Southeast Nerve Net (SENN),* Atlanta, GA.
Mast TG, DA Fadool. 2007. Directing expression of TRPC2 to the plasma membrane in cell culture. *Southeast Nerve Net (SENN),* Wakulla Springs, FL.
Mast TG, Biju KC, DA Fadool. 2007. BDNF immunoreactive periglomerular cells may modulate survival and plasticity of neurons in the olfactory bulb. *Association for Chemoreception Sciences (AChemS),* Sarasota, FL.
Mast TG, Brann JH, DA Fadool. 2008. Signalplex involving protein interactions with the TRPC2 channel in the rat vomeronasal organ. *Southeast Nerve Net (SENN),* Atlanta, GA.
Mast TG, Brann JH, DA Fadool. 2008. The canonical transient receptor potential channel 2 (TRPC2) forms protein-protein interactions with Homer and RTP in the rat

vomeronasal organ. *International Symposium on Olfaction and Taste (ISOT),* San Francisco, CA.

Teaching:

Laboratory-

2001	Anatomy and Physiology I, II, and III	U.C. Biology
2002	Anatomy and Physiology I, II, and III	U.C. Biology
2003	Anatomy and Physiology I and II	U.C. Biology
2003	Comparative and Human Anatomy	U.C. Biology
2004	Microbiology	C.S.C. Biology
2005	Concepts of Biology I	C.S.C. Biology
2007	Anatomy and Physiology I	F.S.U. Biology
2008	Anatomy and Physiology II	F.S.U. Biology
2008	General Biology I	F.S.U. Biology

Lecture-

2004	Microbiology	C.S.C. Biology
2005	Concepts of Biology I	C.S.C. Biology
2008	General Biology I (recitation)	F.S.U. Biology

Collaborative-

2009 & 2010 Lecture on the "Cellular basis of vision" for the course 'Color Theory', Department of Art, Florida State University.

Service:

2002 Secretary, Biology Graduate Student Association, University of Cincinnati.
2007 Assistant Coordinator, Southeast Nerve Net (SENN), 2007 Annual Meeting.
2008 Treasurer, Neuroscience Graduate Student Association, Florida State University.
2008 Reviewer for *Neurochemical Research*.
2009 Assistant Coordinator, Rushton Lecture Series, Florida State University.
2010 Graduate Student Panelist for Tri-Beta National Honor Society, Florida State University.